Analysis and Implementation of an Age Structured Model of the Cell Cycle

Anna Broms

Master's thesis
2017:E51

Lund University

Faculty of Engineering
Centre for Mathematical Sciences
Mathematics

Centrum Scientiarum Mathematicarum

Analysis and Implementation of an Age Structured Model of the Cell Cycle

Anna Broms
broms93@gmail.com

principal supervisor:
Sara Maad Sasane
assistant supervisor:
Gustaf Söderlind

Master's thesis

Lund University

September 2017

Abstract

In an age-structured model originating from cancer research, the cell cycle is divided into two phases: Phase 1 of variable length, consisting of the biologically so called G_1 phase, and Phase 2 of fixed length, consisting of the so called S, G_2 and M phases. A system of nonlinear PDEs along with initial and boundary data describes the number densities of cells in the two phases, depending on time and age (where age is the time spent in a phase). It has been shown that the initial and boundary value problem can be rewritten as a coupled system of integral equations, which in this M.Sc. thesis is implemented in MATLAB using the trapezoidal and Simpson rule. In the special case where the cells are allowed to grow without restrictions, the system is uncoupled and possible to study analytically, whereas otherwise, a nonlinearity has to be solved in every step of the iterative equation solving. The qualitative behaviour is investigated numerically and analytically for a wide range of model components. This includes investigations of the notions of crowding, i.e. that cell division is restricted for large population sizes, and quorum sensing, i.e. that a small enough tumour can eliminate itself through cell signalling. In simulations, we also study under what conditions an almost eliminated tumour relapses after completed therapy. Moreover, upper bounds for the number of dividing cells at the end of Phase 2 at time t are determined for specific cases, where the bounds are found to depend on the existence of so called cancer stem cells. Lastly, a careful error analysis of the MATLAB implementation is performed both in a linear and in a nonlinear case.

Åldersbaserad modell av cellcykeln: Analys och implementering

I en åldersbaserad modell av cellcykeln som härstammar från cancerforskning kan cellcykeln delas in i två faser: en av variabel längd och en av fix längd. Det totala antalet celler i en tumör kan, tillsammans med antalet celler som just avslutat en cykel och ska genomgå celldelning, beskrivas genom ett system av integralekvationer. I arbetet studeras detta system dels analytiskt och dels numeriskt, genom förfinad implementering av modellen i MATLAB och simulering för många olika val av modellens ingående komponenter. Bland annat undersöks huruvida återväxt av en tumör efter avslutad behandling beror av så kallade cancerstamceller.

Cellcykeln är den följd av processer en cell genomgår under sin livstid fram till tidpunkten då cellen delar sig i två dotterceller. I den första av modellens två faser växer cellerna och samlar näring för att i den andra fasen duplicera sitt genetiska material, växa ytterligare, syntetisera nödvändiga proteiner och slutligen dela sig i två. Antalet celler i de två faserna beror av tidpunkt och ålder, där ålder avser hur länge en cell befunnit sig i fasen. I arbetet visas inledningsvis att det går att beskriva antalet celler som befinner sig i var och en av faserna vid en viss tidpunkt genom ett system av olinjära partiella differentialekvationer (PDEer), med tillhörande initial- och randvärden. Randvärdena beskriver hur celler lämnar en fas och går in i nästa, medan initialvärdena beskriver en ursprunglig åldersdistribution för cellerna i respektive fas för tidpunkten då simuleringen startar. För fasen med variabel längd (fas 1) gäller att cellerna lämnar denna fas och övergår i nästa fas enligt en fördelningsfunktion, $F(\tau)$, där det är större chans för en gammal cell att övergå i fas 2 än för en cell som befunnit sig i fas 1 en kortare tid. Modellen är dock helt deterministisk och det som avses med fördelningsfunktionen är *andelen* celler som har övergått från fas 1 i åldersspannet $[0, \tau]$. I modellen förekommer även en så kallad trängselfunktion, $f(p)$, som anger andelen celler som genomgår celldelning efter fas 2 då den totala populationsstorleken är p. Trängselfunktionen används för att ta hänsyn till att celler inte alltid antas växa ohämmat, utan har svårare att dela på sig både vid trängsel, dvs. om systemet innehåller för många celler på liten yta så att näringsbrist råder, och vid eventuell så kallad quorum sensing, där cellerna signalerar varandra på ett sådant sätt att tumören självdör. Vidare antas den första fasen kunna få input från dotterceller från så kallade cancerstamceller. Dottercellerna är vanliga celler som ingår i modellen, medan cancerstamcellerna, som är väldigt få till antalet, inte gör det. Cancerstamcellerna kan vara en förklaring till att cancer inte sällan kommer tillbaka efter avslutat behandling. Det är debatterat huruvida cancerstamceller existerar eller ej och i arbetet undersöks därför kvalitativt skillnaden mellan att ta hänsyn till deras dotterceller och att inte göra det.

I en artikel i *Journal of Mathematical Analysis and Applications* som ligger till grund för detta arbete visar Sara Maad Sasane att initial- och randvärdesproblemet kan skrivas om som ett system av integralekvationer och att detta system har en entydig lösning. Integralekvationerna är enklare att studera än det ursprungliga systemet av PDEer och gör det möjligt att studera modellen numeriskt. Lösningarna till integralekvationerna är funktioner av en variabel, medan lösningarna till det ursprungliga systemet av PDEer är funktioner av två variabler. Detta gör att lösningarna till integralekvationerna är enklare att visualisera. I detta examensarbete presenteras integralekvationerna och den numeriska implementeringen av modellen förfinas genom att lösa systemet av integralekvationer genom trapetsmetoden och Simpsons metod. När trängselfunktionen ej är konstant måste en ickelinjär ekvation lösas i varje steg. En utmaning är att hantera diskontinuiteterna som finns i integralekvationerna och en rigorös felanalys presenteras därför för att undersöka felet i de båda numeriska metoderna. Simuleringar görs för att undersöka lösningarna efter lång tid för många olika val av trängselfunktion, inputfunktion och initiala åldersdistributioner, samt ett par olika val av fördelningsfunktion.

Då det biologiskt är svårt att exakt bestämma modellens konstanter och ingående funktioner, genomförs kvalitativa undersökningar. För specifika parameterval kan en övre gräns för antalet celler som genomgår celldelning vid tid t bestämmas. Trots relativt lite information om de biologiska förhållandena kan det då gå att få fram approximativa resultat om antalet delande celler.

Acknowledgements

I would like to warmly thank my supervisors Sara Maad Sasane and Gustaf Söderlind for generously sharing their knowledge, for encouraging me to tackle the challenges I have encountered in my work and for valuable feedback and discussions along the way. I would also like to thank Ivar Persson for being my sounding board and Carina Dunlop at the University of Surrey for commenting on an early draft of the manuscript.

Contents

1 Introduction

1.1 Background

The cell cycle, i.e. the sequence of processes from the moment a cell is born until it divides into two daughter cells, is for eukaryotic cells (cells with a nucleus) traditionally divided into four different phases: the G_1, S, G_2 and M phases [1, 2]. In the first and longest phase, the G_1 phase (Gap 1 phase), the cell grows and accumulates nutrients. After completion of the G_1 phase, the cell enters the S phase (Synthesis phase) where the cell duplicates its genetic material. In the G_2 phase (Gap 2 phase), the cell grows and prepares for mitosis (cell division), for instance by synthesising necessary proteins. Finally, in the M phase, the Mitotic phase, the two sets of genetic material within the mother cell is separated in two parts, followed by cell division into two daughter cells. Thereafter, the daughter cells enter the G_1 phase of a new cycle, see Figure 1.1 [2]. The four phases are discrete in the way that a cell always must complete one phase to enter the next. The entire cycle is regulated by a complicated process that also regulates signals that monitor the specialisation of cells [2].

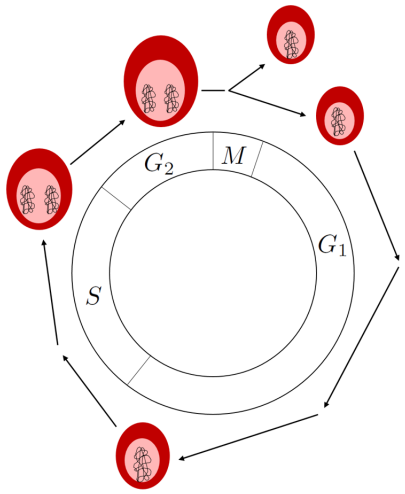

Figure 1.1: Schematic picture of the four phases of the cell cycle of an eukaryotic cell.

In an age structured model originating from cancer research, the phases of the cell cycle is for modelling purposes grouped into two new phases: Phase 1, of variable length, and Phase 2, of fixed length, where Phase 1 corresponds to the G_1 phase and Phase 2 corresponds to the S, G_2 and M phases. The reason for this specific assembling of phases is that it better captures the qualitative behaviour of the system; nothing happens qualitatively that we take into account in the model between the S, G_2 and M phases and therefore they are clustered as one phase. The original phases could have been used, but this would only have resulted in a model with four phases, where three of the phases are mathematically identical (apart from their length). Therefore, it is more sound to combine these phases into one phase. If the age lengths of the S, G_2 and M phases are known however, it is possible to translate the results from the current model to results for a model with the standard four phases.

It is possible to describe the number of cells in each of the two phases at a specific time by a system of nonlinear partial differential equations (PDEs), along with specified initial and boundary data. The number of cells in the two phases depend on the two variables time and age, where age is defined as the time a cell has spent in the phase. Note that neither size nor DNA content of the cells are taken into account. The initial data describe an initial age distribution in each phase, whereas the boundary data describe how cells enter one phase from the previous.

There are advantages of using an age structured model, in comparison to other types of models

where e.g. cell size is considered. The reason for this is that the response to cancer therapies more easily can be modelled, many of which delay or block a specific phase of the cell cycle [10]. In an age structured model, it might be easier to investigate the location of the cells in terms of phase [1]. Having knowledge about how a population of cells move through the cell cycle is crucial to choose the most efficient therapeutic method and, moreover, the effect of a certain therapy depends on where in the cell cycle the cells are [1].

This project is based on the particular age structured model presented in an article by Sara Maad Sasane in *Journal of Mathematical Analysis and Applications* [10]. The model is a simplified version of the CelCyMUS model, developed by Norman Kirkby and collaborators at the University of Surrey, see for instance [1, 5]. Having the advantage of being simple in its structure, the model of this M.Sc. thesis does only address the parts of the cell cycle important for the larger picture of the life of the cells, as they transfer from one state to the other. Despite the overall complexity of the cell cycle, the model does not take into account specific intricate steps of sub phases of the cell cycle or detailed chemical pathways, a property that makes the model an available tool for simulation and analysis that however still captures the main traits of the cell cycle.

A few crucial functions have a large impact on the output of the equations of the model, more thoroughly described in the Model Description chapter (2): In Phase 1, the cells leave the phase and enter the next according to a *cumulative distribution function*, $F(\tau)$. The model is deterministic and what we mean by the cumulative distribution function $F(\tau)$ is the proportion of cells that has left Phase 1 and entered Phase 2 in the age span $[0, \tau]$. The proportion of cells that undergoes mitosis after Phase 2 is described by the so called *crowding function*, f, where the remaining proportion that does not undergo mitosis is assumed to die. Lastly, the so called *input function*, ψ, represents input from an earlier stage as boundary data for Phase 1.

For instance, the input function could be interpreted as daughter cells from so called cancer stem cells. The daughter cells are ordinary (cancer) cells included in the model, whereas the small proportion of mother cells, which have different properties than the other cells and follow a different cycle, are not. It is discussed whether cancer stem cells exist at all and to investigate this issue will be one of the main focuses of this project. The cancer stem cells might be an explanation to relapse of a cancer tumour after completed cancer therapy. Even if the cancer cells themselves might have become extinct after successful medication, the tumour could start growing again via the daughter cells of the cancer stem cells – stem cells that have not been affected by the medication [6, 11]. It is believed that the stem cells not only have the potential of initiating the cancer but also of driving its progression onward [8]. In addition, the amount of cancer stem cells present might affect the aggressiveness of the tumour [8]. A second argument for the existence of cancer stem cells is that they can explain the heterogeneity among cells in a tumour [6]. Cancer mortality has decreased as a consequence of early detection, rather than effective treatment during the last decades [11]. It is a possibility that the cancer drugs of tomorrow must take a new grasp of the problem by focusing on affecting and eliminating the cancer stem cells (if it can be proven that they exist) and not only the cancer cells themselves, to completely cure a cancer [6, 8, 11].

Sara Maad Sasane showed in [10] that the initial and boundary value problem in the model can be written as a system of integral equations and that this system has a unique solution. The integral equations are easier to study than the original system of PDEs and make it possible to study the model numerically. The solutions of the integral equations are functions of one variable only, whereas the solutions of the original system of PDEs are functions of two variables. This fact makes the solutions of the integral equations easier to visualise and it is the set of integral equations that will be the main focus of this project.

1.2 Aim

The aim of the project is threefold:

I. To construct an efficient and accurate implementation of the integral equation representation of the model in MATLAB.

II. To investigate the qualitative behaviour of the system numerically for a wide range of choices of the initial data, the cumulative distribution function, the crowding function and the input function. The existence of cancer stem cells is investigated by examining qualitative differences (e.g. growth properties or boundedness of the solution) in the cases with or without an input function different from zero.

III. To analytically investigate both the impact of the input function and the growth properties of the solution in general.

1.3 Disposition

After the introductory chapter, (2), describing the model in-depth, the report is divided into three main parts: in the chapter *Numerical Methods*, (3), the numerical machinery of the implementation of the model is described in detail. In the chapter *Simulations*, (4), tests with various combinations of model components are carried out in order to numerically gain knowledge about the qualitative behaviour of the system and to reproduce results from the article of Maad Sasane. A case study is conducted, where it is assumed that almost all cells of a cancer tumour have been successfully eliminated by some medical treatment. We investigate under what conditions the imagined tumour will be kept zero-sized and for what conditions the tumour will relapse. In the following chapter, *Qualitative Behaviour*, (5), the properties of the solutions are investigated analytically and we make estimates of the long–term upper bound for the number density of dividing cells at time t. Finally, in the chapter *Investigation of Numerical Error*, (6), a careful error analysis is performed for the MATLAB implementation, where the order of accuracy of the implemented methods used to solve the system of integral equations is validated and analytical expressions for the numerical error are presented.

2 Model Description

The components of the model are next introduced in more detail, leading up to the system of PDEs describing the amount of cells in Phase 1 and Phase 2. In an example, the system is solved for a specific, simple choice of functions. In Section 2.2, the equivalent system of integral equations, which will be the main focus of this project, is presented. For a proof of the equivalence of the two representations of the model however, the reader is referred to [10].

2.1 PDE Representation

The cells in Phase 1 and Phase 2 are described by their number densities (number of cells per age unit) $n_1(t,\tau)$ and $n_2(t,\tau)$ at age τ and time t. Let $T > 0$ be the total time for which the model is investigated and t a specific time in the interval $[0,T]$. The lengths of Phase 1 and 2 are denoted T_1 and T_2 respectively and represent the maximum time a cell can spend in each of the phases. It is throughout this project assumed that $T_1 > T_2$ (This is not the case for all human cancer cells, but is taken as a reasonable assumption based on experimental values from a so called hybridoma cell line in [5]).

Any change of n_i can for both phases be described as the directional derivative in the $(1,1)$ direction,

$$Dn_i(t,\tau) = \lim_{\epsilon\to 0} \frac{n_i(t+\epsilon,\tau+\epsilon) - n_i(t,\tau)}{\epsilon}. \tag{2.1}$$

Remark. The number densities are not necessarily continuous functions, which means that it is not always possible to replace Dn_i with the sum of partial derivatives $\frac{\partial n_i}{\partial t} + \frac{\partial n_i}{\partial \tau}$. When the directional derivative is used, n_i will be continuous and differentiable along lines parallel to $(1,1)$.

Cells grow older at the same pace as time passes, which means that a cell of age τ at time t is of age $\tau+\Delta\tau$ at time $t+\Delta\tau$. Cells from Phase 1 are assumed to enter Phase 2 according to a transition rate h, defined as the rate of transition in the infinitesimal age span $[\tau,\tau+\Delta\tau]$ per time unit. We remark that transition to Phase 2 is the only way a cell can leave Phase 1. Cells that have not transferred from Phase 1 to Phase 2 in the interval $[0,T_1]$ are assumed to die and do not have an impact on the future system. We define by $N_1(t,\tau)$ the number of cells in Phase 1 at time t in the age span $[0,\tau]$, such that

$$N_1(t,\tau) = \int_0^\tau n_1(t,\sigma)\,\mathrm{d}\sigma \tag{2.2}$$

and $n_1(t,\tau) = \frac{\partial N_1}{\partial \tau}(t,\tau)$. Thus, $N_1(t,\tau+\Delta\tau) - N_1(t,\tau)$ denotes the number of cells in Phase 1 at time t in the age span $[\tau,\tau+\Delta\tau]$. The difference in the number of cells between time t and $t+\epsilon$ can therefore be expressed as

$$N_1(t+\epsilon,\tau+\Delta\tau+\epsilon) - N_1(t+\epsilon,\tau+\epsilon) - (N_1(t,\tau+\Delta\tau) - N_1(t,\tau)) \approx -h(\tau)\left(N_1(t,\tau+\Delta\tau) - N_1(t,\tau)\right)\epsilon, \tag{2.3}$$

assuming that ϵ is small. Dividing both sides with $\Delta\tau$ and computing the limit as $\Delta\tau \to 0$, (2.3) can be rewritten as

$$n_1(t+\epsilon,\tau+\epsilon) - n_1(t,\tau) \approx -h(\tau)n_1(t,\tau)\epsilon. \tag{2.4}$$

Taking the limit as $\epsilon \to 0$ yields

$$Dn_1(t,\tau) = -h(\tau)n_1(t,\tau). \tag{2.5}$$

Definition 1. *The cumulative distribution function $F(\tau)$ is a function representing the proportion of the total number of cells that leave Phase 1 and enter Phase 2 in the age span $[0,\tau]$, having the properties that*

i. *$F(T_1) < 1$, (not all cells reach the end of Phase 1),*

ii. *$F(\tau) = 1$ for $\tau > T_1$, (remaining cells die and disappear and all existing cells have transferred after $\tau = T_1$),*

iii. *F is continuous on $[0, T_1]$,*

iv. *$F(0) = 0$ (no cells have left Phase 1 for Phase 2 at $\tau = 0$),*

v. *F is nondecreasing.*

Despite the name of the *cumulative distribution function*, we again stress that the model is deterministic. It is more convenient to work with $F(\tau)$ than the transition rate $h(\tau)$ and the expression in (2.5) (the PDE for Phase 1) will therefore be rewritten in terms of $F(\tau)$.

As $F(\tau)$ denotes a cumulative distribution function, $F'(\tau)$ can be identified as something similar to a probability density function. In this way, $F'(\tau)\Delta\tau$ describes the fraction of the original number of cells leaving Phase 1 and entering Phase 2 in the small age span $[\tau, \tau + \Delta\tau]$ (given that all cells are still available for a transition to Phase 2). The notion of cumulative distribution function also justifies that $1 - F(\tau)$ is the fraction of cells that has not yet transferred from Phase 1 to Phase 2 at age τ. Thus,

$$\frac{F'(\tau)\Delta\tau}{1 - F(\tau)} \tag{2.6}$$

denotes the fraction of cells transferring from Phase 1 to Phase 2 in the age span $[\tau, \tau + \Delta\tau]$, that have not already done so, see Figure 2.1. This amount of cells can also be described in terms of the transition rate $h(\tau)$, as the rate cells are leaving Phase 1 to Phase 2 times an age span $[\tau, \tau + \Delta\tau]$, i.e. $h(\tau)\Delta\tau$. Comparing $h(\tau)\Delta\tau$ with (2.6) for an infinitesimal age span $\Delta\tau \to 0$, it is now possible to conclude that the transition rate $h(\tau)$ and the cumulative distribution function $F(\tau)$ are related through

$$h(\tau) = \frac{F'(\tau)}{1 - F(\tau)}. \tag{2.7}$$

For the sake of completeness, identifying that

$$\frac{\mathrm{d}}{\mathrm{d}\tau}\left(\log(1 - F(\tau))\right) = -\frac{F'(\tau)}{1 - F(\tau)} \tag{2.8}$$

makes it possible to rewrite $F(\tau)$ in terms of $h(\tau)$ as

$$\begin{aligned} &\frac{\mathrm{d}}{\mathrm{d}\tau}\left(\log(1 - F(\tau))\right) = -h(\tau) \\ \Leftrightarrow\ &\log(1 - F(\tau)) = -\int_0^\tau h(s)\,\mathrm{d}s \\ \Leftrightarrow\ &1 - F(\tau) = \exp\left(-\int_0^\tau h(s)\,\mathrm{d}s\right) \\ \Leftrightarrow\ &F(\tau) = 1 - \exp\left(-\int_0^\tau h(s)\,\mathrm{d}s\right). \end{aligned} \tag{2.9}$$

The PDE in (2.5) can now be rewritten in terms of $F(\tau)$ as

$$Dn_1 = -\frac{F'(\tau)}{1 - F(\tau)} n_1(t, \tau), \quad t \in (0, T), \tau \in (0, T_1). \tag{2.10}$$

In Phase 2, which has fixed length, nothing happens to the cells within the phase that we take into account in this model; the cells cannot leave the phase before the end of the phase and similarly as for Phase 1 the cells grow older at the same pace as time passes. We will see that the number density

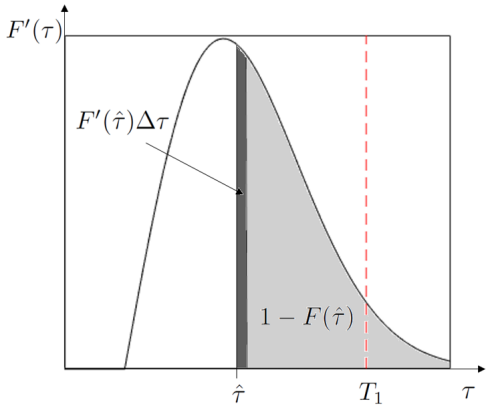

Figure 2.1: The proportion of cells transferring from Phase 1 to Phase 2 in the small age span $[\hat{\tau}, \hat{\tau} + \Delta\tau]$ is given by $\frac{F'(\hat{\tau})\Delta\tau}{1-F(\hat{\tau})}$. The dotted line marks $\tau = T_1$, above which all remaining cells that have not transferred from Phase 1 to Phase 2 are assumed to die.

of cells are described by a transport equation: In correspondence to the derivation of the equation for Phase 1, we define the number of cells in Phase 2 at time t in the age span $[0, \tau]$ by $N_2(t, \tau)$, such that

$$N_2(t, \tau) = \int_0^\tau n_2(t, \sigma)\, \mathrm{d}\sigma \tag{2.11}$$

and $n_2(t, \tau) = \frac{\partial N_2}{\partial \tau}(t, \tau)$. Consequently, $N_2(t, \tau + \Delta\tau) - N_2(t, \tau)$ denotes the number of cells existing at time t in the age span $[\tau, \tau + \Delta\tau]$. Given that there is the same number of cells in Phase 2 at time t and at time $t + \epsilon$ we have

$$N_2(t + \epsilon, \tau + \Delta\tau + \epsilon) - N_2(t + \epsilon, \tau + \epsilon) = N_2(t, \tau + \Delta\tau) - N_2(t, \tau). \tag{2.12}$$

Dividing by $\Delta\tau$ and taking the limit as $\Delta\tau \to 0$ yields $n_2(t + \epsilon, \tau + \epsilon) = n_2(t, \tau)$, i.e.

$$Dn_2 = 0, \quad t \in (0, T), \tau \in (0, T_2). \tag{2.13}$$

Equation (2.13) is recognised as the transport equation.

We have now derived the PDEs for both Phase 1 and Phase 2. It remains to describe the initial and boundary conditions. The initial conditions are less involved and are given by some initial age distributions φ_1 and φ_2 in the two phases such that $n_i(0, \tau) = \varphi_i(\tau)$. The initial age distributions are piecewise continuous functions with the properties that $\varphi_1 : (0, T_1) \to [0, \infty)$ and $\varphi_2 : (0, T_2) \to [0, \infty)$.

The number of dividing cells after Phase 2 at time t is determined as a proportion of the total number of cells p at the same time t by a crowding function $f(p)$.

Definition 2. *The crowding function f is a locally Lipschitz continuous function such that $f : [0, \infty) \to [0, 1]$.*

Remark. *The Lipschitz continuity of the crowding function is for theoretical purposes, making it possible to prove existence and uniqueness properties for the system – proofs which however go beyond the scope of this thesis but are found in [10]. For instance, all functions being C^1 are locally Lipschitz continuous.*

The role of the crowding function is to adjust the behaviour of the system when the state of the system is biologically sub-optimal in some sense. This includes two important cases: cells are less likely to divide either due to space limitations if there are too many cells in the system (a phenomenon that we call *crowding*) or, if the total number of cells are too few (a phenomenon called *quorum sensing*).

In a system where crowding is taken into account, fast growing cells, such as cancer cells, might grow too fast for blood vessels to develop, whose role is to provide the cells with necessary nutrients to grow and duplicate. In addition, it seems realistic that a group of cells never can grow exponentially without restrictions. A consequence is that cells might die in a system with a large population.

According to the theory of quorum sensing, for instance discussed in [9], cells in a cancer tumour might be able to signal to each other similarly as bacteria do to other bacteria. When there are few cells in a system, it might in this way be possible for cells to send signals affecting the gene expression of surrounding cells. The effect can be decreased growth, a prohibited cell division and even cell death, which results in a decrease in the number of cells and possibly to the extinction of a cancer tumour.

In the implementation of the model, it is assumed that none, one or two of these phenomena occur. Crowding corresponds to a crowding function $f(p)$ such that $f(p) \to 0$ as $p \to \infty$, whereas for quorum sensing $f(p) \to 0$ as $p \to 0$, all in accordance with [10]. A constant crowding function corresponds to neither crowding nor quorum sensing and will be used in some of the simulations of this thesis.

Before the boundary condition for Phase 1 can be described, we must introduce notation for the number of cells in the system. Let $P(t)$ denote the total number of cells at time t such that

$$P(t) = \int_0^{T_1} n_1(t,\tau)\,\mathrm{d}\tau + \int_0^{T_2} n_2(t,\tau)\,\mathrm{d}\tau. \tag{2.14}$$

The number of cells that in the end of Phase 2 undergoes mitosis at time t is described by $M(t)$ and is now given by

$$M(t) = f(P(t))n_2(t,T_2). \tag{2.15}$$

To be precise, $M(t)$ denotes the number density of cells (number of cells per age unit) before cell division at time t. The cells that do not undergo mitosis are assumed to die at the end of Phase 2. After mitosis, $2M(t)$ cells per age unit enter Phase 1 of the next cycle along with cells expressed by the input function $\psi(t)$, for instance representing daughter cells from cancer stem cells. That is, the boundary condition at $\tau = 0$ for the number density of Phase 1, n_1, can be written as $n_1(t,0) = 2M(t) + \psi(t)$.

The input function is non-negative, piecewise continuous and has the unit of number of cells per age unit at $\tau = 0$. If $\psi = 0$, it is assumed that cancer stem cells do not exist at all. Regardless of their existence, the proportion of cancer stem cells is assumed to be small and does not affect the crowding of the system. In other words, the cancer stem cells never compete for room with the normal cancer cells. However, the daughter cells – cells represented by ψ – can form a large part of the total number of cells. In the simulations of this thesis we will assume that the number density of daughter cells ψ is constant and compare the cases $\psi = 0$ and $\psi > 0$.

The boundary condition for n_2 at $\tau = 0$ represents the cells that transfer from Phase 1 to Phase 2 at time t. This quantity is obtained by integrating the transition rate, $\frac{F'(\tau)}{1-F(\tau)}$, times the number density in Phase 1, $n_1(t,\tau)$, for all ages. Collected, the boundary conditions for n_1 and n_2 at $\tau = 0$ are given by

$$\begin{aligned} n_1(t,0) &= 2M(t) + \psi(t), \\ n_2(t,0) &= \int_0^{T_1} \frac{F'(\tau)}{1-F(\tau)} n_1(t,\tau)\,\mathrm{d}\tau. \end{aligned} \tag{2.16}$$

We note that the set of PDEs is linear. However, if f is nonconstant, the system of PDEs together with the initial and boundary data is nonlinear.

After this explanation of the components of the PDEs along with initial and boundary data, it is now possible to visualise in a flowchart how cells transfer from Phase 1 to Phase 2 to Phase 1 of the next cycle of the model, see Figure 2.2.

The system can be solved using the method of characteristics, which uses the idea that a first order PDE, which is what we have here, can be rewritten as a system of ODEs. The ODEs are solved along

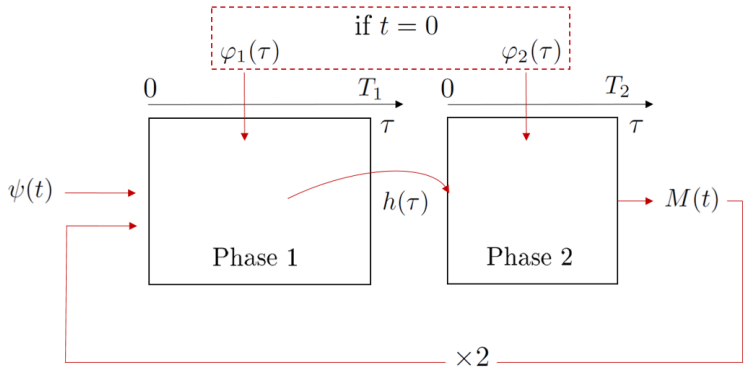

Figure 2.2: Flow chart of the model. Cells transfer from Phase 1 to Phase 2 according to a transition rate $h(\tau)$. The number of cells that undergoes mitosis (per age unit) is represented by $M(t)$ so that $2M(t) + \psi(t)$ cells enter Phase 1 of the next cycle of the model.

so called characteristics, which in this case are lines in the (t, τ)-plane parallel to the vector $(1, 1)$. An example of how this is done is demonstrated in Example 2.1.

Example 2.1. We let the cumulative distribution function take the form of a translated exponential distribution, i.e.

$$F(\tau) = \begin{cases} 1 - e^{-\left(\frac{\tau - c}{a}\right)}, & \text{if } \tau > c, \\ 0, & \text{otherwise.} \end{cases} \tag{2.17}$$

With this choice of cumulative distribution function, the expression for the transition rate $h(\tau)$ becomes particularly easy: $h(\tau) = 1/a$. In addition, we assume that the crowding function f is constant, $f = 1$, that the input function ψ is constant and that the initial age distributions φ_1 and φ_2 are arbitrary. For this choice of f, the expression for $M(t)$ can be simplified to $M(t) = n_2(t, T_2)$. The system of PDEs can be written as

$$\begin{cases} Dn_1 = -h(\tau)n_1(t,\tau), & t \in (0,T), \tau \in (0,T_1), \\ Dn_2 = 0, & t \in (0,T), \tau \in (0,T_2), \\ n_{1,2}(0,\tau) = \varphi_{1,2}(\tau), & \tau \in (0,T_{1,2}), \\ n_1(t,0) = 2n_2(t,T_2) + \psi(t), & t \in [0,T], \\ n_2(t,0) = \displaystyle\int_0^{T_1} \frac{F'(\tau)}{1-F(\tau)} n_1(t,\tau)\,\mathrm{d}\tau = \int_0^{T_1} \frac{1}{a} n_1(t,\tau)\,\mathrm{d}\tau, & t \in [0,T], \end{cases} \tag{2.18}$$

which we solve using the method of characteristics.

We start by looking at the equations for n_1. From the PDEs in (2.18), the ODEs for the characteristics for n_1 are given by

$$\begin{cases} \dfrac{\mathrm{d}t}{\mathrm{d}s} = 1, & t(0) = 0, & \\ \dfrac{\mathrm{d}\tau}{\mathrm{d}s} = 1, & \tau(0) = \tau_0, & \text{if } t \leq \tau, \\ \dfrac{\mathrm{d}n_1}{\mathrm{d}s} = -h(\tau(s))n_1(s), & n_1(0) = \varphi_1(\tau_0), & \end{cases} \\ \begin{cases} \dfrac{\mathrm{d}t}{\mathrm{d}s} = 1, & t(0) = t_0, & \\ \dfrac{\mathrm{d}\tau}{\mathrm{d}s} = 1, & \tau(0) = 0, & \text{if } t > \tau. \\ \dfrac{\mathrm{d}n_1}{\mathrm{d}s} = -h(\tau(s))n_1(s), & n_1(0) = 2M(t_0) + \psi, & \end{cases} \tag{2.19}$$

Using the technique of integrating factor, the two systems in (2.19) yields

$$n_1(t,\tau) = \begin{cases} \left(\dfrac{1-F(\tau)}{1-F(\tau-t)}\right)\varphi_1(\tau-t) = \exp(-t/a)\varphi_1(\tau-t), & \text{if } t \leq \tau, \\ \left(2M(t-\tau)+\psi\right)\left(1-F(\tau)\right) = \left(2n_2(t-\tau,T_2)+\psi\right)\left(1-F(\tau)\right), & \text{if } t > \tau, \end{cases} \tag{2.20}$$

where we in both expressions have used that $\exp(-\int_0^\tau h(\sigma)\,\mathrm{d}\sigma) = (1-F(\tau))$. We note that the solution for $t < \tau$ is given directly by φ_1, whereas the solution for $t > \tau$ depend on the solution for n_2. The characteristics along which a solution for n_2 can be found, are similarly given by

$$\begin{cases} \dfrac{\mathrm{d}t}{\mathrm{d}s} = 1, & t(0) = 0, & \\ \dfrac{\mathrm{d}\tau}{\mathrm{d}s} = 1, & \tau(0) = \tau_0, & \text{if } t \leq \tau, \\ \dfrac{\mathrm{d}n_2}{\mathrm{d}s} = 0, & n_2(0) = \varphi_2(\tau_0), & \end{cases} \\ \begin{cases} \dfrac{\mathrm{d}t}{\mathrm{d}s} = 1, & t(0) = t_0, & \\ \dfrac{\mathrm{d}\tau}{\mathrm{d}s} = 1, & \tau(0) = 0, & \text{if } t > \tau. \\ \dfrac{\mathrm{d}n_2}{\mathrm{d}s} = 0, & n_2(0) = \displaystyle\int_0^{T_1} \frac{1}{a} n_1(t,\tau)\,\mathrm{d}\tau, & \end{cases} \tag{2.21}$$

The system in (2.21) has the solution

$$n_2(t,\tau) = \begin{cases} n_2(0,\tau-t), & \text{if } t \leq \tau, \\ n_2(t-\tau,0), & \text{if } t > \tau. \end{cases} \tag{2.22}$$

We already here remark that the solution for n_2 for $t > \tau$ will always be dependent on n_1 and that the solution for n_1 for $t > \tau$ will be dependent on n_2: We identify that

$$n_2(t,\tau) = \varphi_2(\tau-t), \quad \text{if } t \leq \tau, \tag{2.23}$$

which now can be used to refine the expression for $n_1(t,\tau)$ for $t > \tau$, presented in (2.20):

$$n_1(t,\tau) = \left(2n_2(t-\tau,T_2)+\psi\right)\left(1-F(\tau)\right) = \left(2\varphi_2(T_2-t+\tau)+\psi\right)\left(1-F(\tau)\right). \tag{2.24}$$

The expression in (2.24) is valid for $\tau < t < \tau + T_2$, as φ_2 is defined on the interval $[0, T_2]$. In turn, using (2.24), the equation for $n_2(t,\tau)$ for $t > \tau$ (for $t < T_2$) can now be solved using the boundary condition:

$$\begin{aligned} n_2(t,0) &= \int_0^{T_1} \frac{F'(\tau)}{1-F(\tau)} n_1(t,\tau)\,\mathrm{d}\tau = \int_0^{T_1} \frac{1}{a} n_1(t,\tau)\,\mathrm{d}\tau = \\ &= \int_0^{t} F'(\tau)(2\varphi_2(T_2 - t + \tau) + \psi)\,\mathrm{d}\tau + \int_t^{T_1} \frac{e^{-t/a}}{a}\varphi_1(\tau - t)\,\mathrm{d}\tau, \end{aligned} \tag{2.25}$$

where we in the last equality have used the previously calculated solutions for n_1, both for $t \leq \tau$ and $t > \tau$. Thus,

$$n_2(t-\tau,0) = \int_0^{t-\tau} F'(\tau)(2\varphi_2(T_2 - t + \tau + \sigma) + \psi)\,\mathrm{d}\sigma + \int_t^{T_1} \frac{e^{-t+\tau/a}}{a}\varphi_1(\sigma - t + \tau)\,\mathrm{d}\sigma. \tag{2.26}$$

This solution can be used to compute n_1 on the next interval, by again using the expression in (2.20) valid for $t \geq \tau$,

$$n_1(t,\tau) = (2n_2(t-\tau), T_2) + \psi)\,(1 - F(\tau)). \tag{2.27}$$

In this way, we can continue to compute $n_1(t,\tau)$ and $n_2(t,\tau)$ one interval at the time by finding a solution to one of the equations using the other, up to any final time T we find suitable. For an illustration of the calculations in this example see Figure 2.3. In comparison to the previous flowchart in Figure 2.2, the time dimension is more carefully demonstrated and it is visualised how the solution of the system of PDEs propagate along characteristics.

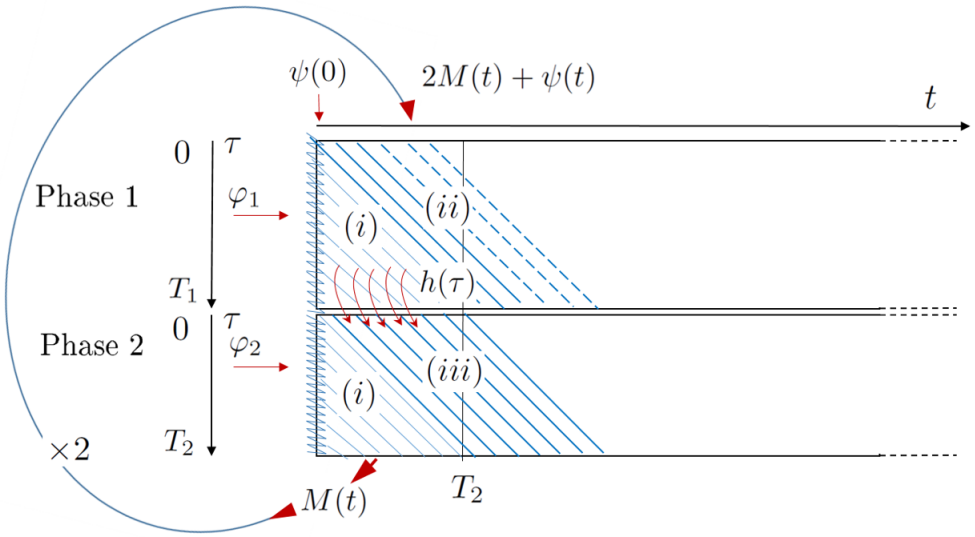

Figure 2.3: Alternative flowchart of the model. The solutions of the system of PDEs propagate along characteristics. The system has to be solved one interval at the time as the solution for n_1 is dependent on the solution for n_2 and vice versa: in region (i), $n_1(t,\tau)$ and $n_2(t,\tau)$ are computed for $t < \tau$ using φ_1 and φ_2, in (ii), $n_1(t,\tau)$ is computed for $\tau < t < \tau + T_2$, using the previously calculated n_2 and in (iii), $n_2(t,\tau)$ is computed using the already computed $n_1(t,\tau)$.

2.2 Integral Equations

The set of PDEs,

$$\begin{cases} Dn_1 = -\dfrac{F'(\tau)}{1-F(\tau)} n_1(t,\tau), & t \in (0,T), \tau \in (0,T_1), \\ Dn_2 = 0, & t \in (0,T), \tau \in (0,T_2), \\ n_{1,2}(0,\tau) = \varphi_{1,2}(\tau), & \tau \in (0,T_{1,2}), \\ n_1(t,0) = 2M(t) + \psi(t), & t \in [0,T], \\ n_2(t,0) = \displaystyle\int_0^{T_1} \frac{F'(\tau)}{1-F(\tau)} n_1(t,\tau)\,\mathrm{d}\tau, & t \in [0,T], \end{cases} \tag{2.28}$$

can be rewritten as an equivalent system of integral equations for $M(t)$ and $P(t)$, presented in Theorem 1 of [10]. It is also proved, in Theorem 2 of [10], that a unique solution of the system of integral equations exists. Therefore, the equivalence of the two representations means that a given solution to either of the representations assures the existence of a unique solution to the other.

Definition 3. *The pair of non-negative functions (n_1, n_2), such that $n_1 : [0,T] \times [0,T_1] \to \mathbb{R}$ and $n_2 : [0,T] \times [0,T_2] \to \mathbb{R}$, is a solution of the system of PDEs in (2.28) up to time t if*

- ***i.*** *The directional derivatives Dn_1 and Dn_2 exist on $[0,T] \times [0,T_1]$ and $[0,T] \times [0,T_2]$ respectively.*
- ***ii.*** *The number densities n_1 and n_2 are absolutely integrable in their second argument on $[0,T_{1,2}]$, i.e. $n_{1,2}(t,\cdot) \in L^1([0,T_{1,2}])$.*
- ***iii.*** *The function $P(t) = \int_0^{T_1} n_1(t,\tau)\,\mathrm{d}\tau + \int_0^{T_2} n_2(t,\tau)\,\mathrm{d}\tau$, $P : [0,T] \to [0,\infty)$, is continuous.*

The relation between the two representations can now be presented as follows, here given without a proof:

Theorem 2.1. *Let (n_1, n_2) be a solution of the system of PDEs in (2.28) up to time t, let the lengths of the phases be such that $T_1 > T_2$ and let the initial data φ_1 and φ_2 be piecewise continuous functions such that $\varphi_1 : (0,T_1) \to [0,\infty)$ and $\varphi_2 : (0,T_2) \to [0,\infty)$. Then the number density of the dividing cells at the end of Phase 2, $M(t)$ defined by $M(t) = f(P(t))n_2(t,T_2)$, and the total number of cells at time t, $P(t)$ defined by $P(t) = \int_0^{T_1} n_1(t,\tau)\,\mathrm{d}\tau + \int_0^{T_2} n_2(t,\tau)\,\mathrm{d}\tau$, satisfy the system of integral equations:*

$$\begin{cases} M(t) = f(P(t)) \left(\displaystyle\int_0^t K(t,\sigma)(2M(\sigma) + \psi(\sigma))\,\mathrm{d}\sigma + \int_0^{T_1} R(t,\sigma)\varphi_1(\sigma)\,\mathrm{d}\sigma + \varphi_2(T_2 - t) \right), \\ P(t) = \displaystyle\int_0^t L(t,\sigma)(2M(\sigma) + \psi(\sigma))\,\mathrm{d}\sigma + \int_0^{T_1} S_1(t,\sigma)\varphi_1(\sigma)\,\mathrm{d}\sigma + \int_0^{T_2} S_2(t,\sigma)\varphi_2(\sigma)\,\mathrm{d}\sigma, \end{cases} \tag{2.29}$$

where the functions K and R are given by

$$K : [0,\infty) \times [0,\infty) \to \mathbb{R}, \quad K(t,\sigma) = \begin{cases} F'(t - T_2 - \sigma), & \text{if } T_2 \le t - \sigma < T_1 + T_2, \\ 0, & \text{otherwise,} \end{cases}$$

$$R : [0,\infty) \times [0,T_1] \to \mathbb{R}, \quad R(t,\sigma) = \begin{cases} \dfrac{F'(\sigma + t - T_2)}{1 - F(\sigma)}, & \text{if } t \ge T_2 \text{ and } 0 \le \sigma < T_1 + T_2 - t, \\ 0, & \text{otherwise.} \end{cases} \tag{2.30}$$

and the functions L, S_1 and S_2 are defined by

$$
\begin{aligned}
L : \mathbb{R}_+ \times \mathbb{R}_+ \to \mathbb{R}, \quad L(t,\sigma) &= \begin{cases} 1, & \text{if } 0 \le t-\sigma < T_2, \\ 1-F(t-T_2-\sigma), & \text{if } T_2 \le t-\sigma < T_1, \\ F(T_1)-F(t-T_2-\sigma), & \text{if } T_1 \le t-\sigma < T_1+T_2, \\ 0, & \text{otherwise,} \end{cases} \\
S_1 : [0,\infty) \times [0,T_1] \to \mathbb{R}, \quad S_1(t,\sigma) &= \begin{cases} 1, & \text{if } t < \min(T_2, T_1-\sigma), \\ \dfrac{F(T_1)-F(\sigma)}{1-F(\sigma)}, & \text{if } T_1-\sigma < t \le T_2 \\ \dfrac{1-F(\sigma+t-T_2)}{1-F(\sigma)}, & \text{if } T_2 \le t < T_1-\sigma \\ \dfrac{F(T_1)-F(\sigma+t-T_2)}{1-F(\sigma)}, & \text{if } \max(T_2, T_1-\sigma) \le t < T_1+T_2-\sigma, \\ 0, & \text{otherwise,} \end{cases} \\
S_2 : [0,\infty) \times [0,T_2] \to \mathbb{R}, \quad S_2(t,\sigma) &= \begin{cases} 1, & \text{if } \sigma+t \le T_2 \\ 0, & \text{otherwise.} \end{cases}
\end{aligned}
\tag{2.31}
$$

Here, $M \in C_p([0,T];[0,\infty)) \cap C([T_2,T];[0,\infty))$ and $P \in C([0,T];[0,\infty))$, where C_p denotes the set of piecewise continuous functions. We remind that the functions φ_i and ψ satisfy $\varphi_1 : (0,T_1) \to [0,\infty)$, $\varphi_2 : (0,T_2) \to [0,\infty)$ and $\psi : [0,T] \to [0,\infty)$ and are all piecewise continuous.

We note that when f is a constant function, the integral equation for $M(t)$ is a so called Volterra equation of the second kind. To get a better grasp on the discontinuities in the integral kernels $K(t,\tau)$ and $L(t,\tau)$, these are illustrated in Figure 2.4 and, for the same purpose, the discontinuities for the functions $S_1(t,\tau)$, $S_2(t,\tau)$ and $R(t,\tau)$ are illustrated in Figure 2.5.

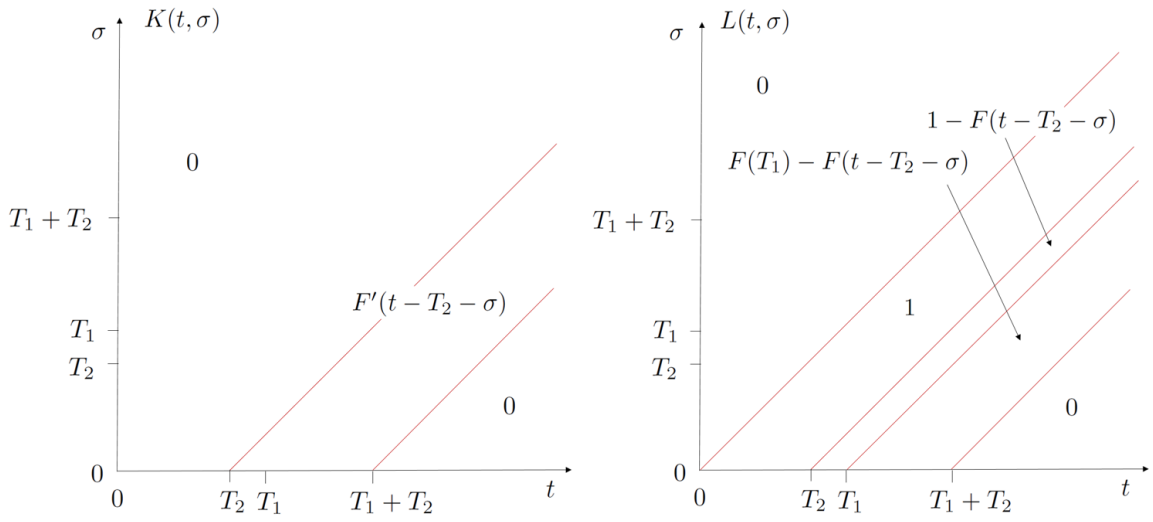

Figure 2.4: Illustration of the discontinuities in the kernels $K(t,\sigma)$ and $L(t,\sigma)$.

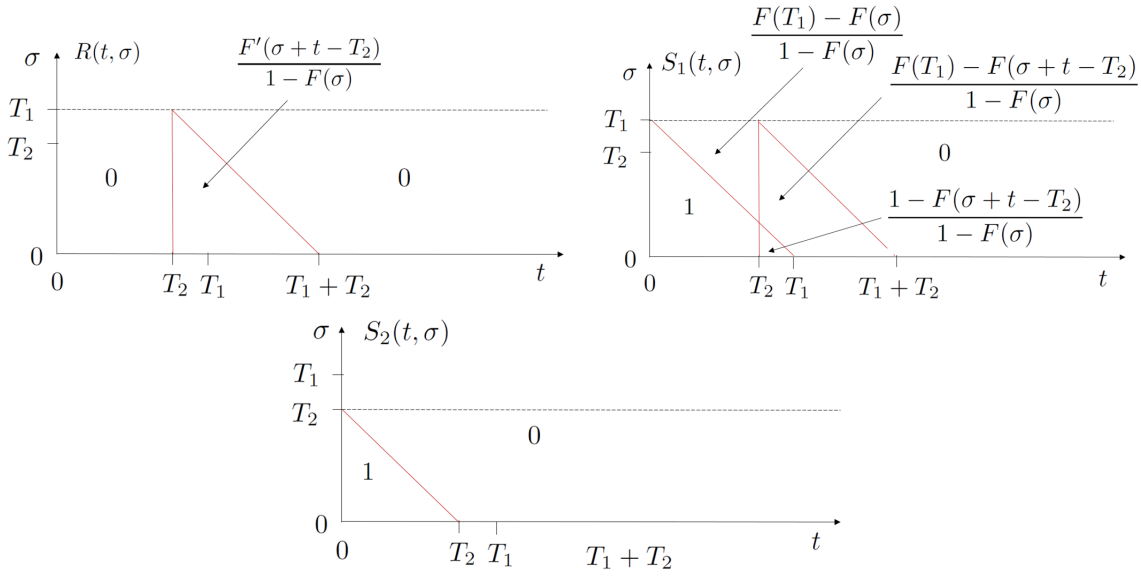

Figure 2.5: Illustration of the discontinuities in $R(t,\sigma)$, $S_1(t,\sigma)$ and $S_2(t,\sigma)$.

3 Numerical Methods

The integral equations for $M(t)$ and $P(t)$ are solved in steps. As the solution of every step is dependent on the previous, it is convenient to compute $M(t)$ and $P(t)$ at equidistant points. The step size h is defined as $h = t/n$, where t is the total time of integration and $n + 1$ is the number of points in the discretization grid on the interval $[0, t]$. The system is solved using three different integration methods: the left point rectangle rule, the trapezoidal rule and Simpson's 1/3rd rule, with an extra step of Simpson's 3/8 rule when n is odd, aiming at yielding first, second and fourth order accuracy respectively. The reason for not implementing Simpson's rule only – the theoretically most accurate method – is both to understand the numerical characteristics of the equations thoroughly and the fact that Simpson's rule turns out to be an inferior choice in the case with a nonconstant crowding function, something that will be discussed in detail in Section 3.5.

In the first section, the left point rectangle rule is mentioned briefly. The choice of discretization grid, which is of great importance in the implementation of the trapezoidal and Simpson's rules, is discussed in the second section, 3.2. In Sections 3.3 and 3.4, it is demonstrated how the equations for $M(t)$ and $P(t)$ are solved using the trapezoidal rule and using Simpson's rule, keeping the crowding function f constant. In the end of the chapter on numerical methods, 3.5, a nonconstant crowding function f is considered in the numerical scheme, yielding a nonlinear equation that must be solved in every step. The order of accuracy and numerical error of the implementations are described in Chapter 6.

Before describing the implementations, we introduce for convenience the notation $A(t)$ for the rightmost term in $M(t)$,

$$A(t) = \int_0^{T_1} R(t, \sigma)\varphi_1(\sigma)\,\mathrm{d}\sigma + \varphi_2(T_2 - t), \tag{3.1}$$

and $B(t)$ for the rightmost term in $P(t)$:

$$B(t) = \int_0^{T_1} S_1(t, \sigma)\varphi_1(\sigma)\,\mathrm{d}\sigma + \int_0^{T_2} S_2(t, \sigma)\varphi_2(\sigma)\,\mathrm{d}\sigma. \tag{3.2}$$

The integrals in $A(t)$ and $B(t)$ are computed using the same integration rule as $M(t)$ and $P(t)$.

——-

3.1 The Left Point Rectangle Rule

In the simulation section in the paper of Maad Sasane [10], the left point rectangle rule was the only implemented method, approximating an integral as

$$\int_a^b g(x)\,\mathrm{d}x \approx \frac{b-a}{n}\sum_{i=0}^{n} g(a + ih). \tag{3.3}$$

Solving the system of integral equations using the left point rectangle rule is a relatively simple task as the system becomes uncoupled, despite the nonlinearity through the crowding function f in the expression

$$M(t) = f(P(t))\left(\int_0^t K(t, \sigma)(2M(\sigma) + \psi(\sigma))\,\mathrm{d}\sigma + \int_0^{T_1} R(t, \sigma)\varphi_1(\sigma)\,\mathrm{d}\sigma + \varphi_2(T_2 - t)\right). \tag{3.4}$$

In other words is it not necessary to know the value of $P(t)$ to compute $M(t)$, which we will see is needed when using Simpson's rule or the trapezoidal rule. However, the drawback is that the method is only first order accurate and we wish to solve the system using a more accurate method. We will therefore hereafter not return to discussions related to the left point rectangle rule.

3.2 Choice of Grid

There are discontinuities in the terms $A(t)$ and $B(t)$ as well as in the kernels, $L(t,\sigma)$ and $K(t,\sigma)$. In order to gain second order accuracy using the trapezoidal rule and fourth order accuracy using Simpson's rule, the grid points must be chosen with great care. By splitting an integral containing a discontinuity into several integrals, each with a continuous integrand, this problem can be handled. The number of steps is chosen so that there is a discretization point exactly in each discontinuity. The first discontinuity occurs in $A(t)$ at the point $t = T_2$, as $\varphi(T_2 - t)$ hereafter is zero, whereas the expression $\int_0^{T_1} R(t,\sigma)\varphi_1(\sigma)\,\mathrm{d}\sigma$ for the first time becomes different from zero. All computations of $M(t)$ and $P(t)$ must therefore be split at this point. For the term related to $S_1(t,\sigma)$ in $B(t)$ there is first a discontinuity at $\sigma = T_2 - t$ for $t \le T_2$ and then also at $\sigma = T_1 + T_2 - t$ for $t \ge T_2$. Finally, for the term related to $S_2(t,\sigma)$ the only discontinuity occurs at $\sigma = T_1 - t$. Again we recall that all discontinuities in $A(t)$ and $B(t)$ are illustrated in Figure 2.5 and that $A(t) = B(t) = 0$ for $t > T_1 + T_2$. It is necessary to keep in mind that the bounds of the integrals in $M(t)$ and $P(t)$ change as t changes. For the discontinuities in the kernels L and K, four different intervals for t are considered, where T is the final point for which we want to compute $M(t)$: $0 < t \le T_2$, $T_2 < t \le T_1$, $T_1 < t \le T_1 + T_2$ and $T_1 + T_2 < t \le T$. Shifts occur at different points:

i. $0 < t \le T_2$:

$$\begin{aligned} K(t,\sigma) &= 0, \quad 0 < \sigma \le t, \\ L(t,\sigma) &= 1, \quad 0 < \sigma \le t, \end{aligned} \tag{3.5}$$

ii. $T_2 < t \le T_1$:

$$\begin{aligned} K &= \begin{cases} F'(t - T_2 - \sigma), & \text{if } 0 < \sigma \le -T_2 + t, \\ 0, & \text{if } -T_2 + t < \sigma \le t, \end{cases} \\ L &= \begin{cases} 1 - F(t - T_2 - \sigma), & \text{if } 0 < \sigma \le -T_2 + t, \\ 1, & \text{if } -T_2 + t < \sigma < t. \end{cases} \end{aligned} \tag{3.6}$$

iii. $T_1 < t \le T_1 + T_2$:

$$\begin{aligned} K &= \begin{cases} F'(t - T_2 - \sigma), & \text{if } 0 < \sigma \le -T_2 + t, \\ 0, & \text{if } -T_2 + t < \sigma \le t, \end{cases} \\ L &= \begin{cases} F(T_1) - F(t - T_2 - \sigma), & \text{if } 0 < \sigma \le -T_1 + t, \\ 1 - F(t - T_2 - \sigma), & \text{if } -T_1 + t < \sigma \le -T_2 + t, \\ 1, & \text{if } -T_2 + t < \sigma < t. \end{cases} \end{aligned} \tag{3.7}$$

iv. $T_1 + T_2 < t \le T$:

$$\begin{aligned} K &= \begin{cases} 0, & \text{if } 0 < \sigma \le -T_1 - T_2 + t, \\ F'(t - T_2 - \sigma), & \text{if } -T_1 - T_2 + t < \sigma \le -T_2 + t, \\ 0, & \text{if } -T_2 + t < \sigma \le t, \end{cases} \\ L &= \begin{cases} 0, & \text{if } 0 < \sigma \le -T_1 - T_2 + t, \\ F(T_1) - F(t - T_2 - \sigma), & \text{if } -T_1 - T_2 + t < \sigma \le -T_1 + t, \\ 1 - F(t - T_2 - \sigma), & \text{if } -T_1 + t < \sigma \le -T_2 + t, \\ 1, & \text{if } -T_2 + t < \sigma < t. \end{cases} \end{aligned} \tag{3.8}$$

It is of course important to notice where T_2 is located in relation to the other three discontinuity points and to split the integrals accordingly. For instance, if $t > T_1 + T_2$ and $-T_1 - T_2 + t < T_2 < -T_1 + t$,

then the integral for $P(t)$ can be rewritten as

$$\begin{aligned} P(t) = &\int_{-T_1-T_2+t}^{T_2} \left(F(T_1) - F(t-T_2-\sigma)\right)\left(2M(\sigma)+\psi(\sigma)\right)\,\mathrm{d}\sigma + \\ &+ \int_{T_2}^{-T_1+t} \left(F(T_1) - F(t-T_2-\sigma)\right)\left(2M(\sigma)+\psi(\sigma)\right)\,\mathrm{d}\sigma + \\ &+ \int_{-T_1+t}^{-T_2+t} \left(1 - F(t-T_2-\sigma)\right)\left(2M(\sigma)+\psi(\sigma)\right)\mathrm{d}\sigma + \\ &+ \int_{-T_2+t}^{t} \left(2M(\sigma)+\psi(\sigma)\right)\,\mathrm{d}\sigma. \end{aligned} \tag{3.9}$$

3.3 The Trapezoidal Rule

The composite trapezoidal rule is a second order method, approximating an integral of the general form $\int_a^b g(x)\,\mathrm{d}x$ as

$$\int_a^b g(x)\,\mathrm{d}x \approx \frac{b-a}{2n}\left[g(a) + 2\left\{\sum_{i=1}^{n-1} g(a+ih)\right\} + g(b)\right], \tag{3.10}$$

where $n+1$ is the number of points on the interval $[a,b]$ (leading to n segments) and $h = (b-a)/n$ is the step size. By denoting the start and end point of the integral in $M(t)$ by t_{start} and t_{end}, where $t_{\text{start}} = \max(0, t-T_1-T_2)$ and $t_{\text{end}} = \max(0, t-T_2)$, the trapezoidal rule can be used to compute $M(t)$ on each of its intervals, assuming that the crowding function f is constant, as

$$\begin{aligned} M(t) = &f\left(\int_{t_{\text{start}}}^{t_{\text{end}}} K(t,\sigma)(2M(\sigma)+\psi(\sigma))\,\mathrm{d}\sigma \approx \frac{h}{2}\Bigg[K(t,t_{\text{start}})(2M(t_{\text{start}})+\psi(t_{\text{start}})) + \right. \\ &+ 2\left\{\sum_{i=1}^{n-1} K(t,t_{\text{start}}+ih)(2M(t_{\text{start}}+ih)+\psi(t_{\text{start}}+ih))\right\} + \\ &\left. + K(t,t_{\text{end}})(2M(t_{\text{end}})+\psi(t_{\text{end}}))\Bigg] + A(t)\right). \end{aligned} \tag{3.11}$$

Here, $n+1$ is the number of points in the discretization of the interval $[t_{\text{start}}, t_{\text{end}}]$. It is noticeable that no point in $M(t)$ has to be computed implicitly as it always holds that $t_{\text{end}} < t$. The equation for $P(t)$ is computed similarly as the one for $M(t)$, with the difference that contributions from integrals on different intervals are added to receive the result. Naturally, all values needed to compute $P(t)$ is for f is constant given directly by the values of $M(t)$. The method is self-starting as we have in the very first step on the first interval that

$$\begin{aligned} M(h) &= f(p)A(h), \\ P(h) &\approx \frac{h}{2}\left[(2M(0)+\psi(0)) + (2M(h)+\psi(h))\right] + B(h), \end{aligned} \tag{3.12}$$

where $M(0) = A(0)$ and $P(0) = B(0)$.

3.4 Simpson's Rule

Using Simpson's 1/3rd rule, which is a fourth order method, an integral of the form $\int_a^b g(x)\,\mathrm{d}x$ is approximated as

$$\int_a^b g(x)\,\mathrm{d}x \approx \frac{h}{3}\left[g(a) + 4g\left(\frac{a+b}{2}\right) + g(b)\right], \tag{3.13}$$

where the step size is $h = (b-a)/2$ and where the function g is assumed to be at least C^3 on $[a,b]$ [3]. Splitting the interval of integration, $[a,b]$, into n multiple segments and using Simpson's rule repeatedly over every two segments, the composite Simpson's rule takes the form of

$$\int_a^b f(x)\,\mathrm{d}x = \frac{b-a}{3n}\left[f(a) + 4\sum_{\substack{i=1\\ i\text{ odd}}}^{n-1} f(a+ih) + 2\sum_{\substack{i=2\\ i\text{ even}}}^{n-2} f(a+ih) + f(b)\right], \tag{3.14}$$

using $n+1$ points and $h = (b-a)/n$. However, this only works well if n is even. When n is odd, the composite Simpson's rule can for instance be used along with an extra step of the trapezoidal rule. For stability, this extra step has to be taken as the last step [4]. An alternative is to use the composite Simpson's rule on the interval $[a, a+hn]$ when n is even and a combination of the composite Simpson's rule on the interval $[a, a+h(n-3)]$ and Simpson's 3/8-rule, a method using four points, on the interval $[a+h(n-3), a+hn]$ when n is odd. Using this last approach, all approximate values are calculated to the same accuracy as both Simpson's 1/3 rule and Simpson's 3/8 rule are fourth order methods [4].

In this section it is still assumed that f is constant so that the system is uncoupled. The expression for the integral in $M(t)$, first corresponding to a time t leading to an even number of segments (n even), is

$$\begin{aligned}
M(t) &= f\left(\int_{t_{\text{start}}}^{t_{\text{end}}} K(t,\sigma)(2M(\sigma)+\psi(\sigma))\,\mathrm{d}\sigma + A(t)\right) \approx \\
&\approx f\Bigg(\frac{h}{3}\Big[K(t,t_{\text{start}})(2M(t_{\text{start}})+\psi(t_{\text{start}})) + \\
&\quad + 4\left\{\sum_{\substack{i=1\\ i\text{ odd}}}^{n-1} K(t,t_{\text{start}}+ih)(2M(t_{\text{start}}+ih)+\psi(t_{\text{start}}+ih))\right\} + \\
&\quad + 2\left\{\sum_{\substack{i=2\\ i\text{ even}}}^{n-2} K(t,t_{\text{start}}+ih)(2M(t_{\text{start}}+ih)+\psi(t_{\text{start}}+ih))\right\} + \\
&\quad + K(t,t_{\text{end}})(2M(t_{\text{end}})+\psi(t_{\text{end}}))\Big]\Bigg).
\end{aligned} \tag{3.15}$$

For n odd there are a few modifications for the same expression: the summation over i odd gets an upper bound of $n-4$, the summation over i even gets an upper bound of $n-5$, the last term has $(t, t_{\text{start}}+h(n-3))$ as its argument and an extra term of

$$\begin{aligned}
&\frac{3h}{8}\Big[K(t,t_{\text{start}}+h(n-3))\,(2M(t_{\text{start}}+h(n-3))+\psi(t_{\text{start}}+h(n-3))) + \\
&+ 3K(t,t_{\text{start}}+h(n-2))(2M(t_{\text{start}}+h(n-2))+\psi(t_{\text{start}}+h(n-2))) + \\
&+ 3K(t,t_{\text{start}}+h(n-1))(2M(t_{\text{start}}+h(n-1))+\psi(t_{\text{start}}+h(n-1))) + \\
&+ K(t,t_{\text{end}})(2M(t_{\text{end}})+\psi(t_{\text{end}}))\Big]
\end{aligned} \tag{3.16}$$

is added to the expression in (3.15). A scheme for calculating $P(t)$ is given similarly, with the difference that terms from different integrals are added to form the final result. In the same manner as with the trapezoidal rule, the method is self-starting, as the values of $M(t)$ up until $t = T_2$ are given directly by $A(t)$ and the values needed to compute $P(t)$ are given by the values of $M(t)$. A fourth order scheme based on Simpson's 1/3rd rule is now ready to be used for the choice of a constant crowding function f.

The described methods approximate the integrand on each segment by a constant, a first degree polynomial or a second degree polynomial, see Figure 3.1 (Simpson's 3/8 rule approximate by a cubic polynomial in the last step for n odd).

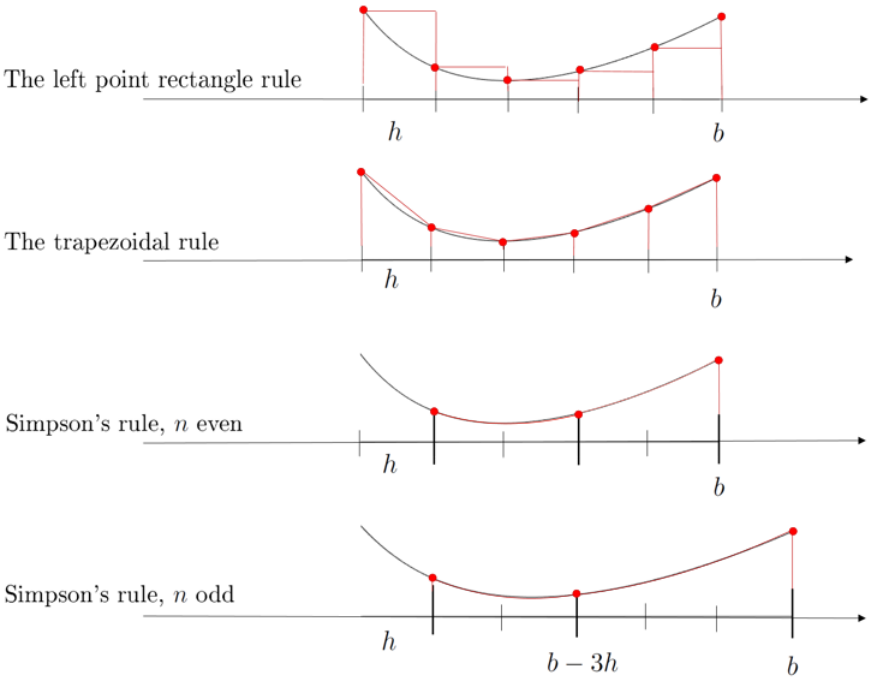

Figure 3.1: Illustration of the three integration methods used (red) to integrate a function (black). Simpson's 1/3rd rule approximates the integrand over every two segments while the left point rectangle rule and the trapezoidal rule approximate the integrand over every segment.

3.5 Impact from Crowding Function

When the crowding function f is nonconstant, the system is coupled and more work is required compared to the linear case. Here, the expression for $P(t)$ is used as argument in f to compute $M(t)$ at every step, as the equations for $M(t)$ and $P(t)$ are linked as

$$\begin{cases} M(t) = f(P(t)) \left(\displaystyle\int_0^t K(t,\sigma)(2M(\sigma) + \psi(\sigma))\,\mathrm{d}\sigma + \int_0^{T_1} R(t,\sigma)\varphi_1(\sigma)\,\mathrm{d}\sigma + \varphi_2(T_2 - t) \right), \\ P(t) = \displaystyle\int_0^t L(t,\sigma)(2M(\sigma) + \psi(\sigma))\,\mathrm{d}\sigma + \int_0^{T_1} S_1(t,\sigma)\varphi_1(\sigma)\,\mathrm{d}\sigma + \int_0^{T_2} S_2(t,\sigma)\varphi_2(\sigma)\,\mathrm{d}\sigma. \end{cases} \tag{3.17}$$

The integrating steps in $P(t)$, i.e. the summation of terms for the trapezoidal or Simpson's rule, up until but not including time t, are now denoted P_{steps} for convenience. The discretized version of the

integral $\int_0^t K(t,\sigma)(2M(\sigma)+\psi(\sigma))\,\mathrm{d}\sigma$ is similarly denoted M_{steps}. We let μ denote the multiple of h that is the factor in front of $(2M(t)+\psi(t))$ in the last step of the discretization of $P(t)$. In general, independently of the choice between our two methods (trapezoidal or Simpson's rule), the expression for $M(t)$,

$$M(t) = f(P(t))\,(M_{\text{steps}} + A(t))\,, \tag{3.18}$$

then takes the form

$$M(t) = f\left(P_{\text{steps}} + \mu(2M(t)+\psi(t)) + B(t)\right)(M_{\text{steps}} + A(t))\,. \tag{3.19}$$

If f is not piecewise linear, (3.19) is a nonlinear equation in $M(t)$. However, this equation can be solved, for instance in MATLAB using the `fzero` command, based on the bisection algorithm. The resulting value for $M(t)$ is subsequently used to compute a solution for $P(t)$, similarly as in the case with a constant f, using the second part of (3.17) and the trapezoidal or Simpson's rule.

The starting step for Simpson's rule becomes a bit more involved than in the case with constant crowding. Simpson's rule uses the values of three points to make an approximation, whereas the trapezoidal rule only needs two points. This fact might cause a problem at the very first step using Simpson's rule, where $M(h)$ and $P(h)$ are to be computed. In the first point at $t = 0$, the solution is straightforward:

$$\begin{aligned} P(0) &= B(0), \\ M(0) &= f(P(0))A(0). \end{aligned} \tag{3.20}$$

However, to get fourth order accuracy at the point $t = h$, the so called Romberg's method must be used, applying the trapezoidal rule for the step sizes h and $h/2$ and combining the expressions of the approximations, as we will demonstrate below. To understand what happens, we introduce the Euler-Maclaurin summation formula, expressing the size of the error for the trapezoidal rule.

Lemma 3.1 (Euler-Maclaurin)**.** *For the trapezoidal rule, the error from the approximation $T(h)$ of the integral*

$$\int_a^b g(x)\,\mathrm{d}x, \tag{3.21}$$

computed using n segments through the approximation formula (3.10)*, is given by the Euler-Maclaurin summation formula:*

$$\begin{aligned} T(h) = \int_a^b g(x)\,\mathrm{d}x + \frac{h^2}{12}[g'(b) - g'(a)] - \frac{h^4}{720}[g'''(b) - g'''(a)] + \frac{h^6}{30240}[g^{(5)}(b) - g^{(5)}(a)] + \\ + \cdots + c_{2r}h^{2r}[g^{(2r-1)}(b) - g^{(2r-1)}(a)] + \mathcal{O}(h^{2r+2}). \end{aligned} \tag{3.22}$$

The generating function for the coefficients c_{2r} is

$$1 + c_2h^2 + c_4h^4 + c_6h^6 + \cdots = \frac{h}{2}\frac{e^h+1}{e^h-1}. \tag{3.23}$$

The Euler-Maclaurin summation formula holds under the assumption that g is sufficiently smooth.

A proof of the lemma is found in [3]. The Euler-Maclaurin summation formula states that the error expansion $E(h)$ for the trapezoidal rule takes the form of $E(h) = C_2h^2 + C_4h^4 + C^6h^6 + \ldots$. For the step size h, $M(h)$ and $P(h)$ are given by

$$\begin{aligned} M(h) &= f(P(h))A(h), \\ P(h) &= B(h) + \frac{h}{2}\left((2M(0)+\psi(0)) + (2M(h)+\psi(h))\right) + C_2h^2 + \mathcal{O}(h^4), \end{aligned} \tag{3.24}$$

where $C_2h^2 + \mathcal{O}(h^4)$ denotes the error. Similarly for the step size $h/2$,

$$
\begin{aligned}
M(h/2) &= f(P(h/2))A(h/2),\\
P(h/2) &= B(h/2) + \frac{h}{4}\left((2M(0) + \psi(0)) + (2M(h/2) + \psi(h/2))\right),\\
M(h) &= f(P(h))A(h),\\
P(h) &= B(h) + \frac{h}{4}\left((2M(0) + \psi(0)) + 2(2M(h/2) + \psi(h/2)) + (2M(h) + \psi(h))\right) + \frac{1}{4}C_2h^2 + \mathcal{O}(h^4).
\end{aligned}
\tag{3.25}
$$

A value of $M(h/2)$ is received by combining the expressions for $M(h/2)$ and $P(h/2)$ in (3.25) and solving for $M(h/2)$. Combining the two expressions for $P(h)$ in (3.24) and (3.25), the error constant C_2 can be eliminated. The simplified expression for $P(h)$ becomes

$$
P(h) = B(h) + \frac{h}{6}(2M(0) + \psi(0)) + \frac{2}{3}h\left[\left(2M\left(\frac{h}{2}\right) + \psi\left(\frac{h}{2}\right)\right)\right] + \frac{h}{6}(2M(h) + \psi(h)), \tag{3.26}
$$

which is recognised as a Simpson approximation of $P(h)$, being of fourth order accuracy. It is now finally possible to compute $M(h)$ to the same accuracy.

In the computations with a nonconstant crowding function f, we find that the discontinuities in the integral equations cause trouble, despite choosing the grid carefully. For the trapezoidal rule, second order accuracy is found to be easily obtained for all $t > 0$ (this result will be validated in Section 6.1). However, Simpson's rule proves to be suboptimal and works properly, yielding fourth order accuracy, only up until $t = T_2$. We will now motivate this behaviour of the Simpson implementation: We let A_- denote $A(t)$ before $t = T_2$ and A_+ denote $A(t)$ after $t = T_2$, i.e.

$$
A(t) = \begin{cases} A_-(t), & t < T_2, \\ A_+(t), & t \geq T_2. \end{cases} \tag{3.27}
$$

An illustration of $A(t)$ is found in Figure 3.2.

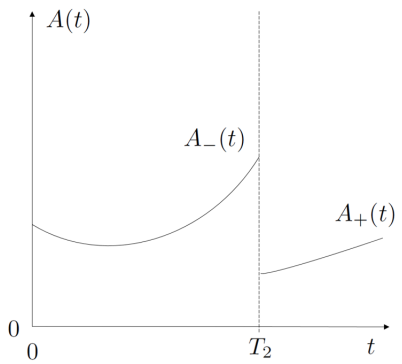

Figure 3.2: Discontinuity in $A(t)$ at T_2.

The discontinuity in $A(t)$ at $t = T_2$ makes it nontrivial to compute $M(T_2)$, as we in P_{steps} must use M for $t < T_2$ based on $A_-(t)$, while $A_+(t)$ is used in the computation of $M(T_2)$:

$$
M(T_2) = f\left(P_{\text{steps}} + \mu(2M(T_2) + \psi(T_2)) + B(T_2)\right)A_+(T_2). \tag{3.28}
$$

An infinite derivative of the type which appears in $M(t)$ at the discontinuity at T_2 creates an error that might be larger than the combined error of all the other steps combined [3]. The integrand is not

C^3, which is demanded if Simpson's rule is to be used in a satisfactory way. The effect of this problem is that it is not possible to obtain fourth order accuracy for Simpson's rule after the point $t = T_2$ with f nonconstant. The scheme based on Simpson's rule performs here no better than the scheme based on the trapezoidal rule. This is contrary to the case with a constant crowding function, where the value of $M(t)$ is given directly by the current value of $A(t)$ and is not dependent on the history of A or of M. The reason is that for f constant, $M(t) = A_-(t)$ for $t \leq T_2$. Then, the mentioned discontinuity causes no problems as we have introduced a grid with an integration point exactly at $t = T_2$. The integral is split at this particular point into two distinct integrals, where each integrand is sufficiently differentiable.

Due to the discontinuity, simulations where crowding is taken into account (i.e. where f is nonconstant) can only be based on the trapezoidal rule and a smaller step size (compared to when the crowding function is constant and Simpson's rule is applied).

However, there is one way to get around the problem and create an implementation of the model that is as accurate as possible without applying Simpson's rule. This is done by instead using combinations of computations from the trapezoidal rule with varied and smaller step sizes. There is still a chance to receive an error of the same magnitude as we would have expected from Simpson's rule by for instance applying Romberg's method of integration, a recursive method that decreases the error and improves the approximation of an integral.

Lemma 3.2 (Romberg's method of Integration)**.** *Suppose that the true value of the integral*

$$\int_a^b g(x)\,\mathrm{d}x \tag{3.29}$$

is I. Let $I_{k,j}$ denote an approximation of I, where k denotes the order of extrapolation and j how accurate the estimate of the integral is. By accuracy we mean that for every step that j is increased, the step size h is halved. Romberg's method can generally be stated as

$$I_{k,j} = I_{k-1,j+1} + \frac{I_{k-1,j+1} - I_{k-1,j}}{2^{2(k-1)} - 1}, \quad k \geq 2. \tag{3.30}$$

Given that the function g is sufficiently smooth so that the Euler-Maclaurin summation formula holds, every step of Romberg's method reduces the error $\mathcal{O}(h^2)$.

For a proof of the lemma, we refer to [3]. We are interested in making an extrapolation of order two, i.e. $k = 2$, and motivate the lemma informally for this case. Note that this is the type of approximation we already made to compute $M(h)$. Let I_1 denote the numerical approximation of the integral (3.29) obtained by using the step h, and I_2 the numerical approximation obtained by using step size $h/2$. Remembering from the Euler-Maclaurin summation formula that the truncated error of the composite trapezoidal rule ideally can be written as $E_t = \frac{\alpha}{n^2}$, where n is the number of segments of the discretization and α is some constant, it holds that

$$\begin{aligned} I &\approx I_1 - \frac{\alpha}{n^2}, \\ I &\approx I_2 - \frac{\alpha}{4n^2}. \end{aligned} \tag{3.31}$$

The constant α can be eliminated by combining the two expressions in (3.31), yielding

$$I \approx I_2 + \frac{1}{3}(I_2 - I_1). \tag{3.32}$$

This is the second order extrapolation of Romberg's method, by comparison with the expression in (3.30).

By using the trapezoidal rule to integrate an arbitrary function $g(t)$, the integral between the points $t = 2(i-1)h$ and $t = 2ih$ can be approximated as

$$\begin{aligned} &h\left[g(2(i-1)h)+g(2ih)\right], && \text{using step size } 2h,\\ &h\left[\frac{1}{2}g(2(i-1)h)+g((2i-1)h)+\frac{1}{2}g(2ih)\right], && \text{using step size } h. \end{aligned} \tag{3.33}$$

Applying Romberg's method of second order from (3.32), the step between $t = 2(i-1)h$ and $t = 2ih$ can be represented as

$$\begin{aligned} &h\left(\frac{1}{2}g(2(i-1)h)+g((2i-1)h)+\frac{1}{2}g(2ih)\right)+\frac{h}{3}\left(-\frac{1}{2}g(2(i-1)h)+g((2i-1)h)-\frac{1}{2}g(2ih)\right)=\\ &=h\left(\frac{g(2(i-1)h)}{3}+\frac{4g((2i-1)h)}{3}+\frac{g(2ih)}{3}\right). \end{aligned} \tag{3.34}$$

We see that this formula agrees with one step of Simpson's 1/3rd rule. By decreasing the step size, the error for the trapezoidal rule can thus be reduced to the same order of magnitude as computations with Simpson's rule ideally would have generated, for instance by repeated use of Romberg's rule.

In conclusion, an accurate implementation of the model where a nonconstant crowding function is applied can be obtained by using the trapezoidal rule only. However, Romberg's method is valid only if the integrand is sufficiently differentiable so that the Euler-Maclaurin summation formula applies, with an error expansion with h in powers of 2: h^2, h^4 etc. We have already seen that there is a discontinuity problem at $t = T_2$ and we cannot guarantee that the integrand is three times differentiable, which is demanded if fourth order accuracy is to be obtained from Romberg's method. Therefore, we cannot guarantee that the method is applicable. However, we will see that it is possible to reduce the error by using Romberg's method greatly. The order of accuracy obtained by applying Romberg's rule is investigated in Section 6.2.

4 Simulations

Tests with various combinations of model components are carried out in order to numerically gain knowledge about the qualitative behaviour of the system and to reproduce some of the analytical and numerical results from the article of Maad Sasane. The simulations also serve to visualise the quality of the new implementation of the model. In Section 4.3, a specific case study is performed where the question is if a tumour decreased in size after medical treatment, so that only a very small number of cancer cells remain, will die off or start growing again when medications have stopped. We also investigate if the result depends on the existence of (daughter cells of) cancer stem cells, i.e. if the result is dependent on whether $\psi \neq 0$ or not.

In all simulations, the cumulative distribution function $F(\tau)$ was chosen to follow a Weibull distribution in accordance with common practice in survival analysis and with the numerical results of Section 7 in [10]:

$$F(\tau) = \begin{cases} 1 - e^{-\left(\frac{\tau - c}{a}\right)^b}, & \text{if } \tau > c, \\ 0, & \text{otherwise.} \end{cases} \tag{4.1}$$

The constant b determines the rate of transition from Phase 1 to Phase 2, depending on age: if $b = 1$, it is as likely to transfer from Phase 1 to Phase 2 for all cells, independently of age spent in Phase 1, if $b < 1$ it is more likely for young cells to transfer than for old ones, whereas if $b > 1$ it is more likely for old cells to transfer than for young cells. In most of the simulations in this chapter, $b = 2$. The delaying parameter, c, was set to $c = 2.5$ hours, corresponding to a first part of Phase 1 where no cells transfer to Phase 2. It was assumed that the proportion $1 - d$ of all cells entering Phase 1 survives to Phase 2 and therefore, the constant a could be calculated to

$$a = \frac{T_1 - c}{\log(1/d)^{1/b}}. \tag{4.2}$$

The remaining proportion of the cells die and disappear at the end of Phase 1, i.e. $F(\tau)$ can be rewritten as

$$F(\tau) = \begin{cases} 0, & \text{if } \tau < c, \\ 1 - e^{-\left(\frac{\tau - c}{a}\right)^b}, & \text{if } c < \tau \leq T_1, \\ 1, & \text{if } \tau > T_1. \end{cases} \tag{4.3}$$

The lengths of Phase 1 and Phase 2 were set to $T_1 = 12.5$ hours and $T_2 = 9$ hours, in correspondence with experimental data in [5]. In all figures illustrating simulations, the scale of the time axis is therefore in hours.

Tests were carried out both with and without crowding (no crowding corresponds to $f(p)$ being constant). In the case with no crowding, it can be good to keep in mind that some kind of space limiting seems realistic. Therefore, one interpretation of the case without crowding is that the number of cells are too few for crowding to contribute to the dynamics of the system. However, in the test with f constant, such interpretations are left aside, and it is somewhat naively assumed that no space limitations exist.

In the tests of Sections 4.1 and 4.2, investigating the system with and without crowding, the input functions φ_1 and φ_2 were both varied as ten different continuous functions in different tests: first degree polynomials, second degree polynomials and exponential functions with alternating parameters. In the examples illustrating the properties of the system, the specific initial data chosen for illustrative figures do not have any particular meaning biologically, but are only chosen to show interesting dynamics.

In order to investigate the contribution to $M(t)$ and $P(t)$ from the input function $\psi(t)$, $\psi(t)$ was varied in different computations to a wide range of constant values, where daughter cells from cancer stem cells were assumed to constitute either a very small or a larger proportion of the total population of cells. When $\psi = 0$, it is assumed that cancer stem cells do not exist at all.

Combined, all the function choices described give a model that is simple to work with. Despite the little or non-existent experimental or theoretical ground for many of the choices, interesting properties

of the model can still be investigated. The step size in the simulations was put to $h = 0.0125$ when Simpson's rule was used (for f constant) and a combination of $h = 0.125$ and $h = 0.125/2$, when the trapezoidal rule was used through Romberg's method (for f nonconstant).

4.1 Constant Crowding Function

Two choices of the surviving proportion from Phase 1 to Phase 2 were considered: $d = 0.05$ and $d = 0.25$. The corresponding cumulative distribution functions are illustrated in Figure 4.1. The constant crowding function was put to five different values, $f(p) = 1$, $f(p) = 0.95$, $f(p) = 0.75$, $f(p) = 0.67$ and $f(p) = 0.6$, and the input function ψ was kept to small constant values relative to the size of $M(t)$. We will start the section by looking at function choices leading to unbounded solutions for M and P in Examples 4.1–4.3.

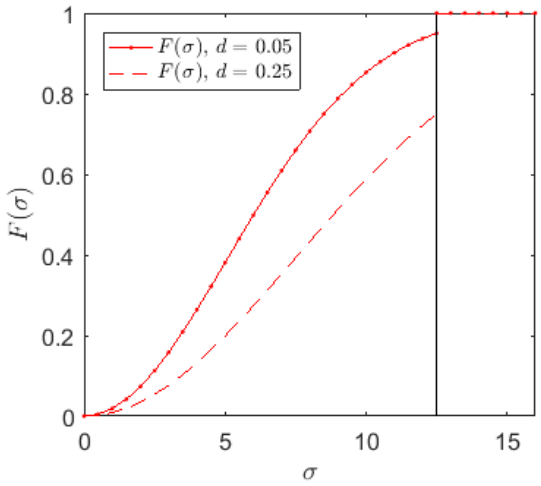

Figure 4.1: Cumulative distribution functions. Horizontal line marks $t = T_1$ after which $F(\tau) = 1$.

Example 4.1. Surviving proportion $d = 0.05$ and $f = 0.95$: All simulations have similar properties, with $M(t) \to \infty$ and $P(t) \to \infty$ as $t \to \infty$. In Figure 4.2 two such simulations are illustrated, where $\psi = 0$. The population size seems to grow exponentially. The constant crowding function is chosen so that more than half of the cells undergoes mitosis in each cycle, which can explain the unbounded solutions. Choosing the input function as $\psi = 0$ or $\psi \neq 0$ give the same growth properties, i.e. ψ does not affect whether the solution is unbounded or not, but only affects how fast the solution grows.

Example 4.2. Surviving proportion $d = 0.25$: The simulations for $f = 1$, $f = 0.95$, $f = 0.75$ and $f = 0.67$ (having a crowding function such that $f > 1/(2F(T_1))$), all have similar properties, with $M(t) \to \infty$ and $P(t) \to \infty$ as $t \to \infty$, as in Example 4.1. It can be noted that for $f = 0.67$, the solution grows very slowly, see Figure 4.3. Again, the size of ψ does not affect the overall behaviour of the system, but only how fast the solution grows.

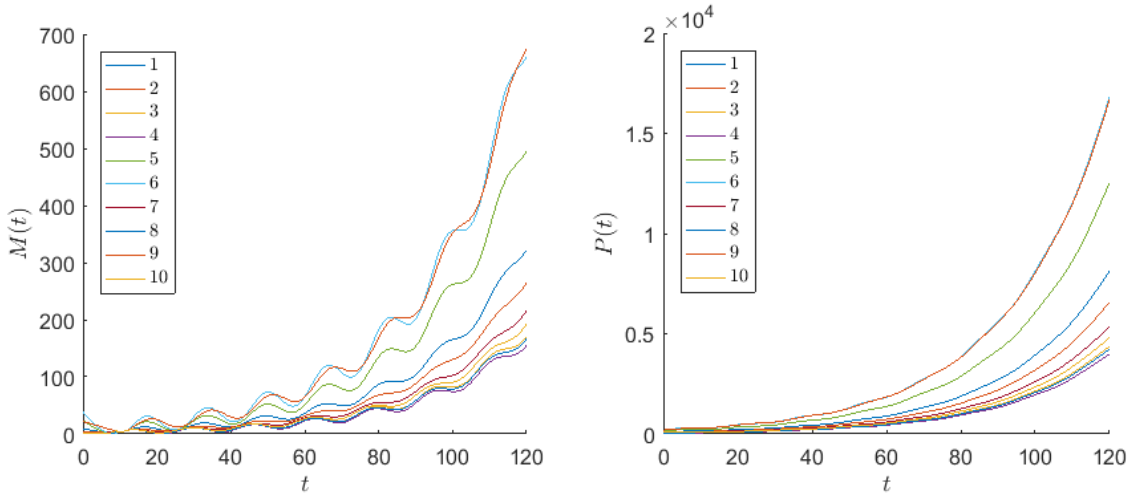

Figure 4.2: Example 4.1: Simulation of $M(t)$ and $P(t)$ for $d = 0.05$, $f = 0.95$, $\psi(t) = 0$, $\varphi_1(\tau) = 25e^{-0.4\tau}$ and ten different choices of $\varphi_2(\tau)$ (The specific choice of the initial data in φ_1 does only serve to illustrate overall trends of the system and does not have any particular meaning in itself.) Ten choices of φ_2 are illustrated and the unit of the time axis is in hours.

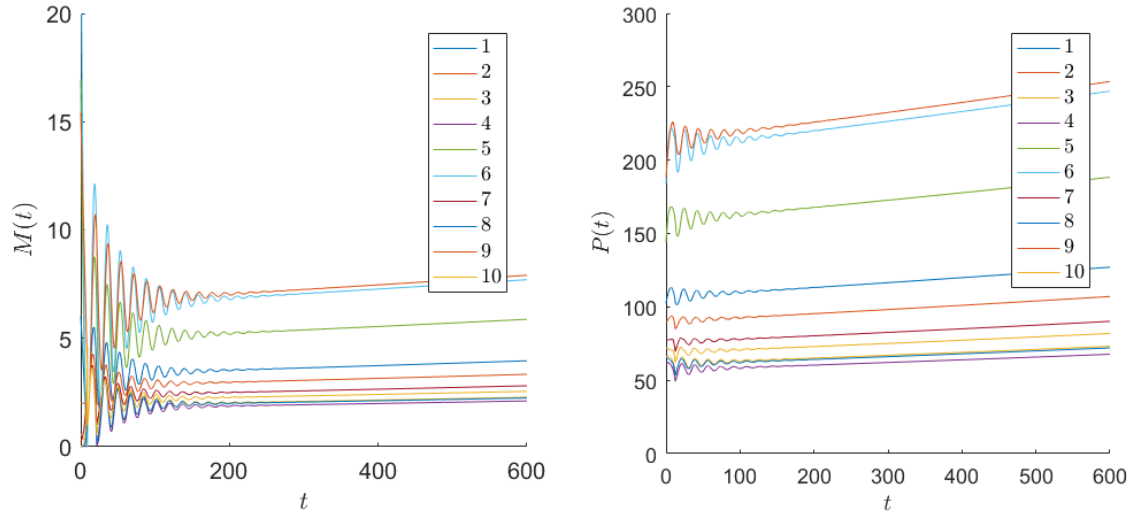

Figure 4.3: Example 4.2: Simulation of $M(t)$ and $P(t)$ for $d = 0.25$, $f = 0.67$, $\psi(t) = 0$, $\varphi_1(\tau) = 25e^{-0.4\tau}$ and ten different choices of $\varphi_2(\tau)$. Approximate solutions grow slowly in comparison to when larger values for f are used. The unit of the time axis is in hours.

Example 4.3. The growth properties of $M(t)$ are more carefully investigated. It can be demonstrated, plotting the y-axis on a logarithmic scale, that $M(t)$ grows exponentially for all investigated constant crowding functions yielding an unbounded solution. For an illustration, see Figure 4.4 where $f = 1$. Exponential solutions are also obtained for varying choices of b and c in the cumulative distribution function ($b = 1$ or $b = 2$, $c = 0$ or $c = 2.5$), varying choices of constant ψ and varying $\varphi_1(\tau)$ and $\varphi_2(\tau)$. The choices of ψ, $\varphi_1(\tau)$ and $\varphi_2(\tau)$ however do affect the growth rate for M and P.

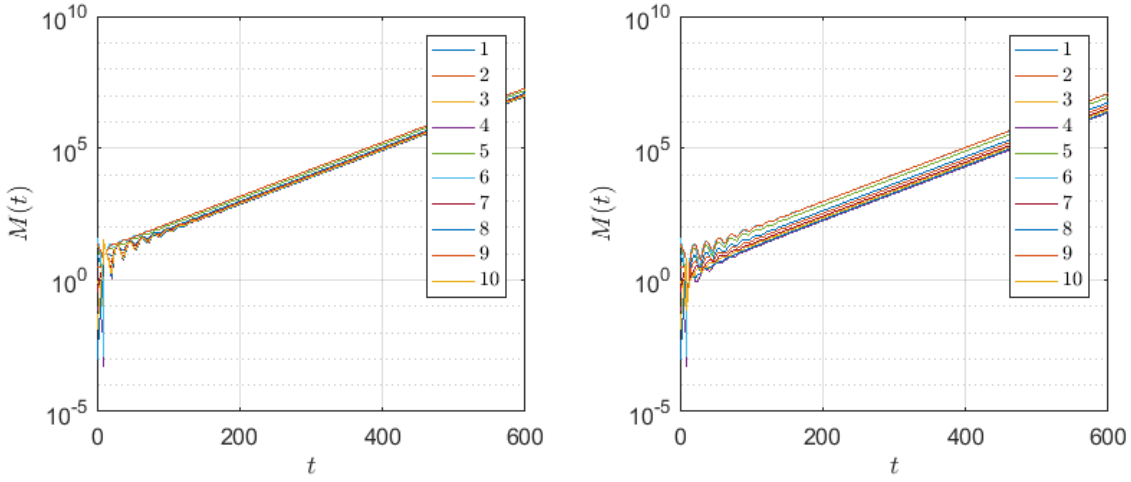

(a) $\varphi_1(\tau) = 2\tau + 5$ (b) $\varphi_1(\tau) = 7e^{-0.7\tau}$

Figure 4.4: Example 4.3: Investigation of the exponential growth of the numerical simulation when no crowding is assumed to affect the system and $f > 1/(2F(T_1))$. Here, $\psi = 1$ and ten different choices of φ_2 are used. The unit of the time axis is in hours. In the cumulative distribution function, $b = 2$ and $c = 2.5$.

If the proportion f of dividing cells at the end of Phase 2 is set to smaller values, we get bounded solutions. This is illustrated in Examples 4.4–4.5 for the choice $f = 0.6$, chosen so that $f < 1/(2F(T_1))$.

Example 4.4. If $\psi > 0$, $M(t)$ and $P(t)$ both tend to constant solutions M_∞ and P_∞ independently of the choices of φ_1, φ_2 or ψ. We note that the choices of φ_1 and φ_2 do not affect the value at the limit. In Figures 4.5] and 4.6, two simulations of this type are illustrated, using $\psi = 1$ and $\psi = 5$ respectively.

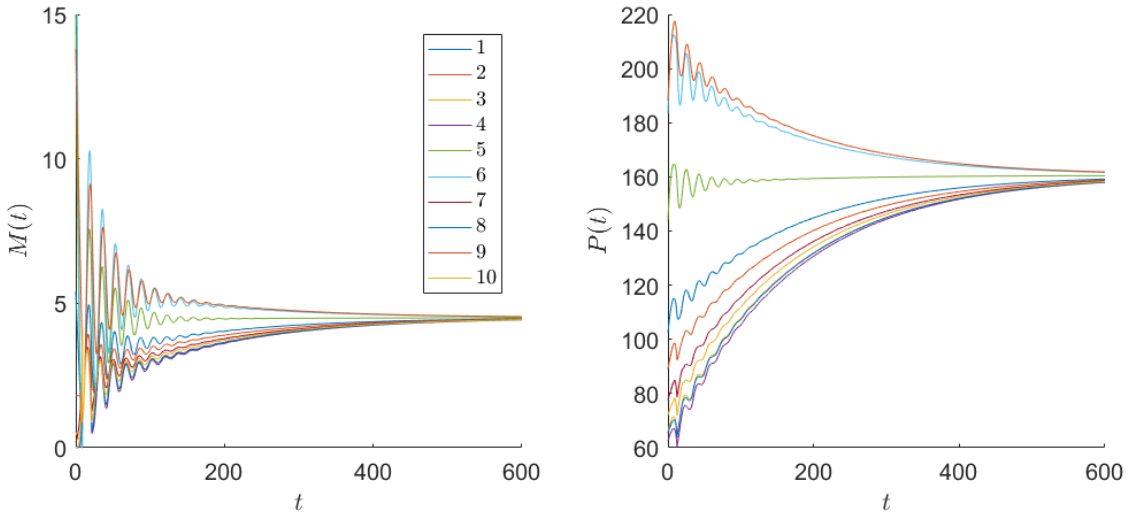

Figure 4.5: Example 4.4: Simulation of $M(t)$ and $P(t)$ for $d = 0.25$, $f = 0.6$, $\psi = 1$, $\varphi_1(\tau) = 25e^{-0.4\tau}$ and ten different choices of $\varphi_2(\tau)$. The unit of the time axis is in hours.

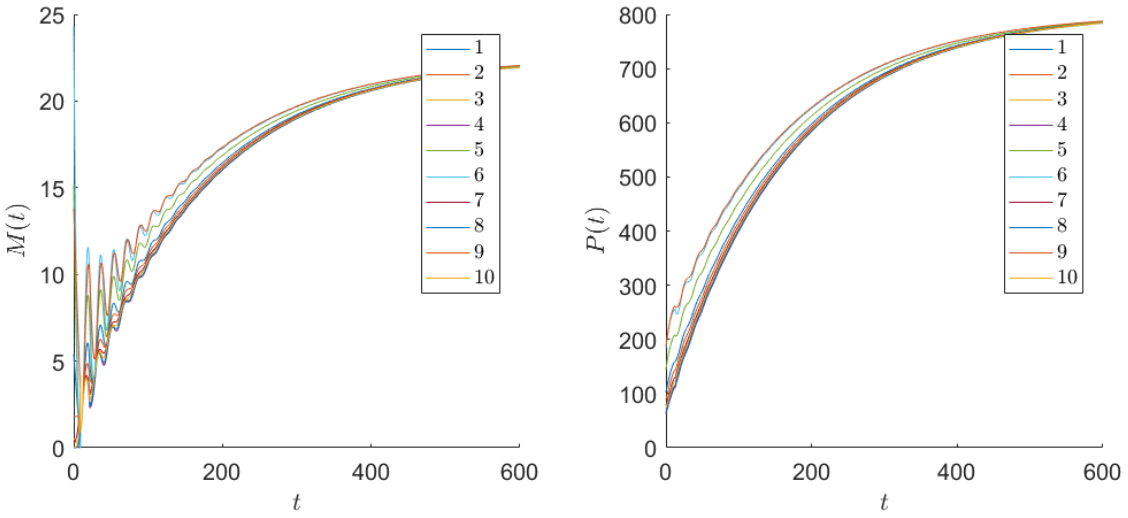

Figure 4.6: Example 4.4: Simulation of $M(t)$ and $P(t)$ for $d = 0.25$, $f = 0.6$, $\psi = 5$, $\varphi_1(\tau) = 25e^{-0.4\tau}$ and ten different choices of $\varphi_2(\tau)$.

Example 4.5. Again, the surviving proportion is set to $d = 0.25$ and the crowding function chosen to $f = 0.6$. When $\psi = 0$, $M \to 0$ and $P \to 0$ as $t \to \infty$. This is illustrated in Figure 4.7 for five different choices of φ_2 and φ_1 set to $\varphi_1(\tau) = 5\tau$. Note that the limit values are independent of the choices of φ_1 and φ_2.

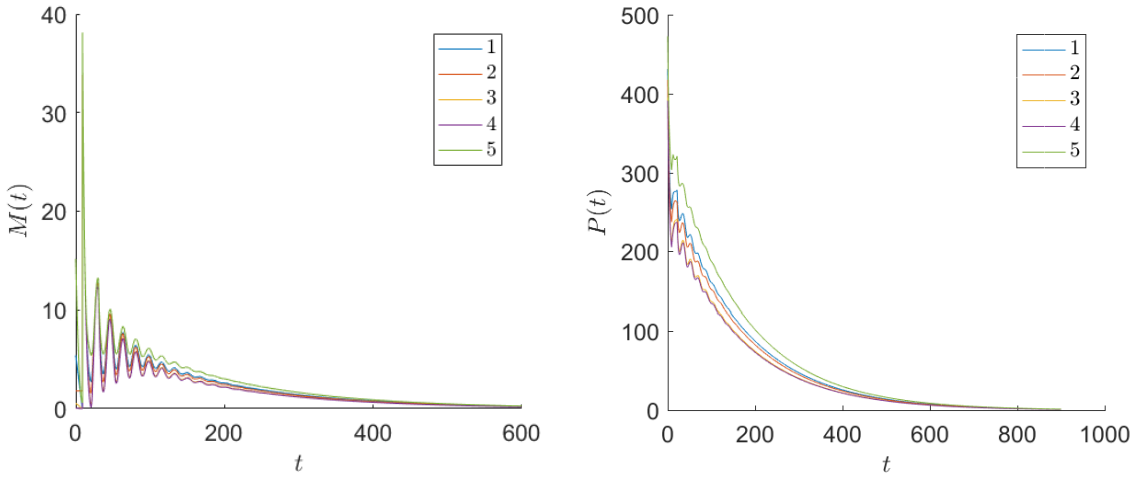

Figure 4.7: Example 4.5: Simulation of $M(t)$ and $P(t)$ for $d = 0.25$, $f = 0.6$, $\psi(t) = 0$, $\varphi_1(\tau) = 5\tau$ and five different choices of $\varphi_2(\tau)$.

4.2 Non-Constant Crowding Function

Three choices of the crowding function are considered: $f_1(p) = 1/\cosh(0.01p)$ and

$$f_2(p) = \begin{cases} 1, & 0 \le p \le 30, \\ -\dfrac{0.95}{70}p + \dfrac{197}{140}, & 30 < p \le 100, \\ 0.05, & p > 100, \end{cases} \tag{4.4}$$

representing *crowding*, i.e. such that $f(p) \to 0$ as $p \to \infty$ and $f(p)$ decreasing, and

$$f_3(p) = \frac{1}{0.09(p + 0.05)} \exp\left(-\ln(0.05(p + 0.05))^2/2\right), \tag{4.5}$$

representing *quorum sensing*, having the property that $f(p) \to 0$ as $p \to 0$ (In fact, f_3 also represents the crowding property for large p). Concerning crowding, the advantage of the piecewise linear f_2, in relation to the smooth f_1, is that the constant value of $f(p) = 1$ in f_2 for small population sizes p allows for exponential growth of the solutions when the number of cells is small. For the crowding function f_1, no such scenario is considered, and the space limiting acts already for very few cells. The crowding functions f_1, f_2 and f_3 are all illustrated in Figure 4.8 and have the desired property that they map to the interval $[0, 1]$, representing a proportion of the total number of cells.

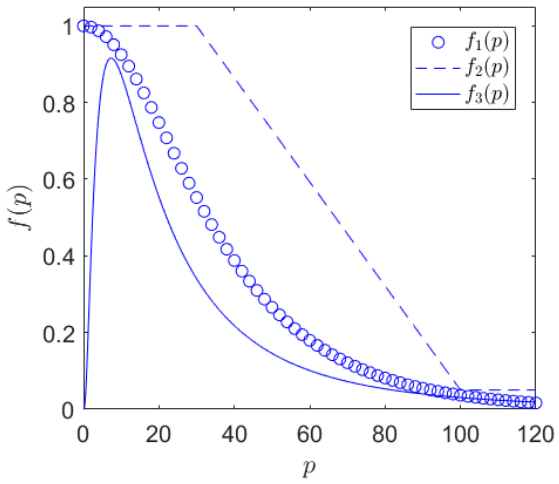

Figure 4.8: Crowding functions

The surviving proportion is chosen to $d = 0.25$ in all simulations, along with five or ten different choices of φ_1 and φ_2, in accordance with tests in the previous section.

Example 4.6. We choose the crowding function $f = f_1$ to investigate the concept of crowding. The input function ψ is chosen in the set $\{0, 0.5, 1, 3, 10, 20\}$. In all investigated cases the solution of M and P tend to some constant limits M_∞ and P_∞. It can again be observed that the limits are independent of the initial data, which can be seen in Figures 4.9 and 4.10 for the choice $\psi = 1$, where the same limits are obtained for ten different choices of φ_2 and two different choices of φ_1. Crowding influences the solutions to a varying extent at the same time t in the two figures due to the varying number of initial cells for the two simulations, given by the initial data. To put it clearer, the number of cells are adjusted to a varying extent by f at the same time t, due to the different sizes of $P(t)$. This is one explanation to the different dynamics in the two figures. The long-term limits are approximated from the graphics to $M_\infty \approx 3.07$ and $P_\infty \approx 115$. The large difference between the number density of

dividing cells in M_∞ and the total number of cells in P_∞ is due to the fact that only a small fraction of the population undergoes cell division when P is large.

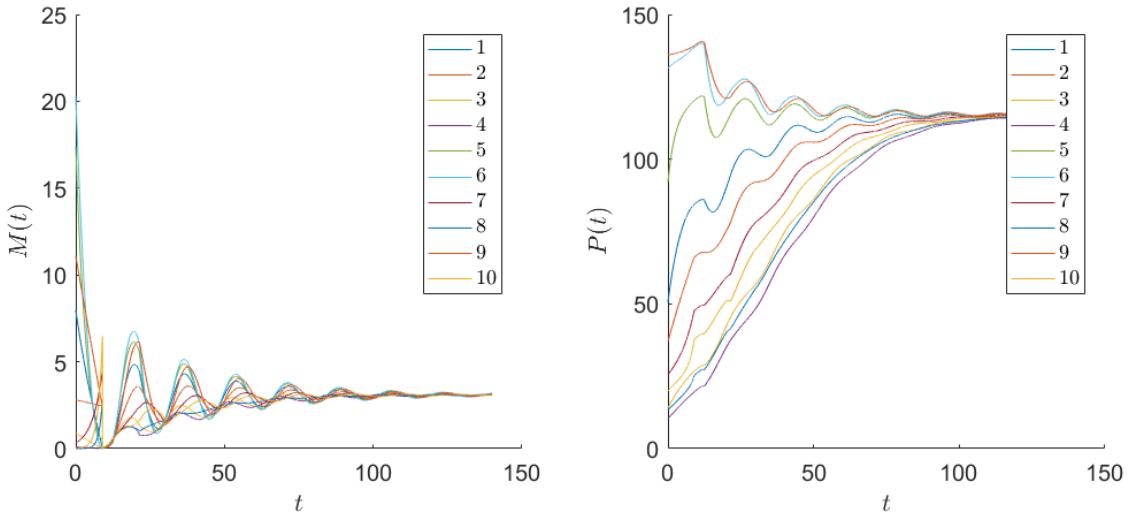

Figure 4.9: Example 4.6, crowding: Simulation of $M(t)$ and $P(t)$ for $d = 0.25$, $f = f_1$, $\psi = 1$, $\varphi_1(\tau) = 7e^{-0.7\tau}$ and ten different choices of $\varphi_2(\tau)$. The limits M_∞ and P_∞ are independent of φ_1 and φ_2.

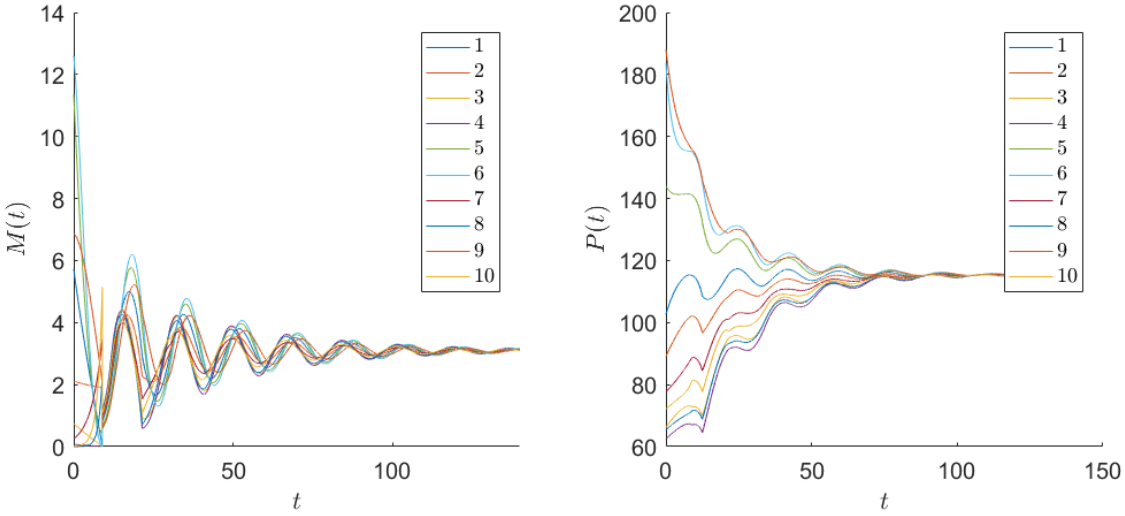

Figure 4.10: Example 4.6, crowding: Simulation of $M(t)$ and $P(t)$ for $d = 0.25$, $f = f_1$, $\psi = 1$, $\varphi_1(\tau) = 25e^{-0.4\tau}$ and ten different choices of $\varphi_2(\tau)$. Again, we see that φ_1 and φ_2 do not affect M_∞ and P_∞.

Observations show that simulations of crowding using the crowding function f_2 give solutions with the same properties in terms of solutions tending to limit values. The limits are different and we will see in Section 5.1 how they can be determined.

Example 4.7. The concept of quorum sensing is next investigated, choosing the crowding function $f = f_3$. For the chosen initial data, $M(t)$ and $P(t)$ tend to constant values M_∞ and P_∞ similarly as in the case with crowding. This is the case both when $\psi = 0$, see Figure 4.11 and when $\psi > 0$, see Figure 4.12 where $\psi = 10$. In the case when $\psi = 0$, the limits can be approximated from the numerical solution to $M_\infty = 0.51$ and $P_\infty = 16.3$, independently of the initial data.

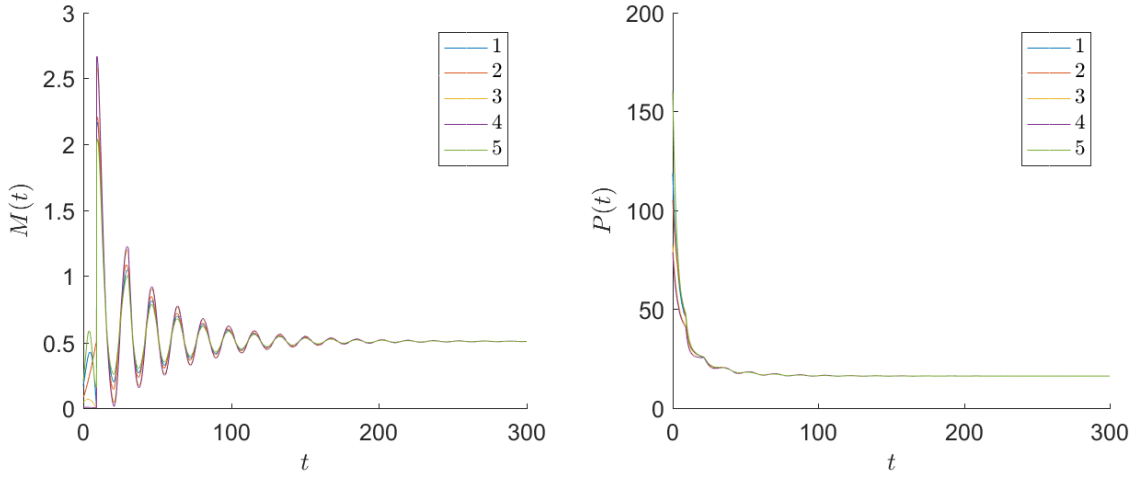

Figure 4.11: Example 4.7, quorum sensing: Simulation of $M(t)$ and $P(t)$ for $d = 0.25$, $f = \frac{1}{0.09(p+0.05)} \exp\left(-\ln(0.05(p+0.05))^2/2\right)$, $\varphi_1(\tau) = \tau$ and five different choices of $\varphi_2(\tau)$. Here, $\psi = 0$.

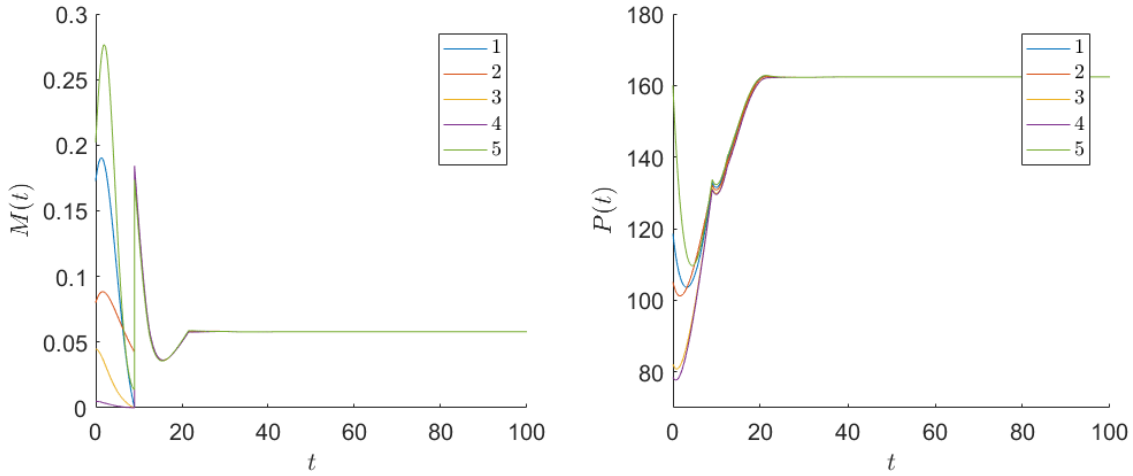

(a) $P(t)$ for $\varphi_1(\tau) = 5$.

(b) $P(t)$ for $\varphi_1(\tau) = 5\tau$

Figure 4.12: Example 4.7, quorum sensing: Simulation of $M(t)$ and $P(t)$ for $d = 0.25$, $f = \frac{1}{0.09(p+0.05)} \exp\left(-\ln(0.05(p+0.05))^2/2\right)$, $\varphi_1(\tau) = \tau$ and five different choices of $\varphi_2(\tau)$. Here, $\psi = 10$.

It is observed that the solutions converge faster to its limits for larger values of the constant ψ than for smaller ψ in Example 4.6 and 4.7. The space limiting property of the crowding function has an effect earlier for a larger ψ, as a large contribution from the input function ψ faster gives a larger population compared to the case when $\psi = 0$. An interpretation can be that a larger value of ψ, which might be interpreted as correspondent to a larger amount of cancer stem cells, results in a more aggressive cancer.

4.3 Possibilities of Eliminating a Tumour

In this section we assume that a cancer tumour has been treated successfully using some medical therapy. All or almost all the cancer cells have been killed off, leading to that not more than a very small fraction of the original amount of cells remains (for practical reasons it is likely to assume that a tiny part of all the cells still remain). What happens to the tumour if it is now left on its own without medication – Does it grow or remain being (almost) zero-sized? Is the long term solution $M = P = 0$? Is the reason behind the relapse of a tumour (when this happens) the cancer stem cells or the small amount of remaining cancer cells? To investigate these questions, we perform tests where the initial age distributions are put to $\varphi_1 = \varphi_2 = 0$ or $\varphi_1 = \epsilon_1$ and $\varphi_2 = \epsilon_2$ for some small $\epsilon_1 > 0$ and $\epsilon_2 > 0$ and simulate the system, both in the case with a constant crowding function $f = 1$ (no crowding) and in the case with crowding, where the crowding function is chosen to be

$$f_4(p) = \begin{cases} 1, & 0 \leq p \leq 50, \\ 1/\cosh(0.015(p-50)), & p > 50, \end{cases} \tag{4.6}$$

leaving room for the cells to grow exponentially when the population size is small ($p \leq 50$), but adjusting the population size when the population (possibly) grows larger and space and nutrients are limited. See Figure 4.13a for an illustration of the nonconstant crowding function. The constant crowding function is assumed to mimic a situation where the cells are too few for crowding to have an effect.

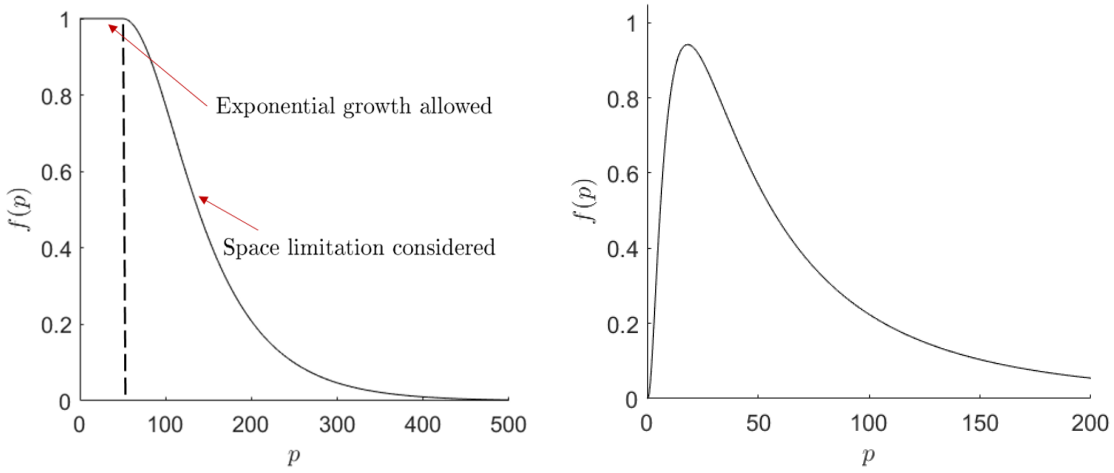

(a) Crowding function f_4 in Examples 4.8 and 4.9 representing crowding.

(b) Crowding function f_5 in Example 4.10 representing quorum sensing.

Figure 4.13

Example 4.8. We assume that all the cells have been killed off. If $\psi = 0$, there is nothing that can drive the growth of the tumour. However, if $\psi = k$ for some $k > 0$, we get in the case with $f = 1$ the behaviour of Figure 4.14 where the solution grows exponentially regardless of the size of k. In the case of crowding, using $f = f_4$, we get the behaviour of Figures 4.15a and 4.15b, where the number density of dividing cells (and the total number of cells) initially grows exponentially, but reaches a limit value after some finite time. The constant total number of cells after long time is larger for a system with a larger contribution from cancer stem cells (ψ larger), than for a system with a smaller contribution from cancer stem cells (Figure 4.15b). The number density of dividing cells, $M(t)$, on the other hand is smaller when the impact from cancer stem cells is larger (Figure 4.15a).

To conclude, a zero-sized tumour can start growing again due to input from daughter cells of cancer stem cells. The crowding function determines the growth properties of the tumour.

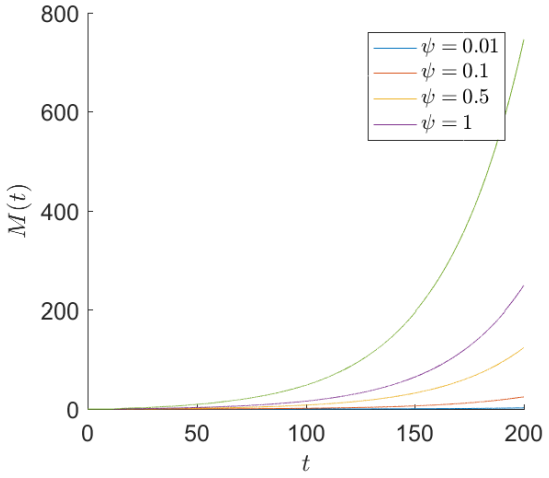

Figure 4.14: Example 4.8: Exponential growth is obtained for a zero-sized tumour that is left to grow without space limitations, if $\psi > 0$.

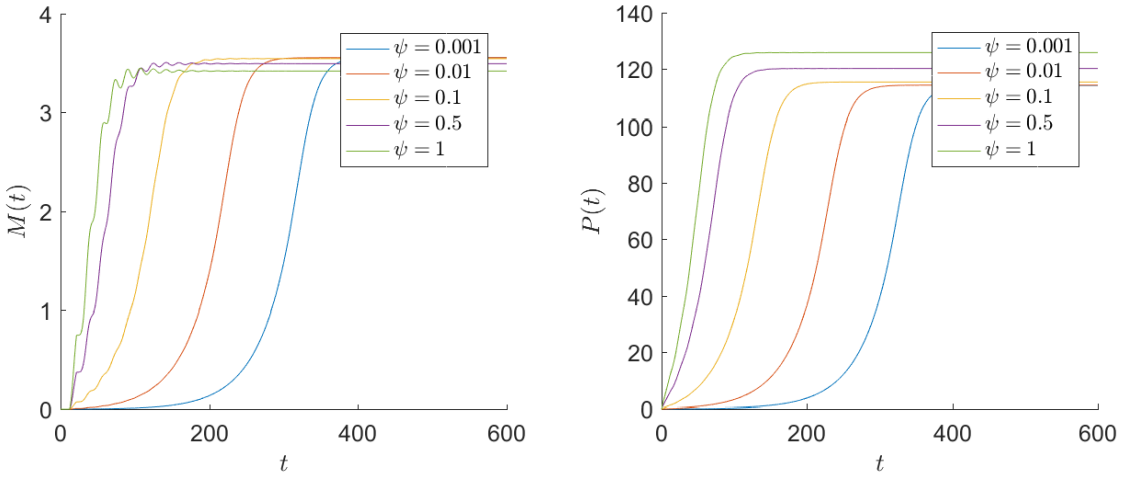

(a) (b)

Figure 4.15: Example 4.8: The number density of dividing cells and the total number of cells reach a steady limit after long time when space limiting is used through the crowding function f_4. The size of the input function ψ affects both the size of the tumour (originally zero sized) and how it grows after long time.

Example 4.9. We next assume that a small amount of the original cells remains after completed therapy and that no cancer stem cells exist, i.e. $\varphi_1 = \varphi_2 = \epsilon$, for some constant $\epsilon << 1$ and $\psi = 0$. Tests are carried out for $\epsilon = 0.001$, $\epsilon = 0.01$, $\epsilon = 0.05$ and $\epsilon = 0.1$.

It is found that solutions reach a nonzero limit when space limiting is considered, the limit for the total number of cells being $P_\infty \approx 114$ (units) for the particular crowding function f_4. The initial number of cells are given from

$$\begin{aligned} P(0) &= \int_0^{T_1} n_1(0,\tau)\,\mathrm{d}\tau + \int_0^{T_2} n_2(0,\tau)\,\mathrm{d}\tau = \\ &= \int_0^{T_1} \varphi_1(\tau)\,\mathrm{d}\tau + \int_0^{T_2} \varphi_2(\tau)\,\mathrm{d}\tau = \epsilon(T_1 + T_2) \end{aligned} \tag{4.7}$$

and are considerably fewer than P_∞, ranging from 2.15 for the largest considered value of ϵ to 0.02 for the smallest value of ϵ in the simulations. The total number of cells thus increases substantially for the simulated cases. The limit is reached faster for larger values of the initial distribution φ_1 than for smaller values, see comparison between Figures 4.16a and 4.16b, where $\varphi_1 = \epsilon = 0.001$ and $\varphi_1 = \epsilon = 0.1$ respectively. An interpretation is that if a larger number of malignant cells are left after the cancer treatment, the tumour returns faster. We note that if also cancer stem cells contribute to the system so that $\psi = k$ for some $k > 0$, some other limit values M_∞ and P_∞ are obtained, depending on the size of ψ. It is observed that the larger the contribution from the input function ψ, the larger is the limit value P_∞, i.e. the total number of cells asymptotically.

The conclusion from the simulations where crowding is applied as a whole is that if the tumour is not completely eliminated, it can start growing again due only to the remaining cancer cells. If there in addition is a contribution from cancer stem cells, the tumour relapses to a different size, larger than the final size for the case where no cancer stem cells are present. Mathematically, the crowding function determines the growth properties of the tumour. We will see how in Section 5.1. We note by comparing the solutions of Figure 4.15 and Figure 4.16 that the solutions for M and P have a more oscillatory behaviour initially for $\varphi_1 = \varphi_2 = \epsilon$ and $\psi = 0$ than for $\varphi_1 = \varphi_2 = 0$ and $\psi \neq 0$.

With constant crowding, solutions grow exponentially despite the small number of initial cells, see Figure 4.17. In both Figure 4.16 and 4.17, the legends of the graphs correspond to different choices of $\varphi_2 = \epsilon$.

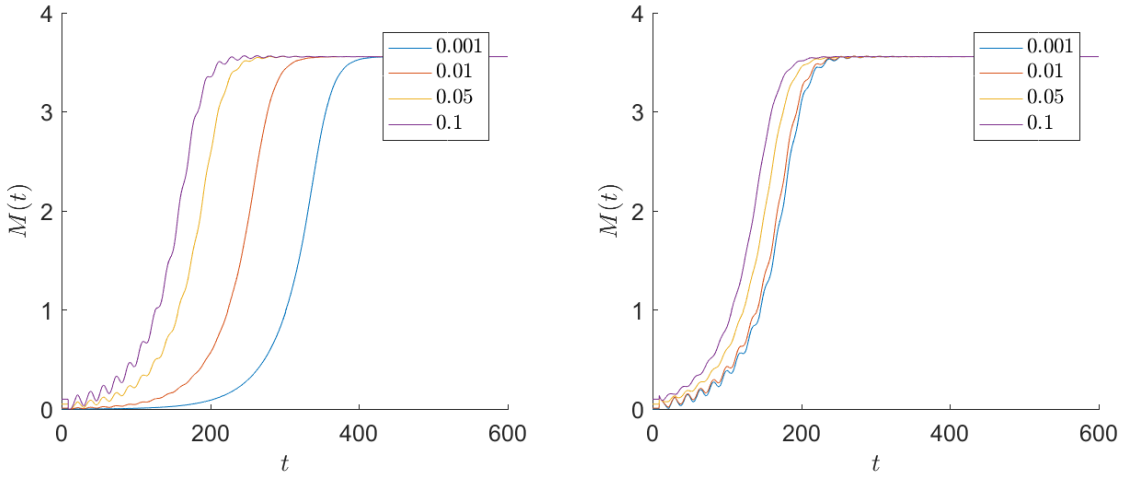

(a) The initial age distribution in Phase 1 is $\varphi_1 = \epsilon = 0.001$.

(b) The initial age distribution in Phase 1 is $\varphi_1 = \epsilon = 0.1$.

Figure 4.16: Example 4.9: The number density of dividing cells reach a steady limit after long time when space limiting is applied using the crowding function f_4. The limit is reached faster when the initial age distributions are larger. Legend represents choices of $\varphi_2 = \epsilon$. There is no contribution from cancer stem cells, i.e. $\psi = 0$.

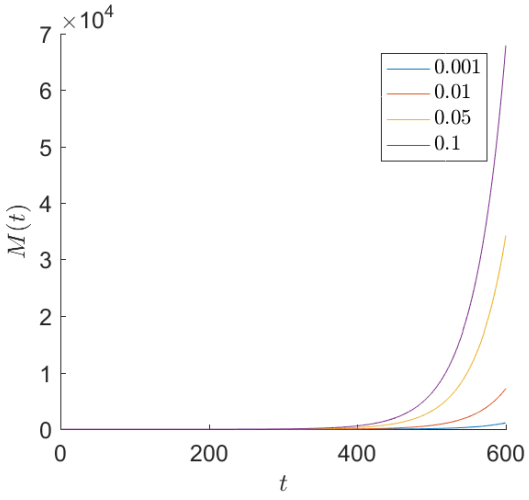

Figure 4.17: Example 4.9: Exponential growth is obtained for a tumour of size ϵ that is left to grow without space limitations. Here, $\varphi_1 = \epsilon = 0.001$ and if also $\varphi_2 = \epsilon$, the total number of initial cells are 0.02 (units unspecified). Legend represents different choices of $\varphi_2 = \epsilon$. There is no contribution from cancer stem cells, i.e. $\psi = 0$.

Lastly, we illustrate that we do not necessarily get the same behaviour of the system with growing solutions and a relapsing tumour if quorum sensing is assumed to exist. For this purpose, we choose the crowding function

$$f_5(p) = \frac{1}{0.035(p+0.05)} \exp\left(-\ln(0.05(p+0.05))^2/2\right), \tag{4.8}$$

illustrated in Figure 4.13b.

Example 4.10. First, the same test as in Example 4.9 is carried out, with $\varphi_1 = \varphi_2 = \epsilon$ and $\psi = 0$, but in this example with $f(p) = f_5(p)$. For every small initial age distribution ϵ tested, it holds that $M \to 0$ and $P \to 0$ when t increases, see Figure 4.18. In a second approach, the small initial age distributions are kept but $\psi = k$, where $k > 0$, is varied. The dynamics of the system changes and even for a very small input function such as $\psi = 0.01$, the solutions reach a nonzero limit. An illustration is seen in Figure 4.19 for $\psi = 0.5$ and $\varphi_1 = 0.001$.

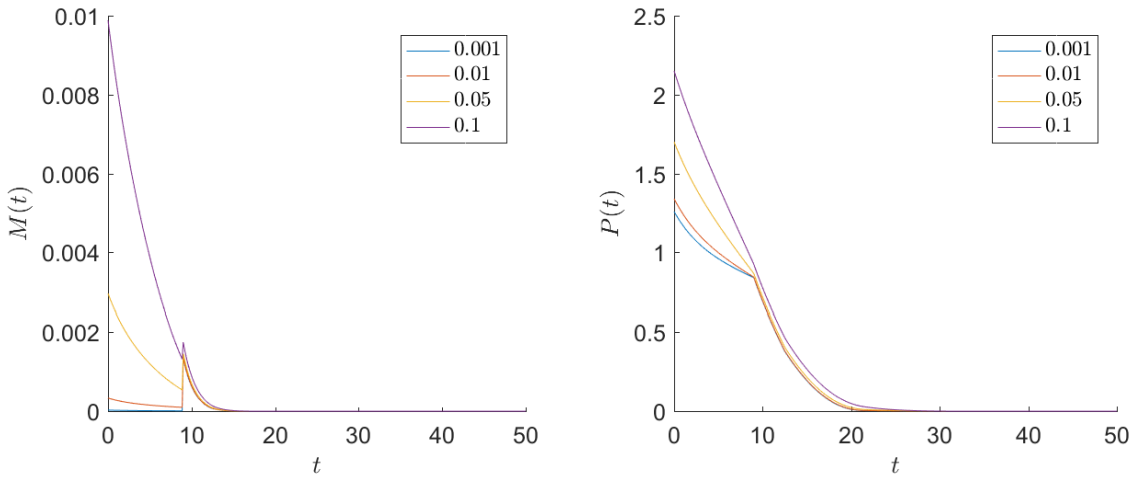

Figure 4.18: Example 4.10: When $\psi = 0$, the number density of dividing cells, $M(t)$, and the total number of cells, $P(t)$, decreases to zero when quorum sensing is applied through the crowding function f_5.

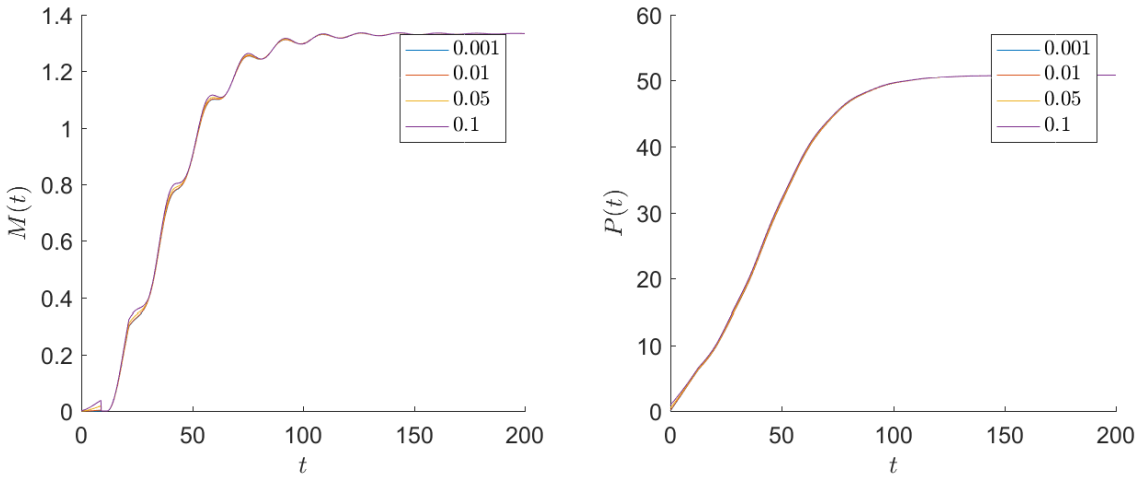

Figure 4.19: Example 4.10: When $\psi \neq 0$, the number density of dividing cells, $M(t)$, and the total number of cells, $P(t)$, reaches a nonzero limit when quorum sensing is applied through the crowding function f_5.

5 Qualitative Behaviour

In this part of the report, the qualitative behaviour of the system is investigated. As many components of the model are hard to determine experimentally, it is of importance to be able to detect overall properties of the solutions. In the first section, 5.1, the results of the simulations using a constant or nonconstant crowding function in Sections 4.1 and 4.2 are investigated theoretically. In particular, equations for the long-term solutions or limit values for $M(t)$ and $P(t)$ are presented (under the condition that the solution is not unbounded). In the subsequent section, 5.2, we analyse the results of the simulations in Section 4.3, where it is investigated whether an almost eliminated tumour still can cause harm. In Section 5.3, upper bounds for $M(t)$ are computed for $f = 1$ and $F(T_1) > 1/2$. In accordance with all other numerical investigations of this M.Sc. thesis, we assume that $T_2 > T_1 - T_2$. In the case with a constant crowding function f, the properties of $P(t)$ are given directly by the properties of $M(t)$ and we therefore choose to focus on the properties of $M(t)$ only. Finally, in Section 5.4, the difference between the solutions with a constant $\psi > 0$ and $\psi = 0$ are computed analytically for a constant crowding function f.

5.1 Long-Term Solutions

The unbounded, exponentially growing solutions in Examples 4.1–4.3, where the constant crowding function f was chosen so that $f > 1/(2F(T_1))$, can be described as follows: after mitosis, $2M(t) = 2f(P(t))n_2(t, T_2) = 2fn_2(t, T_2)$ expresses the number density of cells already in the model entering Phase 1 of the next cycle, whereas $F(T_1)$ denotes the proportion of cells transferring from Phase 1 to Phase 2. Collected, the factor $2fF(T_1)$ can be thought of as the proportion of surviving cells through one cell cycle, see Figure 5.1. When this quantity is larger than one, we get exponential growth. It was mentioned in Example 4.2 that the solution for $f = 0.67$ grows very slowly compared to when f was chosen to a larger constant. The reason is that the factor $2fF(T_1)$ in the case with $f = 0.67$ is only slightly larger than one.

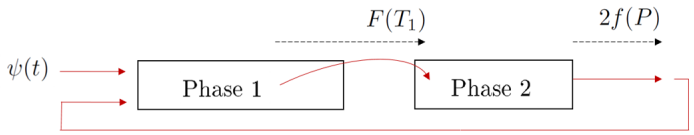

Figure 5.1: The factor $F(T_1)2f(P)$ is a measure of the proportion of surviving cells through one cell cycle.

The remaining numerical results presented in Sections 4.1 and 4.2 can be summarized theoretically using the results of Proposition 4 from the article of Maad Sasane [10]. In this report, the proposition is reformulated in Theorem 5.1, here stated without proof (for a proof, the reader is referred to [10]). The theorem explains the behaviour of the solutions as $t \to \infty$ in Examples 4.4–4.7, observed in Figures 4.6–4.7 and 4.9 – 4.11. In all these cases, the solution of M and P tend to constant limits M_∞ and P_∞. Note that the theorem does not assure that such limits exist, but only what the limits are if they exist. However, in the case with bounded solutions, Maad Sasane reasons that parameter choices that do not lead to limits are very rare [10].

Theorem 5.1. *Given that the limits* $\psi_\infty := \lim_{t\to\infty} \psi(t)$, $M_\infty := \lim_{t\to\infty} M(t)$ *and* $P_\infty := \lim_{t\to\infty} P(t)$ *exist, then* M_∞ *and* P_∞ *in the two cases* $\psi_\infty = 0$ *and* $\psi_\infty > 0$ *can be computed as follows:*

i.) If $\psi_\infty = 0$, *then either* $M_\infty = P_\infty = 0$ *or*

$$\begin{aligned} f(P_\infty) &= 1/(2F(T_1)), \\ M_\infty &= \frac{P_\infty}{2\left(T_1 + F(T_1)T_2 - \int_0^{T_1} F(\sigma)\,\mathrm{d}\sigma\right)}, \end{aligned} \tag{5.1}$$

ii.) If $\psi_\infty > 0$, then $f(P_\infty) < 1/(2F(T_1))$ and P_∞ and M_∞ satisfy

$$\begin{aligned}(1 - 2f(P_\infty)F(T_1))P_\infty &= \psi_\infty \left(T_1 + F(T_1)T_2 - \int_0^{T_1} F(\sigma)\,\mathrm{d}\sigma \right), \\ M_\infty &= \frac{1}{2}\left(\frac{P_\infty}{T_1 + F(T_1)T_2 - \int_0^{T_1} F(\sigma)\,\mathrm{d}\sigma} - \psi_\infty \right).\end{aligned} \tag{5.2}$$

We note that the limit values M_∞ and P_∞ are independent of the choices of φ_1 and φ_2, a result that we observed in our simulations. This is a property worth to put some emphasis on: regardless of initial data, the long term solutions will be the same. We also remark that the theorem can be used in an application only if f, $F(T_1)$ and $\int_0^{T_1} F(\sigma)\,\mathrm{d}\sigma$ somehow are biologically known.

In the case with a constant crowding function $f = 0.6$ and no input ($\psi = 0$), the theoretical limit values taken from the first part of Theorem 5.1 are $M_\infty = P_\infty = 0$, which also was the result obtained in Example 4.5. In Example 4.6, with crowding and $\psi = 1$, the limit values where approximately determined to $M_\infty \approx 3.07$ and $P_\infty \approx 115$ from the graphics. By using the second part of Theorem 5.1, a similar result is obtained, $M_\infty \approx 3.09$ and $P_\infty \approx 115$. In the case with quorum sensing and $\psi = 0$, the values from the graphics of Figure 4.11 read $M_\infty = 0.51$ and $P_\infty = 16.3$, while the values from the first part of Theorem 5.1 becomes $M_\infty = 0.51$ and $P_\infty = 16.3$. These few examples illustrate that the numerical implementation seem to correspond well with the theorem.

We end the section by further studying how the size of ψ affects the limit values M_∞ and P_∞. As mentioned in Example 4.7 and in Section 4.3, *Possibilities of Eliminating a Tumour*, a larger value for the total number of cells after long time is obtained when ψ is large than for small ψ. We also observed that the limit for M_∞ was smaller for a larger values of ψ than for a smaller values of ψ.

Example 5.1. We compute limit values M_∞ and P_∞ using Theorem 5.1 for different values of ψ and using two different crowding functions: $f_1(p) = 1/\cosh(0.01p)$, representing crowding, and $f_3(p) = \frac{1}{0.09(p+0.05)} \exp\left(-\ln(0.05(p+0.05))^2/2\right)$, representing quorum sensing and crowding. See Figure 5.2 for an illustration of the result. It can be concluded that the observations from our simulations correspond to the theorem.

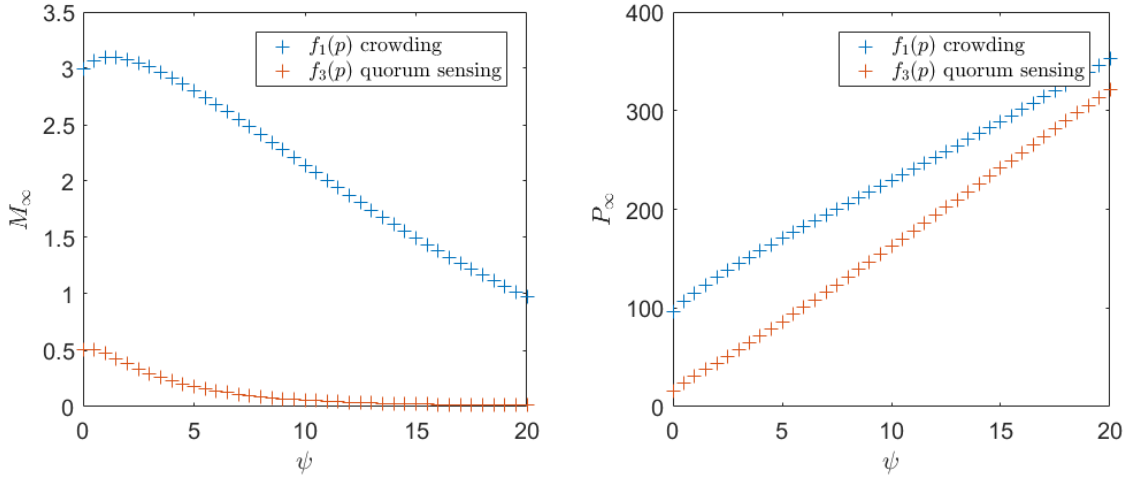

Figure 5.2: Limit values M_∞ and P_∞ as functions of ψ, computed using Theorem 5.1. Observe that $M_\infty > 0$ for all ψ also in the case with quorum sensing.

5.2 Possibilities of Eliminating a Tumour

We head back to the question of whether an almost eliminated tumour will cause any future harm, according to our model. When the tumour initially was eliminated entirely ($\varphi_1 = \varphi_2 = 0$), there is a clear distinction between the cases with or without cancer stem cells: In the case with no cancer stem cells ($\psi = 0$), nothing drives the growth of the tumour and therefore it remains being zero sized, while in the case when there is a nonzero sized input from daughter cells of cancer stem cells ($\psi > 0$), the tumour will re-establish itself, regardless of the choice of crowding function. The tumour also relapses when a tiny fraction of the original tumour is left ($\varphi_1 = \epsilon_1$ and $\varphi_2 = \epsilon_2$). The conclusion is that as long as there is some input to the system, either from daughter cells of cancer stem cells ($\psi > 0$) or from a few remaining cancer cells ($\varphi_1 = \epsilon_1$ and $\varphi_2 = \epsilon_2$) that starts dividing again, the tumour will grow if no space limitations are considered ($f = 1$). In this case, the number of cells will be very large regardless of initial age distribution after some finite time. The explanation is again the growth factor $f2F(T_1)$, causing exponential growth.

With crowding, the solutions will reach limit values M_∞ and P_∞, again according to Theorem 5.1. As the initial data do not affect the long term solution, this result is not surprising, i.e. large or small initial data lead to the same limit values. However, for smaller initial age distributions ϵ, a longer time (and more generations through the cell cycle) is required to reach the limit. An interpretation might be that if a larger number of the cancer cells initially are removed so that a tinier fraction of the original tumour remains, there is more time to detect a recurring tumour. Nevertheless, as the solution grows until it reaches its limit, the final size of the tumour might still be many times larger than the post-treatment size and as large as if a larger proportion of the original tumour had been left untreated. The final size is depending on the properties of the crowding function and on the size of the input function.

In conclusion, it is difficult to visually draw a distinction between the cases of having input from cancer stem cells and not having, both when using a constant crowding function and when using a crowding function representing crowding. The reason is that remaining cancer stem cells themselves can cause relapse of a tumour. However in the case where limit values are reached, the size of the limits M_∞ and P_∞ are determined by ψ. Theorem 5.1 states that the values for $\psi = 0$ and $\psi \neq 0$ fulfils different equations and in this sense it is possible to separate the cases $\psi = 0$ and $\psi \neq 0$. In addition, there is a more oscillatory behaviour initially for $\varphi_1 = \varphi_2 = \epsilon$ and $\psi = 0$ than for $\varphi_1 = \varphi_2 = 0$ and $\psi \neq 0$ in Figures 4.15 and 4.16, which means that it could be possible to distinguish the cases $\psi = 0$ and $\psi \neq 0$ also visually. This is something that should be investigated further.

There is a possibility that a tumour decreased to being almost zero sized does not relapse if quorum sensing exists. If there is no contribution from cancer stem cells, such a tumour dies off completely. Observe that this is all in accordance with the first part of Theorem 5.1. However, if there is a nonzero contribution from cancer stem cells, the solutions again reach limits, P_∞ and M_∞. The limits obtained for P are larger for larger values of ψ than for smaller values. An interpretation can be that the tumour is more aggressive the more cancer stem cells it contains, which was proposed in [8].

5.3 Investigation of Upper Bound

As seen in Examples 4.1–4.3 of the *Simulations* chapter, the solution is unbounded and grows exponentially for choices of the constant crowding function f such that $f > 1/(2F(T_1))$. In this section we want to investigate the growth properties of such unbounded solutions further. Approximations and general properties of the solutions will be given both in the case $\psi = 0$ and $\psi > 0$, valid also when not all model components (φ_1, φ_2 and properties of $F(\tau)$) are known. It is often necessary to work with approximate solutions when the knowledge about biological parameters is scarce.

An analytical expression for $M(t)$ becomes complicated to handle even for the simplest of parameter choices. This is true already for the very first interval $t \in [T_1 + T_2]$, as illustrated in Example 5.2.

Example 5.2. We use the specific choice of cumulative distribution function

$$F(\tau) = 1 - \exp\left(-\frac{\tau - c}{a}\right), \tag{5.3}$$

for which $F'(\tau)$ and the transition rate $h(\tau)$ become particularly easy ($h(\tau) = 1/a$), along with constant φ_1, φ_2 and ψ. On the very first interval, $M(t)$ can be computed as

$$M(t) = \begin{cases} \varphi_2, & 0 < t \le T_2, \\ \left(1 - e^{-\frac{t-T_2-c}{a}}\right)(2\varphi_2 + \psi) + \frac{\varphi_1}{a} e^{-\left(\frac{t-T_2}{a}\right)}(T_1 + T_2 - t), & T_2 < t \le 2T_2, \\ (2\varphi_2 + \psi)e^{-\left(\frac{t-T_2-c}{a}\right)}\left(e^{T_2/a} - 1\right) + \\ \quad + (2\varphi_2 + \psi)\left(\left(2e^{\frac{c}{a}} - 2e^{-\left(\frac{t-2T_2-c}{a}\right)}\right) - \frac{2}{a}e^{-\frac{t-2T_2-2c}{a}}(t - 2T_2)\right) + \\ \quad + \frac{2\varphi_1}{a^2}e^{\left(\frac{-t+2T_2+c}{a}\right)}\left((T_1 + T_2)(t - 3T_2) - \frac{t^2}{2} + tT_2\right) + & 2T_2 < t \le T_1 + T_2. \\ \quad + \psi e^{\frac{c}{a}}\left(1 - e^{\frac{-t+2T_2}{a}}\right) + \\ \quad + \frac{\varphi_1}{a}e^{-\left(\frac{t-T_2}{a}\right)}(T_1 + T_2 - t), \end{cases} \tag{5.4}$$

See Appendix A for computations of this result.

The example motivates the need of approximate results. A further motivation comes from the computational difficulty of determining both exact and approximate results, as the integral determining $M(t)$ (and the integral determining $P(t)$) must be split on intervals, whose boundaries are dependent on t. As we already know, this is a consequence of the properties of the kernels $K(t, \sigma)$ and $L(t, \sigma)$ in the integral equations and of the terms involving the initial age distributions, which have an impact on the solution only up until $t = T_1 + T_2$. As a reminder, the equation determining $M(t)$ for the case $f = 1$ is given by

$$M(t) = \int_{\max(t-T_1-T_2,0)}^{\max(t-T_2,0)} (2M(\sigma) + \psi(\sigma))F'(t - T_2 - \sigma)\,\mathrm{d}\sigma + \varphi_2(t - T_2) + \int_0^{T_1} R(t, \sigma)\varphi_1(\sigma)\,\mathrm{d}\sigma. \tag{5.5}$$

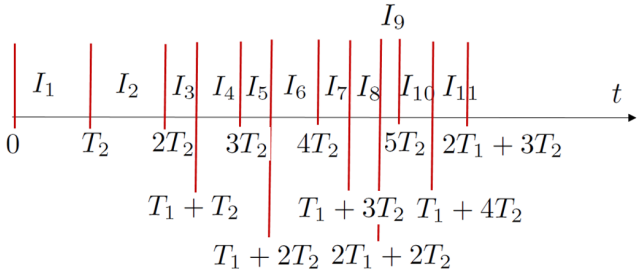

Figure 5.3: Intervals needed to compute exact (and approximate) solutions for $M(t)$.

An illustration of how the intervals for $M(t)$ must be split can be seen Figure 5.3. For the computation of $M(t)$ on the first few intervals, the solution is constructed as follows:

– On interval $I_1 = [0, T_2]$, there is no contribution from the integral or from the term involving $R(t, \sigma)$, but only from φ_2.

– On interval $I_2 = [T_2, 2T_2]$, the integral has lower bound 0 and upper bound $t - T_2$ and only M from interval I_1 contributes. There is also a contribution from the term involving $R(t, \sigma)$, but $\varphi_2 = 0$.

– On interval $I_3 = [T_2, T_1 + T_2]$, the limits of the integral are still 0 and $t - T_2$, but here M from both I_2 and I_3 contribute. Again, there is also a contribution from the term involving $R(t, \sigma)$.

– On interval $I_4 = [T_1 + T_2, 3T_2]$, the integral has lower bound $t - T_1 - T_2$ and gets a contribution from intervals I_1, I_2 and I_3.

– On interval $I_5 = [T_1 + 2T_2, 4T_2]$, there is a contribution from intervals I_2, I_3 and I_4.

This is valid for our current choices $T_1 = 12.5$ and $T_2 = 9$, for which the first intervals of Figure 5.3 have boundaries at $0, 9, 18, 21, 27, 30.5, 36, 39.5, 43, 45, 48.5, 52 \ldots$ In other words is it a demanding job to compute $M(t)$ when t is large.

In this section we find an upper bound for $M(t)$. As the properties of $P(t)$ are given by $M(t)$, we choose to focus on $M(t)$ only. Before approximating M, we make a coarse approximation of the integral involving $R(t, \sigma)$:

$$\begin{aligned}\int_0^{T_1+T_2-t} R(t,\sigma)\,\mathrm{d}\sigma &= \int_0^{T_1+T_2-t} \frac{F'(\sigma+t-T_2)}{1-F(\sigma)}\,\mathrm{d}\sigma \le \frac{1}{1-F(T_1)}\int_0^{T_1+T_2-t} F'(\sigma+t-T_2)\,\mathrm{d}\sigma = \\ &= \frac{F(T_1)-F(t-T_2)}{1-F(T_1)} \le \frac{F(T_1)}{1-F(T_1)}.\end{aligned} \tag{5.6}$$

We will also make use of the estimate

$$0 \le \int_0^t K(t,\sigma)\,\mathrm{d}\sigma = \int_{\max(t-T_1-T_2,0)}^{\max(t-T_2,0)} F'(t-T_2-\sigma)\,\mathrm{d}\sigma \le F(T_1) - F(0) = F(T_1) \tag{5.7}$$

to find upper bounds for $M(t)$ on the intervals $I_k = [k(T_1 + T_2), (k + 1)(T_1 + T_2)]$, $k \ge 1$. Both estimates are based directly on the integral equation determining M, presented in total in Theorem 2.1.

Theorem 5.2. *Let $\gamma_k := \max_{t \in I_k} \psi(t)$. The upper bound M_k for $M(t)$ on interval I_k is given by*

$$M_k = M_0 \left(8F(T_1)^3\right)^k + \sum_{j=1}^{k} \left(8F(T_1)^2\right)^{k-j} \left(4F(T_1)^3 + 2F(T_1)^2 + F(T_1)\right) \max(\gamma_{k-1}, \gamma_k), \tag{5.8}$$

where M_0 is the upper bound on the interval $[0, T_1 + T_2]$, depending on φ_1, φ_2 and ψ.

Proof. It can be shown by using induction that $M(t) < M_k$ on interval I_k, where M_k is given by

$$M_k = 8F(T_1)^3 M_{k-1} + \left(4F(T_1)^3 + 2F(T_1)^2 + F(T_1)\right) \max(\gamma_{k-1}, \gamma_k). \tag{5.9}$$

We can find an estimate M_0 such that $M(t) \le M_0$ – we will return to what this estimate becomes. Assume that $M(t) \le M_{k-1}$ on interval I_{k-1}. The interval $[k(T_1 + T_2), (k + 1)(T_1 + T_2)]$ is divided into subintervals of length T_2. On the first of these intervals we have from the approximation of the integral involving $K(t, \sigma)$ in (5.7) that

$$M(t) \le 2F(T_1) M_{k-1} + F(T_1) \max(\gamma_k, \gamma_{k-1}), \tag{5.10}$$

(and from the integral equation for $M(t)$ directly, see the expression in (5.5)). On the next subinterval of length T_2, the estimate (5.10) is used along with (5.7) and we get

$$\begin{aligned} M(t) &\leq 2F(T_1)\left(2F(T_1)M_{k-1} + F(T_1)\max(\gamma_{k-1},\gamma_k)\right) + F(T_1)\max(\gamma_{k-1},\gamma_k) = \\ &= 4F(T_1)^2 M_{k-1} + \left(2F(T_1)^2 + F(T_1)\right)\max(\gamma_k,\gamma_{k-1}). \end{aligned} \tag{5.11}$$

Finally, on the last subinterval of length $T_1 - T_2$ (we still assume that $2T_2 > T_1 > T_2$), we get

$$\begin{aligned} M(t) &\leq 2F(T_1)\left(4F(T_1)^2 M_{k-1} + \left(2F(T_1)^2 + F(T_1)\right)\max(\gamma_k,\gamma_{k-1})\right) + F(T_1)\max(\gamma_{k-1},\gamma_k) = \\ &= 8F(T_1)^3 M_{k-1} + \left(4F(T_1)^3 + 2F(T_1)^2 + F(T_1)\right)\max(\gamma_{k-1},\gamma_k). \end{aligned} \tag{5.12}$$

The estimate of M_k on interval I_k gives rise to a recursion equation with the solution:

$$M_k = C\left((2F(T_1))^3\right)^k + \sum_{j=1}^{k}\left((2F(T_1))^3\right)^{k-j}\left(4F(T_1)^3 + 2F(T_1)^2 + F(T_1)\right)\max(\gamma_{k-1},\gamma_k), \tag{5.13}$$

where C is given by M_0, the upper bound for $M(t)$ on the interval $[0, T_1 + T_2]$. □

By assuming that ψ is constant and identifying the geometric sum in (5.13), we can rewrite M_k as

$$M_k = \begin{cases} M_{0_\psi}\left((2F(T_1))^3\right)^k + \left(4F(T_1)^3 + 2F(T_1)^2 + F(T_1)\right)\left(\dfrac{(2F(T_1))^3)^k - 1}{(2F(T_1))^3 - 1}\right)\psi, & \text{if } \psi \neq 0, \\ M_0\left((2F(T_1))^3\right)^k, & \text{if } \psi = 0, \end{cases} \tag{5.14}$$

where M_{0_ψ} represents a value of M_0 dependent on ψ which can be approximated using that

$$M(t) = \int_0^{t-T_2}(2M+\psi)\,F'(t-T_2-\sigma)\,\mathrm{d}\sigma + \int_0^{T_1} R(t,\sigma)\varphi_1(\sigma)\,\mathrm{d}\sigma \leq M_0 + \psi F(t-T_2) = M_0 + \psi F(T_1). \tag{5.15}$$

One estimate of M_0 is computed in Appendix B to

$$M_0 = \|\varphi_2\|_\infty\left(2F(T_1) + 2(2F(T_2)-1)F(T_1-T_2)\right) + \|\varphi_1\|_\infty\left(\frac{2F(T_1)}{1-F(T_1)}F(T_1-T_2) + \frac{F(T_1)}{1-F(T_1)}\right). \tag{5.16}$$

Using the expression for M_{0_ψ}, the upper bound M_k from (5.14) can be rewritten as

$$M_k = \begin{cases} \left(M_0 + \psi F(T_1)\right)\left((2F(T_1))^3\right)^k + \left(4F(T_1)^3 + 2F(T_1)^2 + \right. \\ \quad \left. + F(T_1)\right)\left(\dfrac{(2F(T_1))^3)^k - 1}{(2F(T_1))^3 - 1}\right)\psi, & \text{if } \psi \neq 0, \\ M_0\left((2F(T_1))^3\right)^k, & \text{if } \psi = 0, \end{cases} \tag{5.17}$$

A comparison between the upper bound for $M(t)$ given by M_k in (5.17) and the numerical solution from the Simpson's implementation is found in Figure 5.4a. We have found a coarse approximation for the upper bound.

Subtracting the term $M_0((2F(T_1))^3)^k$ from M_k in (5.17), it is possible to tell a difference between the cases $\psi = 0$ and $\psi \neq 0$. An illustration of this is seen in Figure 5.4b for the choice $\varphi_1 = \varphi_2 = 1$. This distinction is only possible to make if it is manageable to get a good approximation of M_0, i.e. if all function values and constants needed to determine M_0 are known – in the way described in Appendix B or in some other way. Here, we assume that this is the case. The remaining term for $\psi \neq 0$ does not depend on the choices of φ_1 and φ_2, but only on ψ and $F(T_1)$ – quantities that we assume that we have good knowledge of.

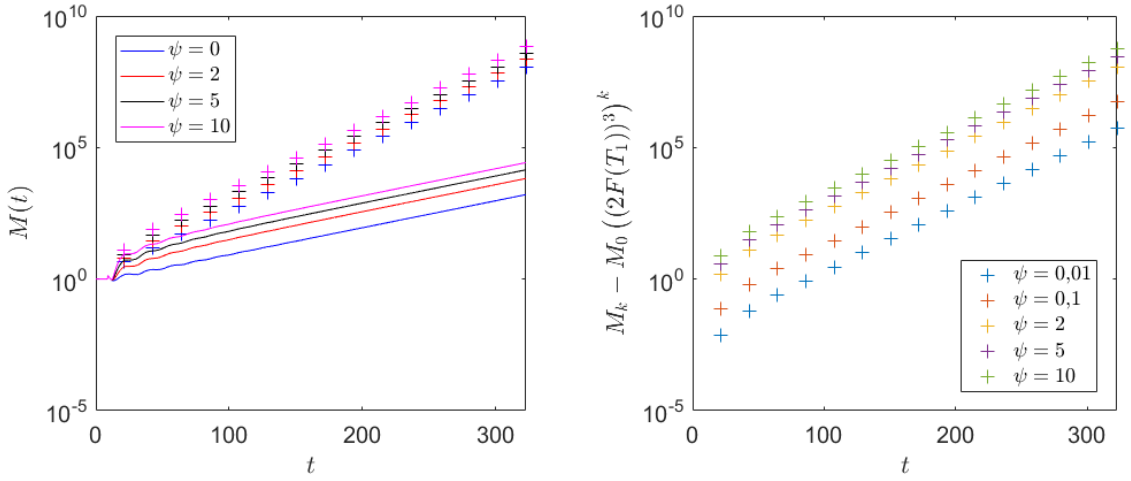

(a) The solution to $M(t)$ computed using Simpson's rule (solid line) compared to an upper bound from (5.17) (marked as +).

(b) Distinction between $\psi = 0$ and $\psi \neq 0$ seen by subtracting the term $M_0((2F(T_1))^3)^k$ from the expression M_k for the upper bound in (5.17). For $\psi = 0$ the remaining quantity is zero.

Figure 5.4: Simulation of $M(t)$ for $\varphi_1(\tau) = \varphi_2(\tau) = 1$ and ψ constant.

We end the section by making a new, coarser approximation of M_{0_ψ} for the interval $[0, T_1 + T_2]$, where only knowledge of $F(T_1)$ and the maximum values of φ_1 and φ_2 are needed. We proceed similarly as in the proof of Theorem 5.2. On the first interval, $t \in [0, T_2]$, $M(t)$ can be approximated by

$$M(t) \leq \|\varphi_2\|_\infty. \tag{5.18}$$

On the subsequent interval of length T_2, using the upper bound of the integral involving $K(t, \sigma)$ from (5.7) and the upper bound of the integral involving $R(t, \sigma)$, (5.6), we have

$$M(t) \leq (2\|\varphi_2\|_\infty + \psi)F(T_1) + \|\varphi_1\|_\infty \frac{F(T_1)}{1 - F(T_1)}, \tag{5.19}$$

where the upper bound from the first interval, $\|\varphi_2\|_\infty$, is used as an approximate value of M. On the last interval of length $T_1 + T_2 - 2T_2 = T_1 - T_2$, the upper approximation from the second interval is used, (5.19), yielding

$$M(t) \leq \left(2\left((2\|\varphi_2\|_\infty + \psi)F(T_1) + \|\varphi_1\|_\infty \frac{F(T_1)}{1 - F(T_1)}\right) + \psi\right) F(T_1) + \|\varphi_1\|_\infty \frac{F(T_1)}{1 - F(T_1)}. \tag{5.20}$$

The expression in (5.20) gives a value for the approximation M_{0_ψ}.

5.4 Impact from the Input Function in the Linear Case

In this section, we investigate the impact from the input function ψ by computing the differences $M_\psi(t) - M_0(t)$ and $P_\psi(t) - P_0(t)$ analytically for a constant crowding function f. Here, $M_\psi(t)$ depends on a constant $\psi > 0$, whereas for $M_0(t)$, $\psi = 0$. From the set of integral equations of Theorem 2.1, $M_\psi(t)$ is given by

$$M_\psi(t) = \int_{\max(t-T_2-T_1,0)}^{\max(t-T_2,0)} (2M(\sigma) + \psi(\sigma))F'(t - T_2 - \sigma)\,\mathrm{d}\sigma + \varphi_2(t - T_2) + \int_0^{T_1} R(t,\sigma)\varphi_1(\sigma)\,\mathrm{d}\sigma, \quad (5.21)$$

leading to the difference

$$M_\psi(t) - M_0(t) = f\left(\int_0^t K(t,\sigma)\psi\,\mathrm{d}\sigma\right) = \psi f\left(\int_{\max(0,t-T_1-T_2)}^{\max(0,t-T_2)} F'(t - \sigma - T_2)\,\mathrm{d}\sigma\right). \quad (5.22)$$

The expression in (5.22) can easily be computed for a general choice of the cumulative distribution function $F(\tau)$:

$$M_\psi(t) - M_0(t) = \begin{cases} 0, & t \le T_2, \\ \psi f F(t - T_2), & T_2 < t < T_1 + T_2, \\ \psi f F(T_1), & t > T_1 + T_2. \end{cases} \quad (5.23)$$

Note that for $t > T_1 + T_2$, we only need to have knowledge of the constants f, ψ and $F(T_1)$ to visualise the difference for M. We next study the difference in the total of number of cells, $P_\psi(t) - P_0(t)$, which can be calculated using the expression from $P(t)$ from the integral equations of Theorem 2.1 given by

$$P(t) = \int_0^t L(t,\sigma)(2M(\sigma) + \psi(\sigma))\,\mathrm{d}\sigma + \int_0^{T_1} S_1(t,\sigma)\varphi_1(\sigma)\,\mathrm{d}\sigma + \int_0^{T_2} S_2(t,\sigma)\varphi_2(\sigma)\,\mathrm{d}\sigma, \quad (5.24)$$

so that

$$P_\psi(t) - P_0(t) = \int_0^t L(t,\sigma)\psi\,\mathrm{d}\sigma. \quad (5.25)$$

We remind of the expression for $L(t,\sigma)$:

$$L(t,\sigma) = \begin{cases} 1, & \text{if } 0 \le t - \sigma < T_2, \\ 1 - F(t - T_2 - \sigma), & \text{if } T_2 \le t - \sigma < T_1, \\ F(T_1) - F(t - T_2 - \sigma), & \text{if } T_1 \le t - \sigma < T_1 + T_2, \\ 0, & \text{otherwise.} \end{cases} \quad (5.26)$$

Let $G(\tau)$ denote the primitive function of $F(\tau)$. Then the difference $P_\psi(t) - P_0(t)$ is given by

$$P_\psi(t) - P_0(t) = \begin{cases} \psi t, & t \le T_2, \\ \psi\left(t + G(0) - G(t - T_2)\right), & T_2 < t \le T_1, \\ \psi\left(F(T_1)(t - T_1) + G(0) - G(t - T_2) + T_1\right), & T_1 < t \le T_1 + T_2, \\ \psi\left(F(T_1)T_2 + G(0) - G(T_1) + T_1\right), & t > T_1 + T_2. \end{cases} \quad (5.27)$$

Note that we in general only have knowledge of $G(\tau)$ if the function $F(\tau)$ is completely known.

Example 5.3. We investigate the differences $M_\psi(t) - M_0(t)$ and $P_\psi(t) - P_0(t)$ for the specific choice of cumulative distribution function

$$F(\tau) = 1 - \exp\left(-\frac{\tau - c}{a}\right), \quad (5.28)$$

with $c = 2.5$, $d = 0.25$ and $a = \frac{T_1 - c}{\log(1/d)}$, similarly as in previous simulations of this M.Sc. thesis. The result is visualised in Figure 5.5 for $f = 1$ and ψ of varying magnitude.

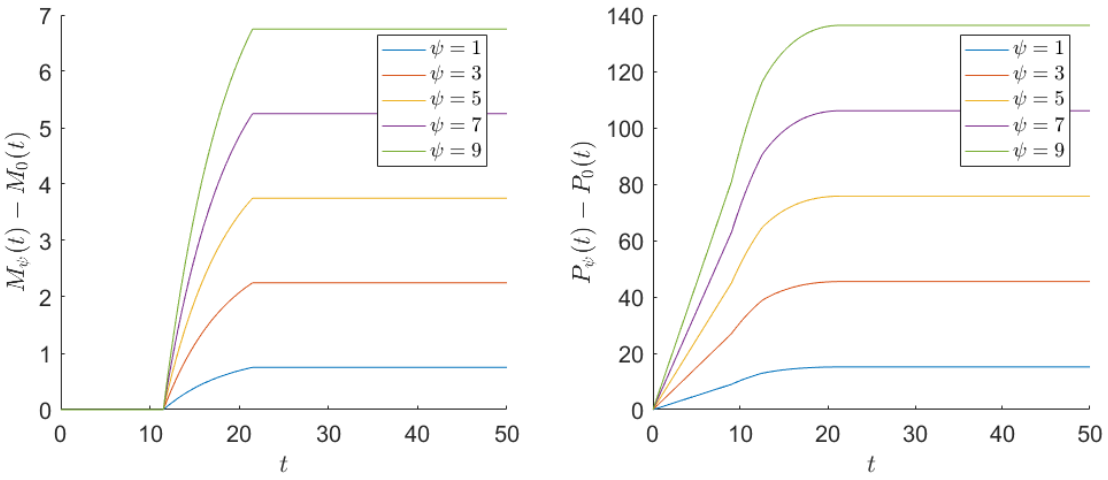

Figure 5.5: Impact from input function ψ computed by analytically taking the difference between the solutions where $\psi > 0$ and $\psi = 0$.

Computations of the difference $M_\psi(t) - M_0(t)$ and $P_\psi(t) - P_0(t)$ are not possible to do analytically if the crowding function f is nonconstant. However, the result from the case with f constant has an important role as a constant crowding function is valid for a system where the population size yet is too small for space limitations to have an effect.

6 Investigation of Numerical Error

The error and order of accuracy of the trapezoidal and Simpson's implementations are investigated for a few numerical examples, to validate that the implementations are as accurate as stated in the chapter *Numerical Methods*, (3), and that the error is kept sufficiently small. First, in Section 6.1, the order of accuracy of the implementations is studied, both for f constant and f nonconstant. In Section 6.2, the error is computed against a reference taken to be the correct solution, obtained numerically using a very small step size. Finally, in Sections 6.3 and 6.4, we derive analytical expressions for the error in the linear and the nonlinear case (f constant and f nonconstant), in the linear case using both the trapezoidal rule and Simpson's rule and in the nonlinear case using the trapezoidal rule only.

6.1 Numerical Investigation on the Order of Accuracy

A method of order p has an error expansion of the form $E(h) = Ch^p + \mathcal{O}(h^r)$, where C is some fixed constant determined by the integrand and where $p < r$. See the Euler-Maclaurin summation formula of Lemma 3.1, valid for the trapezoidal rule with a sufficiently smooth integrand, for comparison. Supposing that the error from the computation of $M(t)$ can be expressed in this way, we let M_h denote $M(T)$ approximated using step size h and form the quotient

$$\frac{M_h - M_{h/2}}{M_{h/2} - M_{h/4}} = \frac{Ch^p - C(h/2)^p + \mathcal{O}(h^{p+1})}{C(h/2)^p - C(h/4)^p + \mathcal{O}(h^{p+1})} = \frac{1 - 2^{-p} + \mathcal{O}(h)}{2^{-p} - 2^{-2p} + \mathcal{O}(h)} = 2^p + \mathcal{O}(h). \tag{6.1}$$

A value p for the order of accuracy can thus be estimated as

$$p = \log_2 \left(\left| \frac{M_h - M_{h/2}}{M_{h/2} - M_{h/4}} \right| \right). \tag{6.2}$$

The quotient (6.2) is computed multiple times to get a reliable measure of the order of accuracy using a sequence of different step sizes, $h, h/2, h/4, h/8, h/16, \ldots$. This is to assure that we have reached the asymptotic region of the problem, i.e. that the step size h is made sufficiently small to get approximately the same value of p in subsequent computations of (6.2). The order of accuracy for $P(T)$ is computed in the same manner. It is of importance to compare the very same point in the discretized solution of $M(T)$ and $P(T)$ for the various step sizes, i.e. to compare the points $M_h(ih)$, $M_{h/2}(2i \cdot \frac{h}{2})$, $M_{h/4}(4i \cdot \frac{h}{4})$ etc., where $T = ih$. If values are compared for points that are one step of length h off from each other, i.e. if we for instance compare $M_h(ih)$ and $M_{h/2}(2i \cdot \frac{h}{2} - h)$, it is not possible to get a reliable measure of the accuracy. The quotient (6.2) does not tell anything about the size of the error, but only about the relative error when solutions computed with varying step sizes are compared. It is here assumed that the correct, analytical value of M and P are unknown.

In this way, it is possible to validate the numerical implementation and assure that the expected order of accuracy is obtained. If this is not the case, there might be an error in the implementation. Alternatively, in the case with crowding, the discontinuity at $t = T_2$ might cause a reduction in the order of accuracy. In the case with a constant crowding function, $f = 1$, the order of accuracy was validated numerically both for the trapezoidal and for Simpson's rule, yielding second and fourth order accuracy ($p = 2$ and $p = 4$ respectively), see Figure 6.1. In the case with crowding (f nonconstant), second order accuracy was validated using the scheme based on the trapezoidal rule, see Figure 6.2. The order of accuracy was determined for the four intervals $0 < t \leq T_2$, $T_2 < t \leq T_1$, $T_1 < t \leq T_1 + T_2$ and $T_1 + T_2 < t \leq T$. In the example calculations documented here, $T = 100$ (larger values of T were also tested). Tests were performed for $h = 1/2^k$, $k = 1, 2, \ldots, 9$.

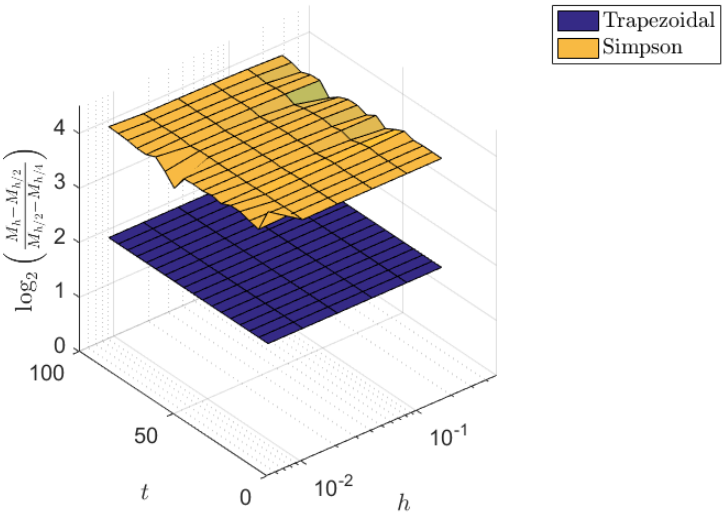

Figure 6.1: Investigation of the order of accuracy for the case $f = 1$. Fourth order accuracy is obtained for Simpson's rule and second order accuracy for the trapezoidal rule. The choice of ψ, φ_1 and φ_2 does not affect the result.

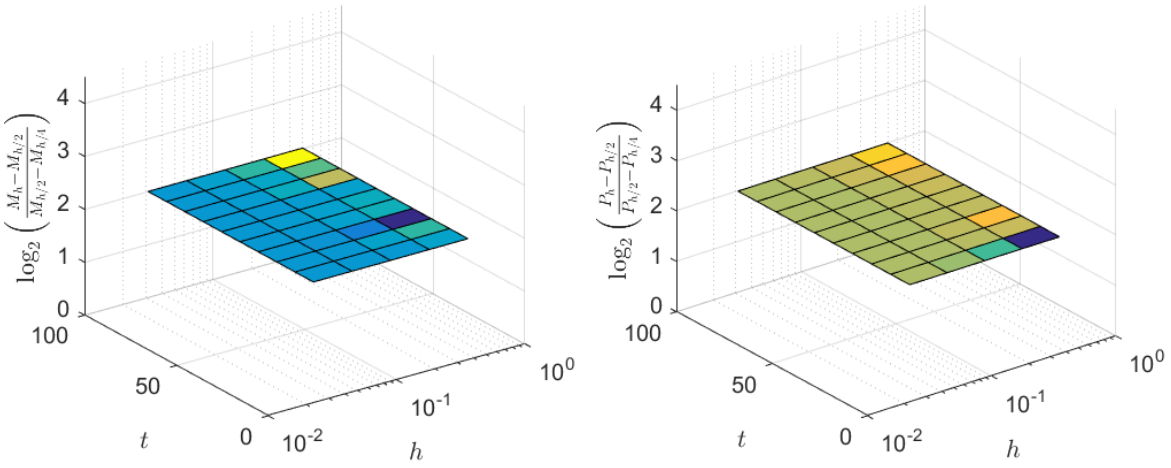

Figure 6.2: Investigation of the order of accuracy for the case $f(p) = 1/\cosh(0.01p)$ and the trapezoidal implementation. Dark blue, dark yellow and green fields indicate an order of accuracy slightly different from $p = 2$ for the largest step size $h = 1/2$. However, the discrepancy is small. The choices of ψ, φ_1 and φ_2 do not affect the result.

6.2 Numerical Investigation of the Error

We are now interested in determining the size of the absolute error in the implementation. This is done numerically, where we assume that the correct, analytical value of $M(T)$ and $P(T)$ now are given and want to determine the error introduced by approximating the true values M and P by M_h and P_h, computed using the step size h. In practice, M and P are computed using a much smaller step size than what is normally chosen (in this particular case we choose $h = 0.001$ and $T = 100$, solving

the system using 10^5 points). The error can be written as an expansion of the form

$$M_h - M = C_1 h^p + C_2 h^r + \ldots, \tag{6.3}$$

where C_1 and C_2 are some constants given by the problem and where $p < r$. Ideally, $p = 2$ for the trapezoidal rule and $p = 4$ for Simpson's rule (under the condition that the integrand is sufficiently differentiable). In Section 6.1, we obtained the expected results for the both methods (where Simpson's rule was used only for a constant crowding function where the integrand always is C^3). We will now give further evidence for this. Using (6.3), we can approximate the constant p_1 from

$$\log |M_h - M| = \log |C_1| + p_1 \log h + \mathcal{O}(h). \tag{6.4}$$

In Figures 6.3–6.5, the error is plotted against the step size h for varying crowding functions f. The largest step size that theoretically can be used is $h = 0.5$ for our current choice of T_1, as we must choose the grid so that a grid point hits T_1 exactly. It is again validated that we obtain second order accuracy using the trapezoidal rule and fourth order accuracy using Simpson's rule. The absolute error is slightly larger in the computations for P than in the computations for M. As Simpson's rule for a constant crowding function is fourth order accurate, the error can be decreased with an increased number of integration point much more rapidly than in the case with a nonconstant crowding function.

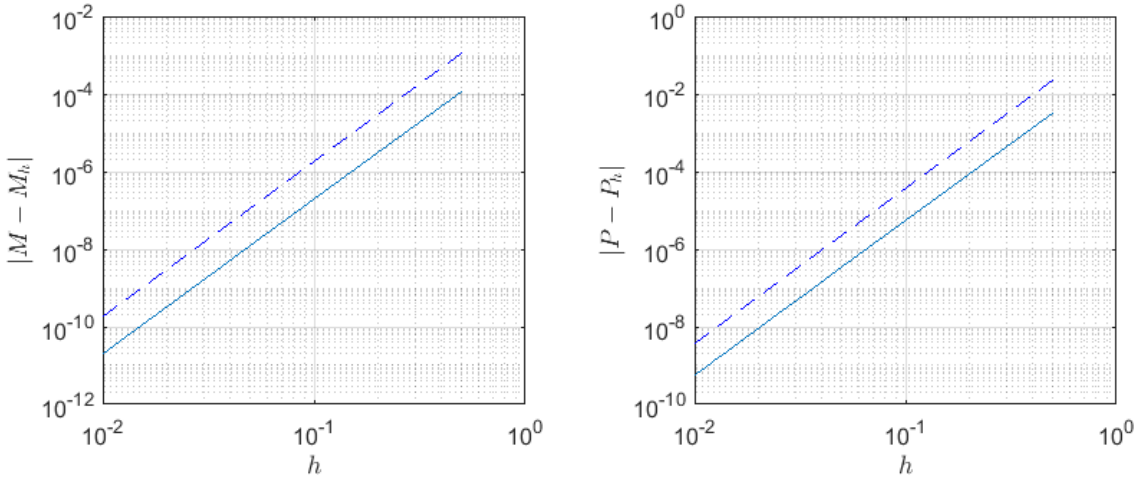

Figure 6.3: Error (solid line) plotted against step size for constant crowding function $f = 1$ and input function $\psi = 0$. Dotted line has slope four and a comparison yields that the solution is fourth order accurate using Simpson's rule.

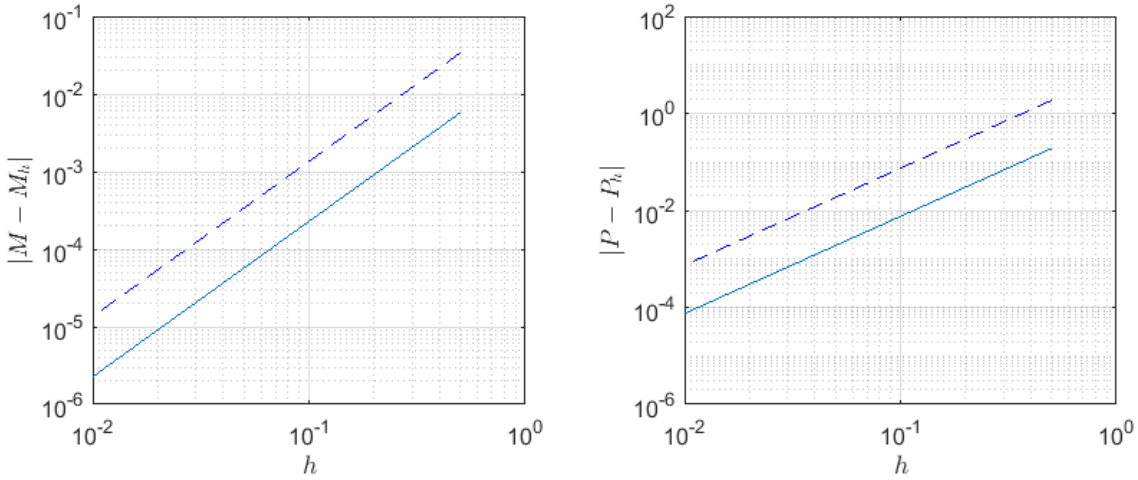

Figure 6.4: Error (solid line) plotted against step size for a crowding function representing crowding, $f(p) = f_1(p) = 1/\cosh(0.01p)$. The input function is chosen to $\psi = 0$. Dotted line has slope two (note that the slope is the same for M and P) and a comparison yields that the solution is second order accurate using the trapezoidal rule.

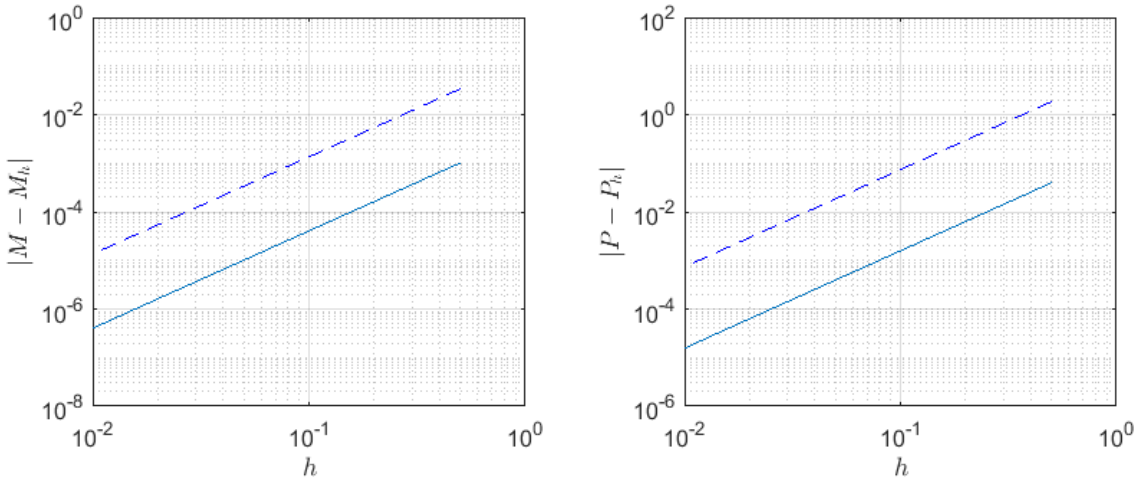

Figure 6.5: Error (solid line) plotted against step size for a crowding function representing quorum sensing and crowding, $f(p) = f_5(p)$. The input function is chosen to $\psi = 2$. Dotted line has slope two and a comparison yields that the solution is second order accurate using the trapezoidal rule.

We return to Romberg's method, described in Lemma 3.2, and ask the question whether it is possible to improve the second order accuracy obtained through the trapezoidal rule to fourth order accuracy by using this method. The result is visualised in Figures 6.6–6.8. It can be validated both for crowding functions representing crowding and crowding functions representing quorum sensing that it is possible to obtain an order of accuracy of at least three. Tests are performed for various end points T, to study whether the same order of accuracy is obtained for the computations regardless of in what point the solution is investigated. The results are visualised here for $T = 12$, $T = 50$ and $T = 100$. For large T, fourth order accuracy is obtained, see Figures 6.6-6.7. The reason why we have a more accurate solution for larger T than for e.g. $T = 12$, close to the discontinuity, is that the discontinuity

does not affect the computation of M or P for large t. Third order accuracy is obtained for $T = 12$, see Figure 6.8. This is a much better result than the second order accuracy obtained using Simpson's rule. In the latter case, the error caused by the discontinuity at the point $t = T_2$ propagates and introduces an error for $t > T_2$, Using Romberg's method, the error does not have as large an impact.

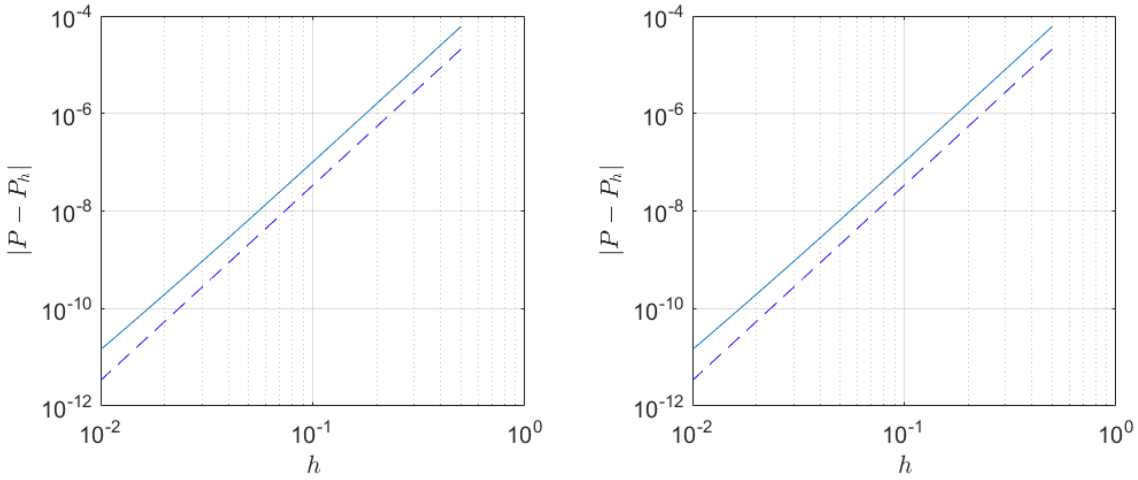

Figure 6.6: Applying Romberg's method: Error (solid line) plotted against step size for a crowding function representing crowding, $f(p) = f_1(p)$. The input function is chosen to $\psi = 0$ and $T = 100$. Dotted line has now slope four and a comparison yields that the solution is fourth order accurate.

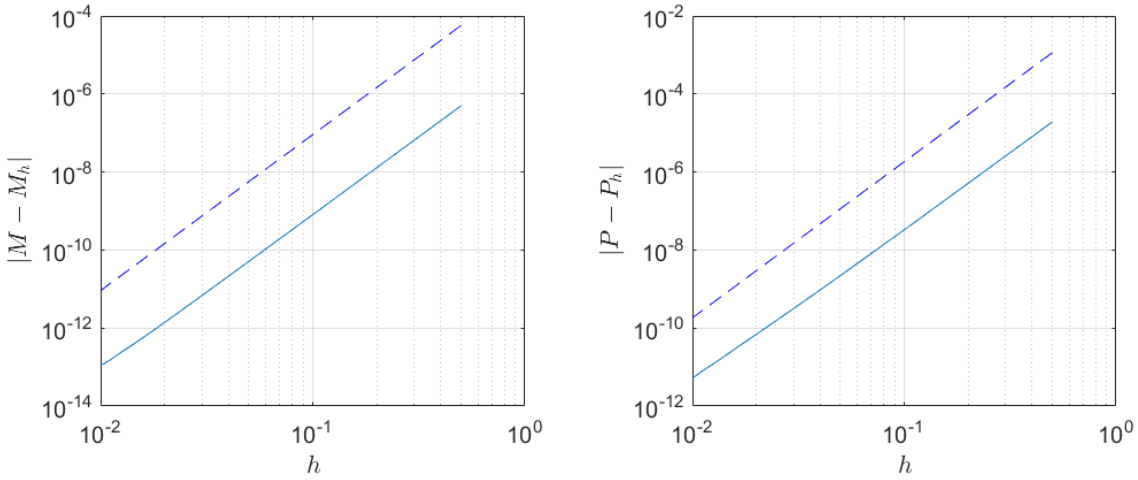

Figure 6.7: Applying Romberg's method: Error (solid line) plotted against step size for $f(p) = f_1(p)$. The input function is now chosen to $\psi = 2$ and $T = 60$. Dotted line has slope four and a comparison yields that the solution is fourth order accurate.

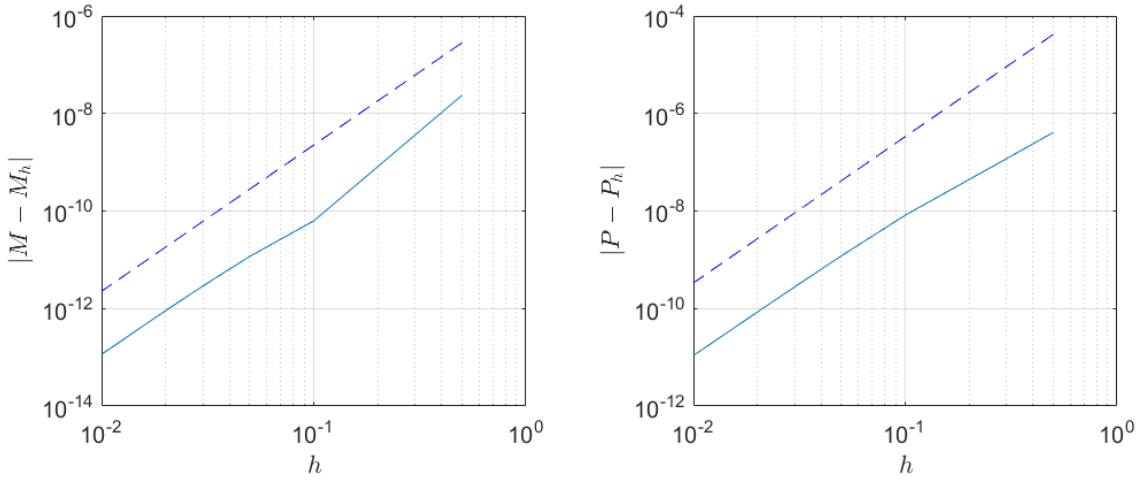

Figure 6.8: Applying Romberg's method: Error (solid line) plotted against step size for a crowding function representing quorum sensing and crowding, $f(p) = f_5(p)$. Now, $T = 12$ and $\psi = 0$. Dotted line has slope three. A comparison yields that the solution is third order accurate.

We saw in Section 3.5 that Romberg's method of order two, which is here applied, agrees with Simpson's rule and yields fourth order accuracy under the condition that the integrand is C^3. If this was the case when crowding is taken into account, we should have obtained a slope of four, illustrating fourth order accuracy, in Figures 6.6–6.8 and in fact, we do for large t. The order of accuracy obtained is maximally four and always considerably larger than two in the examples. It can thus be concluded that it is possible to improve the order of accuracy notably using Romberg's method. However, the degree of improvement seems to vary between different T. We also note that for small h, the absolute size of the error is very small.

6.3 Analytical Investigation of the Error - the Linear Case

After having assured numerically that the size of the error decreases as expected when h is increased and that the numerical error is sufficiently small, we end the chapter by finding analytical expressions for the error, in this section first in the linear case (for a constant crowding function f). We will see that is not trivial to make such computations. A constant input function ψ is used, similarly as in the simulations section, and in accordance with all other numerical work of this report, we assume that $2T_2 > T_1 > T_2$. We choose to focus on the case $t > T_1 + T_2$ and to find an expression for the error in the equation determining $M(t)$:

$$M(t) = \int_{t-T_1-T_2}^{t-T_2} F'(t - T_2 - \sigma)(2M(\sigma) + \psi)\,\mathrm{d}\sigma. \tag{6.5}$$

We note that the distance between the end points of the integral in (6.5) is T_1.

Returning to the Euler-Maclaurin summation formula from Lemma 3.1, we remember that the trapezoidal rule approximates the integral $\int_a^b g(x)\,\mathrm{d}x$ as $\int_a^b g(x)\,\mathrm{d}x \approx T(h)$, where

$$\begin{aligned} T(h) = \int_a^b g(x)\,\mathrm{d}x + \frac{h^2}{12}[g'(b) - g'(a)] - \frac{h^4}{720}[g'''(b) - g'''(a)] + \frac{h^6}{30240}[g^{(5)}(b) - g^{(5)}(a)] + \\ + \cdots + c_{2r}h^{2r}[g^{(2r-1)}(b) - g^{(2r-1)}(a)] + \mathcal{O}(h^{2r+2}), \end{aligned} \tag{6.6}$$

for some constants c_{2r}. Neglecting higher order terms, the error E from computing $\int_a^b g(x)\,\mathrm{d}x$ in one

step (so that $h = b - a$), can be written as

$$E = \frac{(b-a)^3}{12} g''(\xi) = \frac{h^3}{12} g''(\xi), \quad \text{for some } \xi \in [a, b]. \tag{6.7}$$

This follows from the mean value theorem, stating that

$$\frac{g'(b) - g'(a)}{b-a} \approx g''(\xi), \quad \text{for some } \xi \in [a, b] \tag{6.8}$$

(given that g is C^2). Using a composite method, the global truncation error is obtained by taking the sum of the local truncation errors [3]. Thus, using the composite trapezoidal rule with n segments, where each segment is given by $[a + (i-1)h, a + ih]$ and the step size is $h = (b-a)/n$, the total error E_t is given by a summation of the errors on each segment, E_i. In other words,

$$E_t = \sum_{i=1}^{n} E_i = \frac{h^3}{12} \sum_{i=1}^{n} g''(\xi_i) = \frac{(b-a)^3}{12n^3} \sum_{i=1}^{n} g''(\xi_i), \tag{6.9}$$

where ξ_i is a point on segment i. The total error can be rewritten as

$$E_t = \frac{(b-a)^3}{12n^2} \sum_{i=1}^{n} \frac{g''(\xi_i)}{n}, \tag{6.10}$$

where $\dfrac{g''(\xi_i)}{n}$ can be interpreted as a mean value of g'' on the interval $[a, b]$.

In the equation determining $M(t)$, E_i is given by

$$E_i = \frac{T_1^3}{12n^3} \Big(2M''(\xi_i) F'(t - T_2 - \xi_i) - F''(t - T_2 - \xi_i) 4M'(\xi_i) + (2M(\xi_i) + \psi) F^{(3)}(t - T_2 - \xi_i) \Big) \tag{6.11}$$

for $\xi_i \in (t - T_1 - T_2, t - T_2)$. The value of $M(t)$ must be known to calculate the error, which is an issue, as $M(t)$ hardly can be calculated analytically. We must therefore replace $M(t)$ by some approximated upper bound, for instance the one determined in Section 5.3. The error formula then reduces to

$$E_i = \frac{T_1^3}{12n^3} (2M(\xi_i) + \psi) F^{(3)}(t - T_2 - \xi_i). \tag{6.12}$$

For Simpson's rule, the error E from calculating $\int_a^b g(x)\,\mathrm{d}x$, using one segment only and neglecting higher order terms, becomes

$$E = -\frac{(b-a)^5}{2880} g^{(4)}(\xi) = -\frac{h^5}{90} g^{(4)}(\xi), \text{ where } a < \xi < b \text{ and } b - a = 2h \quad [7]. \tag{6.13}$$

For a multiple-segment implementation of Simpson's rule, the error for one segment, $[a + 2(i-1)h, a + 2ih]$, becomes

$$E_i = -\frac{(a + 2(i-1)h - (a + 2ih))^5}{2880} g^{(4)}(\xi) = -\frac{h^5}{90} g^{(4)}(\xi), \text{ where } a + 2(i-1)h < \xi_i < a + 2ih, \tag{6.14}$$

leading to the total error

$$E_t = \sum_{i=1}^{n/2} E_i = -\frac{h^5}{90} \sum_{i=1}^{n/2} g^{(4)}(\xi_i) = -\frac{(b-a)^5}{90n^5} \sum_{i=1}^{n/2} g^{(4)}(\xi_i) = -\frac{(b-a)^5}{90n^4} \sum_{i=1}^{n/2} \frac{g^{(4)}(\xi_i)}{n}. \tag{6.15}$$

The upper summation bound $n/2$ is due to the fact that two segments of length h are joined to compute one approximate value using Simpson's rule. In the trapezoidal implementation, an approximation is computed for every segment of length h. It is now possible to identify from (6.13) that the local error in the Simpson implementation is $\mathcal{O}(h^5)$ whereas the global error, in (6.15), is $\mathcal{O}(h^4)$, as stated earlier. In the computation of $M(t)$, using an upper bound for M on each interval, the total error can be written as

$$E_t = -\frac{(T_1)^5}{90n^5}\sum_{i=1}^{n/2}(2M(\xi_i)+\psi)F^{(5)}(t-T_2-\xi_i). \tag{6.16}$$

This holds under the assumption that $M(t)$ is calculated at a time t such that the number of integration points n are even. As we know that the distance between the end points of the integral determining M is T_1, we can for the computation of M specifically choose $n = T_1/h$ in such a way that n is even. However, for the sake of completeness, we also investigate the error in the case when n is odd. The error formula is slightly different in this case, as one step of Simpson's 3/8 rule is applied in the last step of the computations. In general, computing the integral $\int_a^b g(x)\,\mathrm{d}x$ using one step of Simpson's 3/8 rule yields the error

$$E_t = -\frac{(b-a)^5}{6480n^5}g^{(4)}(\xi) = -\frac{3h^5}{80}g^{(4)}(\xi), \text{ where } a<\xi<b \text{ and } b-a=3h \quad [7]. \tag{6.17}$$

The total error for $M(t)$ when n is odd thus becomes

$$E_t = -\frac{(T_1-3h)^5}{90n^5}\sum_{i=1}^{(n-3)/2}(2M(\xi_i)+\psi)F^{(5)}(t-T_2-\xi_i) - \frac{3h^5}{80}(2M(\xi_i)+\psi)F^{(5)}(t-T_2-\xi_{\text{end}}), \tag{6.18}$$

where $\xi_i \in (t-T_1-T_2, t-T_2-3h)$ and $\xi_{\text{end}} \in (t-T_2-3h, t-T_2)$.

However, using a very coarse estimate as the upper bound for M on each interval, the estimates of the error becomes coarse, both for the trapezoidal and for the Simpson implementation. As the methods are convergent, meaning that $|M - M_h| \to 0$ as $h \to 0$, the reference computed numerically in Section 6.2 gives a reliable measure of the error that fits our purpose well and we do therefore not compute an upper bound of the error using the derived analytical expression.

6.4 Analytical Investigation of the Error - the Nonlinear Case

For a nonconstant crowding function f, the numerical error is investigated analytically only for the trapezoidal rule. We start by introducing the notation in Table 1.

Table 1: Notation used in the nonlinear error analysis

Notation	**Explanation**
$P_{\text{corr}}(t)$, $M_{\text{corr}}(t)$	Correct, analytical value of $P(t)$ and $M(t)$,
$P_{\text{dist}}(t)$, $M_{\text{dist}}(t)$	Disturbed value of $P(t)$ and $M(t)$, influenced by errors,
$P_{\text{err}}(t)$, $M_{\text{err}}(t)$	Total error in $P(t)$ and $M(t)$ at time t,
$\Delta P(t)$, $\Delta M(t)$	Truncation error from the trapezoidal scheme in the computation of the main integrals in $P(t)$ and $M(t)$,
$R_{\text{corr}}(t)$	Correct, analytical value of the integral $\int_0^{T_1} R(t,\sigma)\varphi_1(\sigma)\,\mathrm{d}\sigma$,
$\Delta R(t)$, $\Delta S_1(t)$, $\Delta S_2(t)$	Error from the computation of the respective integrals (exist only up to $t = T_1 + T_2$.).

The error in the equation determining $P(t)$ is given by

$$\begin{aligned} P_{\text{err}}(t) = P_{\text{dist}}(t) - P_{\text{corr}}(t) &= \int_0^t L(t,\sigma)(2M_{\text{err}}(\sigma))\,\mathrm{d}\sigma + \Delta S_1(t) + \Delta S_2(t) + \Delta P(t) \\ \Leftrightarrow\ P_{\text{err}}(t) - \frac{h}{2}L(t,t)M_{\text{err}}(t) &= \sum[M_{\text{err}} : L_{\text{terms}}] + \Delta S_1(t) + \Delta S_2(t) + \Delta P(t) \\ \Leftrightarrow\ P_{\text{err}}(t) - \frac{h}{2}M_{\text{err}}(t) &= \sum[M_{\text{err}} : L_{\text{terms}}] + \Delta S_1(t) + \Delta S_2(t) + \Delta P(t), \end{aligned} \tag{6.19}$$

where we denote by $\sum[M_{\text{err}} : L_{\text{terms}}]$ the summation of terms approximating the integral $\int_0^t L(t,\sigma)2M_{\text{err}}(\sigma)\,\mathrm{d}\sigma$ with the trapezoidal rule, (involving the computations on separate intervals given by the discontinuities in $L(t,\sigma)$). To get an estimate of the error from the equation determining $M(t)$ we start be linearising f around $P_{\text{corr}}(t)$,

$$f(P_{\text{dist}}(t)) \approx f(P_{\text{corr}}(t)) + f'(P_{\text{corr}}(t))P_{\text{err}}(t). \tag{6.20}$$

Then,

$$\begin{aligned} M_{\text{dist}}(t) = \Big(f(P_{\text{corr}}(t)) + f'(P_{\text{corr}}(t))P_{\text{err}}(t)\Big) \Bigg(\int_{t_{\text{start}}}^{t_{\text{end}}} K(t,\sigma)(2M(\sigma) + 2M_{\text{err}}(\sigma) + \psi(\sigma))\,\mathrm{d}\sigma + \\ + R_{\text{corr}}(t) + \Delta R(t) + \varphi_2(T_2 - t) + \Delta M(t)\Bigg), \end{aligned} \tag{6.21}$$

where t_{start} and t_{end} are the boundaries of the integral determining $M(t)$. We introduce the notation

$$\Phi(t) = \int_{t_{\text{start}}}^{t_{\text{end}}} K(t,\sigma)(2M(\sigma) + 2M_{\text{err}}(\sigma) + \psi(\sigma))\,\mathrm{d}\sigma + R_{\text{corr}}(t) + \Delta R(t) + \varphi_2(T_2 - t) + \Delta M(t) \tag{6.22}$$

to simplify the expression for $M_{\text{dist}}(t)$ so that

$$M_{\text{dist}}(t) = \Big(f(P_{\text{corr}}(t)) + f'(P_{\text{corr}}(t))P_{\text{err}}(t)\Big)\Phi(t). \tag{6.23}$$

Subtracting the correct solution,

$$M_{\text{corr}}(t) = f(P_{\text{corr}}(t)) \left(\int_{t_{\text{end}}}^{t_{\text{start}}} K(t,\sigma)(2M(\sigma) + \psi(\sigma))\,\mathrm{d}\sigma + R_{\text{corr}}(t) + \varphi_2(T_2 - t)\right), \tag{6.24}$$

from $M_{\text{dist}}(t)$ gives an equation in $P_{\text{err}}(t)$ and $M_{\text{err}}(t)$:

$$\begin{aligned} M_{\text{err}}(t) - f'(P_{\text{corr}}(t))P_{\text{err}}(t)\Phi(t) = f(P_{\text{corr}}(t)) \left(\int_{t_{\text{end}}}^{t_{\text{start}}} K(t,\sigma)(2M_{\text{err}}(\sigma))\,\mathrm{d}\sigma + \Delta R(t) + \Delta M(t)\right) \approx \\ \approx f(P_{\text{corr}}(t)) \left(\sum[M_{\text{err}} : K_{\text{terms}}] + \Delta R(t) + \Delta M(t)\right), \end{aligned} \tag{6.25}$$

where we denote by $\sum[M_{\text{err}} : K_{\text{terms}}]$ the summation of terms approximating the integral $\int_{t_{\text{end}}}^{t_{\text{start}}} K(t,\sigma)(2M_{\text{err}}(\sigma))\,\mathrm{d}\sigma$. Collected, the system from which $P_{\text{err}}(t)$ and $M_{\text{err}}(t)$ can be determined thus becomes

$$\begin{bmatrix} 1 & -f'(P_{\text{corr}}(t))\Phi(t) \\ -\frac{h}{2} & 1 \end{bmatrix} \begin{bmatrix} M_{\text{err}}(t) \\ P_{\text{err}}(t) \end{bmatrix} = \begin{bmatrix} f(P_{\text{corr}}(t)) \left(\sum[M_{\text{err}} : K_{\text{terms}}] + \Delta R(t) + \Delta M(t)\right) \\ \sum[M_{\text{err}} : L_{\text{terms}}] + \Delta P(t) + \Delta S_1(t) + \Delta S_2(t) \end{bmatrix}. \tag{6.26}$$

The system is of the form

$$\begin{bmatrix} 1 & a \\ b & 1 \end{bmatrix} \begin{bmatrix} M_{\text{err}}(t) \\ P_{\text{err}}(t) \end{bmatrix} = \begin{bmatrix} C \\ D \end{bmatrix}. \tag{6.27}$$

Assuming the matrix is non-singular, a solution is given by

$$\begin{cases} M_{\text{err}}(t) = \dfrac{C - aD}{1 - ab}, \\ P_{\text{err}}(t) = \dfrac{D - bC}{1 - ab}. \end{cases} \tag{6.28}$$

For the very first interval, where $t < T_2$, the system reduces to

$$\begin{bmatrix} 1 & -f'(P_{\text{corr}}(t))\varphi_2(T_2 - t) \\ -\frac{h}{2} & 1 \end{bmatrix} \begin{bmatrix} M_{\text{err}}(t) \\ P_{\text{err}}(t) \end{bmatrix} = \begin{bmatrix} 0 \\ \sum[M_{\text{err}} : L_{\text{terms}}] + \Delta P(t) + \Delta S_1(t) + \Delta S_2(t) \end{bmatrix}. \tag{6.29}$$

Using upper estimates for all terms denoting an error, ΔP, ΔM, ΔS_1 and ΔS_2, it can be concluded that

$$\begin{aligned} M_{\text{err}}(t) &\lessapprox \frac{(f'(P_{\text{corr}}(t))\varphi_2(T_2 - t))\left(\sum[M_{\text{err}} : L_{\text{terms}}] + \Delta P(t) + \Delta S_1(t) + \Delta S_2(t)\right)}{1 - \frac{h}{2} f'(P_{\text{corr}}(t))\varphi_2(T_2 - t)}, \\ P_{\text{err}}(t) &\lessapprox \frac{\sum[M_{\text{err}} : L_{\text{terms}}] + \Delta P(t) + \Delta S_1(t) + \Delta S_2(t)}{1 - \frac{h}{2} f'(P_{\text{corr}}(t))\varphi_2(T_2 - t)}. \end{aligned} \tag{6.30}$$

It now remains to find expressions for the terms involved in the solutions, in order to be able to draw a conclusion about the order of the error:

- The expressions M_{corr} and P_{corr} are treated as constants and if the error is to be determined numerically, M_{corr} and P_{corr} are replaced by the numerical solution for $M(t)$ and $P(t)$.
- The trapezoidal approximations $\sum[M_{\text{err}} : K_{\text{terms}}]$ and $\sum[M_{\text{err}} : L_{\text{terms}}]$ are given by αh and βh, for some constants α and β. The integrals are divided in different intervals depending on for what t we investigate the error and the properties of $K(t, \sigma)$ and $L(t, \sigma)$.
- The errors ΔP and ΔM are given from the calculations of the integrals $\int_0^t L(t, \sigma)(2M(\sigma) + 2M_{\text{err}}(\sigma) + \psi(\sigma))\,\mathrm{d}\sigma$ and $\int_{t_{\text{start}}}^{t_{\text{end}}} K(t, \sigma)(2M(\sigma) + 2M_{\text{err}}(\sigma) + \psi(\sigma))\,\mathrm{d}\sigma$, where the error can be approximated using the error formula for the trapezoidal rule in (6.9) and where $M(\sigma)$ and $M_{\text{err}}(\sigma)$ are approximated from above by constants determined by the maximum value on the interval of integration for the numerical solution of $M(t)$ and M_{err} respectively.
- The errors ΔS_1, ΔS_2 and ΔR can be computed directly using the error formula for the trapezoidal rule in (6.9).
- The expression $\Phi(t)$ can be computed as

$$\Phi(t) = \frac{M_{\text{corr}}(t)}{f(P_{\text{corr}}(t))} + \sum[M_{\text{err}} : K_{\text{terms}}] + \Delta R(t) + \Delta M(t), \tag{6.31}$$

  for $t > T_2$.

Computing the error in the very first points, $t = 0$ and $t = h$, we get

$$\begin{aligned} P_{\text{err}}(0) &= \Delta S_1(0) + \Delta S_2(0) = A_1 h^2, \\ M_{\text{err}}(0) &= f'(P_{\text{corr}}(0)) P_{\text{err}}(0) \varphi(T_2) = A_2 h^2, \end{aligned} \tag{6.32}$$

for some constants A_1 and A_2 and

$$\begin{aligned} M_{\text{err}}(h) &\lessapprox \frac{f'(P_{\text{corr}}(h))\varphi(T_2-h)\left[(h/2)M_{\text{err}}(0)+\Delta P(t)+\Delta S_1(h)+\Delta S_2(h)\right]}{1-\frac{h}{2}f'(P_{\text{corr}}(h))\varphi_2(T_2-h)} = A_3h^2, \\ P_{\text{err}}(h) &\lessapprox \frac{(h/2)M_{\text{err}}(0)+\Delta P(t)+\Delta S_1(h)+\Delta S_2(h)}{1-\frac{h}{2}f'(P_{\text{corr}}(h))\varphi_2(T_2-h)} = A_4h^2, \end{aligned} \tag{6.33}$$

for some constants A_3, A_4. By recursive computation of $M_{\text{err}}(t)$ and $P_{\text{err}}(t)$ in this way, it is possible to see that the error at every point is $\mathcal{O}(h^2)$.

Sample calculations are not performed to compute a bound for the error using the derived formulas. However, the section demonstrates how an error analysis could be performed for the problem.

7 Discussion and Future Work

In this M.Sc. thesis, the system of PDEs describing the number densities in the two phases of the cell cycle was initially derived. The equivalent system of integral equations was implemented and solved numerically in MATLAB using the trapezoidal and Simpson rules, and in the former case, also by applying Romberg's method. Simulations of the notions of crowding and quorum sensing have been done along with simulations with constant crowding, visualising systems that grow exponentially or approach a steady state for the total number of cells. In a case study examining whether an almost zero sized tumour can relapse, it was found that the choices of crowding function, input function and initial age distributions all contribute. A tumour is kept zero sized only if it is assumed that quorum sensing exists or if the tumour is removed completely and no cancer stem cells exist.

Due to the characteristics of the coupled integral equations, it was not manageable to solve the system involving nonlinearities (the system for f nonconstant) using Simpson's rule, but only using the trapezoidal rule, a second order method. An improvement of the solution could therefore have been to adopt a method of variable step length to solve the set of coupled integral equations, yielding a more accurate implementation. An alternative is to use so called Richardson extrapolation to eliminate the constants of the error expansion

$$E = C_1 h^p + C_2 h^r + \dots \tag{7.1}$$

Romberg's method is a special version of Richardson extrapolation useful when the powers of h are multiples of 2. We have been able to demonstrate the usefulness of the method for our particular problem. It was shown, in Section 6.2, where the order of accuracy and numerical error were studied using Romberg's rule, that the order of accuracy could be improved using Romberg's method of second order to third or even fourth order accuracy. As the integrand of the integral determining M is not C^3 at the point $t = T_2$, the error expansion (7.1) for M does not have only even powers of h when t is small and therefore, only third order accuracy is obtained.

For choices of f such that f is constant for small population sizes and where the initial population size for $t \leq T_2$ is below this value, it could in fact be possible to avoid the problem with the discontinuity totally. However, such an f, being piecewise differentiable, adds further complications as the integrals determining M and P must be split wherever the population size reaches a level P where $f(P)$ is nondifferentiable. This is not taken into account in the current implementation and therefore it is equally difficult to use Simpson's rule in a satisfactory way in the case with such a crowding function described.

Despite the issues with Simpson's rule, the numerical implementation has served its purpose well also in the case with f nonconstant, enabling qualitative studies of the model through numerical simulations. In addition, we have been able to numerically validate second order accuracy for the trapezoidal rule and fourth order accuracy using Simpson's rule (when applicable). For step sizes in the order of $h = 10^{-4}$, the error in the computations could be decreased to machine epsilon.

An advantage of the current implementation of the model is that model components easily can be altered. On a long term, it would be interesting to compare the model to experimental data to gain knowledge about reasonable choices of the initial age distributions φ_1 and φ_2, the crowding function f, the cumulative distribution function $F(\tau)$ and the duration of each phase, T_1 and T_2. In its current stage, the model should be thought of as a simplified model of the cell cycle, yielding qualitative results. As no experimental data is used to design a precise crowding function or the initial age distributions, the results of the simulations will of course not tell the size in number of cells of some real life tumour. Nor are the function choices scaled in such a way that the time in number of hours for a solution to reach its limits M_∞ and P_∞ are the ones stated in the chapter, in real life.

Concerning the investigations on qualitative behaviour, it might be challenging to experimentally have knowledge about the values of the cumulative distribution function at more points than only $F(T_1)$, i.e. for instance $F(T_2)$ and $F(T_1 - T_2)$. The choice of a Weibull distribution for the cumulative distribution function in the simulations of this M.Sc. thesis was only theoretical. The lack of information is a strong reason to why an approximation where as few data as possible are needed is

preferred to use, to find for instance the upper bound for M. The upper bounds obtained in this study are very coarse. It would therefore be beneficial if the numerical scheme introduced could be used to analytically approximate a narrow upper and/or lower bound for $M(t)$. However, the lengths of the phases T_1 and T_2, being such that $T_2 < T_1 < 2T_2$, in combination with the characteristics of the kernels of the integral equations, complicates the analytical computations of such approximations of the solutions even in the easiest of settings. The reason is that the time line must be split into many small intervals, where the solution for M from multiple of these small intervals contribute to the computation of $M(t)$, a situation described in the section *Investigation of Upper Bound*, 5.3. The consequence is that computations quickly become hard to overlook. Returning to the coarse upper approximation, it might however still be useful in a situation where a constant crowding function is applied to model the system only for small population sizes, before space limitations have an impact on the system.

The differences between $\psi = 0$ and $\psi \neq 0$ can be seen in simulations where quorum sensing is assumed to exist and the initial number of cells is small. The total number of cells turns to zero if no cancer stem cells are present ($\psi = 0$), but grows otherwise to some limit value (determined by Theorem 5.1). The value of ψ also matters where a constant crowding function is chosen such that $f < 1/(2F(T_1))$. The solution decreases to zero if $\psi = 0$ but reaches a nonzero limit if $\psi > 0$. Moreover, there are differences between $\psi = 0$ and $\psi > 0$ in the upper bound for the number density of dividing cells at time t for f constant, as discussed in Section 5.3. The impact of ψ can also be investigated by analytically studying the difference in $M(t)$ for $\psi = 0$ and $\psi \neq 0$ with f constant, as in Section 5.4.

7.1 Future Work

Future work includes to further investigate the impact from cancer stem cells. One possibility is to create an input function dependent on the total number of cells in the system, i.e. $\psi(t) = \psi(P(t))$. In this way it could be possible to model cancer stem cells that act only when the total number of cells is small. The consequence could be for a tumour with this property that it relapses more easily, as the cancer stem cells always take over for small enough population sizes. In the altered model, there would be competition between the effect of the crowding function and the input function.

Other questions of interest are:

- The growth properties and growth rate of $M(t)$ and $P(t)$ in general and how they depend on input from cancer stem cells, $\psi(t)$,
- The convergence rate to limits M_∞ and P_∞ dependent on ψ (already briefly discussed at the end of Section 4.2),
- The fluctuating behaviour of $M(t)$ before it reaches a steady limit. For small initial data it was found in Section 4.3 that the solutions are more fluctuating if the system is driven by remaining cancer cells than if it is driven by daughter cells of cancer stem cells only. Investigating this difference could be a useful approach to distinguish the cases $\psi = 0$ and $\psi \neq 0$ for small initial data.
- The study of the impact from cancer stem cells represented by ψ using statistical methods, where the model is compared to and used together with experimental data. A goal would be to try the hypothesis $\psi = 0$.

References

[1] G. Chaffey. *Modelling the cell cycle*. PhD thesis, University of Surrey, United Kingdom, 2014.

[2] G. M. Cooper. *The cell: a molecular approach*. Sinauer Associates, 2 edition, 2000. ISBN-10: 0-87893-106-6.

[3] G. Dahlqvist and A. Björk. *Numerical methods*. Prentice-Hall, Inc., 1974. ISBN-10: 0136273157.

[4] L. M. Delves and J. L. Mohamed. *Computational methods for integral equations*. Cambridge University Press, 1985. ISBN: 9780521266291.

[5] D. B. F. Faraday, P. Hayter, and N. F. Kirkby. A mathematical model of the cell cycle of a hybridoma cell line. *Biochemical Enginereering Journal*, 7(1):49–68, 2001. ISSN: 1369-703X.

[6] J. X. Gao. Cancer stem cells: the lessons from pre-cancerous stem cells. *Journal of Molecular Medicine*, 12(444):67–96, 2008. ISSN: 15821838.

[7] F. B. Hildebrand. *Introduction to numerical analysis*. New York : Dover, 2 edition, 1987. ISBN-10: 0486653633.

[8] M. D. Johnston, P. K. Maini, S. Jonathan Chapman, C. M. Edwards, and W. F. Bodmer. On the proportion of cancer stem cells in a tumour. *Journal of Theoretical Biology*, 266(4):708–711, 2010. ISSN: 00225193.

[9] A. S. Kumar, J. N. Bryan, and S. R. Kumar. Bacterial quorum sensing molecule N-3-Oxo-Dodecanoyl-L-Homoserine lactone causes direct cytotoxicity and reduced cell motility in human pancreatic carcinoma cells. *PLoS ONE*, 9(9), 2014. ISSN: 19326203.

[10] S. Maad Sasane. An age structured cell cycle model with crowding. *Journal of Mathematical Analysis and Applications*, 444(1):768–803, 2016. ISSN: 0022-247X.

[11] I. Sánchez-García, C. Vicente-Dueñas, and C. Cobaleda. The theoretical basis of cancer-stem-cell-based therapeutics of cancer: can it be put into practice? *BioEssays*, 29(12):1269–1280, 2007. ISSN: 02659247.

Appendices

A Solution on First Interval

The solution for $M(t)$ on the interval $t \in [0, T_1 + T_2]$ is computed, using the cumulative distribution function

$$F(\tau) = 1 - \exp\left(-\frac{\tau - c}{a}\right) \tag{A.1}$$

and arbitrary constant φ_1, φ_2 and ψ.

On the first subinterval of length T_2, $M(t)$ is given directly by

$$M(t) = \varphi_2. \tag{A.2}$$

For the consecutive subintervals, we need the computation

$$\begin{aligned}\int_0^{T_1} R(t,\sigma)\varphi_1(\sigma)\,\mathrm{d}\sigma &= \int_0^{T_1+T_2-t} \frac{F'(\sigma + t - T_2)}{1 - F(\sigma)}\varphi_1\,\mathrm{d}\sigma = \\ &= \int_0^{T_1+T_2-t} \frac{1}{a}e^{-\left(\frac{t-T_2}{a}\right)}\varphi_1\,\mathrm{d}\sigma = \frac{\varphi_1}{a}e^{-\left(\frac{t-T_2}{a}\right)}(T_1 + T_2 - t) := R_{\mathrm{term}}(t).\end{aligned} \tag{A.3}$$

On the second interval of length T_2, i.e. where $t \in [T_2, 2T_2]$, $M(t)$ is calculated as

$$\begin{aligned}M(t) &= \int_0^{t-T_2} F'(t - T_2 - \sigma)(2M(\sigma) + \psi)\,\mathrm{d}\sigma + \int_0^{T_1} R(t,\sigma)\varphi_1\,\mathrm{d}\sigma = \\ &= F(t - T_2)(2\varphi_2 + \psi) + R_{\mathrm{term}}(t) := \\ &= \left(1 - e^{-\frac{t-T_2-c}{a}}\right)(2\varphi_2 + \psi) + \frac{\varphi_1}{a}e^{-\left(\frac{t-T_2}{a}\right)}(T_1 + T_2 - t).\end{aligned} \tag{A.4}$$

Finally, on the last subinterval, where $t \in [2T_2, T_1 + T_2]$, $M(t)$ is given in all its ugliness from

$$\begin{aligned}M(t) &= \int_0^{t-T_2} F'(t - T_2 - \sigma)(2M(\sigma) + \psi)\,\mathrm{d}\sigma + \int_0^{T_1} R(t,\sigma)\varphi(\sigma)\,\mathrm{d}\sigma = \\ &= \int_0^{T_2} F'(t - T_2 - \sigma)(2\varphi_2 + \psi)\,\mathrm{d}\sigma + \int_{T_2}^{t-T_2} F'(t - T_2 - \sigma)(2M(\sigma) + \psi)\,\mathrm{d}\sigma + R_{\mathrm{term}}(t),\end{aligned} \tag{A.5}$$

where

$$\int_0^{T_2} F'(t - T_2 - \sigma)(2\varphi_2 + \psi)\,\mathrm{d}\sigma = e^{-\left(\frac{t-T_2-c}{a}\right)}\left(e^{T_2/a} - 1\right)(2\varphi_2 + \psi) \tag{A.6}$$

and

$$\begin{aligned}&\int_{T_2}^{t-T_2} F'(t - T_2 - \sigma)(2M_{ii} + \psi)\,\mathrm{d}\sigma = \\ &= (2\varphi_2 + \psi)\left(\left(2e^{\frac{c}{a}} - 2e^{-\left(\frac{t-2T_2-c}{a}\right)}\right) - \frac{2}{a}e^{-\frac{t-2T_2-2c}{a}}(t - 2T_2)\right) + \\ &+ \frac{2\varphi_1}{a^2}e^{\left(\frac{-t+2T_2+c}{a}\right)}\left((T_1 + T_2)(t - 3T_2) - \frac{t^2}{2} + tT_2\right) + \psi e^{\frac{c}{a}}\left(1 - e^{\frac{-t+2T_2}{a}}\right) + R_{\mathrm{term}}(t).\end{aligned} \tag{A.7}$$

All in all, $M(t)$ on the third interval is thus given by

$$\begin{aligned} M(t) = (2\varphi_2+\psi)e^{-\left(\frac{t-T_2-c}{a}\right)}\left(e^{T_2/a}-1\right) + (2\varphi_2+\psi)\left(\left(2e^{\frac{c}{a}} - 2e^{-\left(\frac{t-2T_2-c}{a}\right)}\right) - \frac{2}{a}e^{-\frac{t-2T_2-2c}{a}}(t-2T_2)\right) + \\ + \frac{2\varphi_1}{a^2}e^{\left(\frac{-t+2T_2+c}{a}\right)}\left((T_1+T_2)(t-3T_2) - \frac{t^2}{2} + tT_2\right) + \psi e^{\frac{c}{a}}\left(1-e^{\frac{-t+2T_2}{a}}\right) + \\ + \frac{\varphi_1}{a}e^{-\left(\frac{t-T_2}{a}\right)}(T_1+T_2-t). \end{aligned} \tag{A.8}$$

It is possible to continue calculating an expression for $M(t)$ for arbitrary t in a similar manner. Only a slight modification of the calculations gives an upper approximation of $M(t)$ in the case with arbitrary, non-constant φ_1 and φ_2 where φ_1 and φ_2 in the expressions are replaced by the constant maximal values of the functions, $\|\varphi_1\|_\infty$ and $\|\varphi_2\|_\infty$. However, calculations show that it is beyond doubt quite exhausting to handle the expressions from the integral equations analytically, even in the simplest of settings!

To get a coarse upper approximation of $M(t)$ for the entire interval $[0, T_1+T_2]$, which can be used to calculate approximations and upper bounds for M further, we may take the maximum of $M(t)$ for the entire interval.

B Upper Bound on First Interval

We try to approximate an upper bound M_0 for $M(t)$ on the interval $t \in [T_1+T_2]$ for $f=1$ and $\psi=0$ along with arbitrary $F(\tau)$, $\varphi_1(\tau)$ and $\varphi_2(\tau)$. The value is needed to calculate an upper bound M_k on interval $I_k = [k(T_1+T_2), (k+1)(T_1+T_2)]$, $k \geq 1$ in Theorem 5.2.

For the first interval of length T_2, i.e. where $t \in [0, T_2]$, there is only contribution from φ_2 and we get an upper bound M_A as

$$M_A := \|\varphi_2\|_\infty. \tag{B.1}$$

On the second interval of length T_2, i.e. where $t \in [T_2, 2T_2]$, we have

$$\begin{aligned} M(t) &= \int_0^{t-T_2} (2M(\sigma))\, F'(t-T_2-\sigma)\,\mathrm{d}\sigma + \int_0^{T_1} R(t,\sigma)\varphi_1(\sigma)\,\mathrm{d}\sigma \leq \\ &\leq \int_0^{t-T_2} (2M_A)\, F'(t-T_2-\sigma)\,\mathrm{d}\sigma + \int_0^{T_1} R(t,\sigma)\varphi_1(\sigma)\,\mathrm{d}\sigma \leq \\ &\leq 2M_A F(t-T_2) + \|\varphi_1\|_\infty \frac{F(T_1)}{1-F(T_1)} \leq \\ &\leq 2M_A F(T_2) + \|\varphi_1\|_\infty \frac{F(T_1)}{1-F(T_1)} =: M_B, \end{aligned} \tag{B.2}$$

where we have used that $F(\tau)$ is monotonically increasing and attains larger values the larger the argument. In a general setting it depends on the characteristics of $F(T_2)$, φ_1 and φ_2 whether $M_B > M_A$. If $2F(T_2) < 1$ and $\varphi_1 = 0$ this is not the case. However, if we have an F such that $F(T_2) > 1$ it always holds that $M_B > M_A$ and many choices of φ_1 and φ_2 for other choices of $F(T_2)$ lead to the same situation. With this function choices in mind, we compute the upper bound M_C for the final

interval, $t \in [2T_2, T_1 + T_2]$, as

$$\begin{aligned} M(t) &= \int_0^{t-T_2} 2M(\sigma)F'(t - T_2 - \sigma)\,\mathrm{d}\sigma + \int_0^{T_1} R(t,\sigma)\varphi_1(\sigma)\,\mathrm{d}\sigma \leq \\ &\leq 2M_A \int_0^{T_2} F'(t - T_2 - \sigma)\,\mathrm{d}\sigma + 2M_B \int_{T_2}^{t-T_2} F'(t - T_2 - \sigma)\,\mathrm{d}\sigma + \|\varphi_1\|_\infty \int_0^{T_1} R(t,\sigma)\,\mathrm{d}\sigma = \\ &\leq 2M_A F(t - T_2) + (2M_B - 2M_A)F(t - 2T_2) + 2M_B F(0) + \|\varphi_1\|_\infty \frac{F(T_1)}{1 - F(T_1)} \leq \\ &\leq 2M_A F(T_1) + (2M_B - 2M_A)F(T_1 - T_2) + \|\varphi_1\|_\infty \frac{F(T_1)}{1 - F(T_1)} =: M_C. \end{aligned} \tag{B.3}$$

Comparing M_B and M_C, we see that $M_C > M_B$ as $F(T_1) > F(T_2)$ and as the second term in M_C is positive. For the chosen parameters, the upper bound on the entire interval $[0, T_1 + T_2]$ is thus given by

$$\begin{aligned} M_0 := M_C &= 2M_A F(T_1) + (2M_B - 2M_A)F(T_1 - T_2) + \|\varphi_1\|_\infty \frac{F(T_1)}{1 - F(T_1)} = \\ &= \|\varphi_2\|_\infty \left(2F(T_1) + 2(2F(T_2) - 1)F(T_1 - T_2)\right) + \|\varphi_1\|_\infty \left(\frac{2F(T_1)}{1 - F(T_1)} F(T_1 - T_2) + \frac{F(T_1)}{1 - F(T_1)}\right). \end{aligned} \tag{B.4}$$

However, this approximation of M on the first interval relies on that we know or can approximate a maximum value of φ_1 and φ_2 and that we know $F(T_2)$ and $F(T_1 - T_2)$. If this is not possible, we have to rely on a coarser approximation.

Master's Theses in Mathematical Sciences 2017:E51
ISSN 1404-6342

LUTFMA-3327-2017

Mathematics
Centre for Mathematical Sciences
Lund University
Box 118, SE-221 00 Lund, Sweden

http://www.maths.lth.se/